Diss. ETH No 9489

LASER INDUCED FLUORESCENCE AND SCATTERING NEAR INTERFACES

A dissertation submitted to the

SWISS FEDERAL INSTITUTE OF TECHNOLOGY ZURICH

for the degree of

Doctor of Natural Sciences

presented by

Martin Lieberherr

Dipl. Phys. ETH

born April 19th, 1962

citizen of Krummenau SG and St. Gallen

accepted on the recommendation of

Prof. Dr. W. Lukosz, examiner

Prof. Dr. U. Wild, co-examiner

1991

CONTENTS

ABSTRACT

We investigated experimentally the fluorescence (electric dipole transitions) of molecules in solutions and/or near interfaces and the Rayleigh (dipole) scattering by dielectric particles on interfaces. These processes were compared with the radiation of a classical electric dipole near interfaces. We investigated the possibility to measure orientations and quantum efficiencies of molecules in ensembles by using interface effects on the angular distribution of power (radiation pattern) and total emitted power of a dipole.

The fluorescence lifetimes τ_F of rhodamine dyes (R110, R6G, R101, and SR101) in very dilute solutions (concentration $\leq 10^{-7}$ mol/l) were measured as a function of the refractive indices n_0 of the solvents. Because theory stated a proportionality between total emitted power of an electric dipole and the refractive index of the surrounding medium, a linear regression of the measured total transition rate $A_{tot} = 1/\tau_F$ on n_0 was made ($A_{tot} = n_0 A_{r,vac} + A_{nr}$) and showed high correlations (> 0.9) but negative values for the fit parameter A_{nr} (the non-radiative transition rate, in contrast to the spontaneous emission rate A_r), which is an impossible result. The modified relation $A_{tot} = \{3n_0^2/(2n_0^2 + 1)\}^2 n_0 A_{r,vac} + A_{nr}$ with a local field correction for the radiative power showed high correlations too and additionally positive values for A_{nr}. Quantum efficiencies in the range 70-100 % were calculated from these A_{tot}, A_{nr}, and n_0.

Submonomolecular layers of the dyes R110, R6G, RB, SRB, R101, SR101, R700, and R800 with surface concentration $\leq 10^{15}$ m^{-2} have been prepared with a spin-coat technique on glass with refractive index n_2. Their radiation pattern showed that the mean angle between the surface normal and the molecules' emission dipole moment was $\theta = (77 \pm 2)°$, i.e. that they were preferentially parallel to the surface. The static depolarization of the fluorescence showed that the angle between absorption and emission dipole moments of the dye molecules was smaller than 15°-25°. A linear regression ($A_{tot} = l_\parallel(n_2) A_{r,vac} + A_{nr}$) of the measured transition rate A_{tot} on the calculated total radiated power $l_\parallel(n_2)$ yielded high correlations (> 0.9) but negative values for A_{nr} too. The local field correction above was not appli-

cable in this case, but optical contact experiments were made instead where the optical but not the chemical environment was continuously varied (a glass plate was pressed against the dye layer and the gap width continuously monitored). The total transition rate A_{tot} and the emitted intensity changed reversibly and continuously with the qualitative behaviour as predicted by theory but the accuracy of the data did not allow a determination of the non-radiative transition rate A_{nr} and hence the quantum efficiency.

Unspecific adsorption on glass surfaces of rabbit-anti-human immunoglobulin (Gamma chains) labelled with the fluorescent dye TRITC in phosphate buffer solution was observed via the emission of the dye tracer. An initial bulk concentration of $3 \cdot 10^{-6}$ mol/l yielded after several hours an adsorbate surface concentration of approx. 1 molecule/$(7$ nm$)^2$. From radiation patterns adsorbate film thicknesses of ≈ 10 nm, refractive indices of ≈ 1.4, and an isotropic orientation of the emitters was obtained. With the assumption of isotropic orientation, a refractive index of 1.37 ± 0.02 was calculated from the values of the radiation pattern at the critical angle of total internal reflection.

Radiation patterns of the light scattered by latex particles on air/glass interfaces were measured. The thin latex layers were produced with a spin-coat technique. The size and surface coverage of the latex particles deduced from light scattering were confirmed with raster electron micrographs.

KURZFASSUNG

Wir untersuchten experimentell die Fluoreszenz (elektrische Dipolübergänge) von Molekülen in freier Lösung und/oder nahe an Grenzflächen sowie die Rayleigh-Streuung durch dielektrische Teilchen auf Grenzflächen. Wir verglichen diese Prozesse mit der Strahlung eines klassischen elektrischen Dipols nahe einer Grenzfläche. Wir untersuchten, ob Orientierung und Quantenwirkungsgrad von Molekülen in Ensembles gemessen werden können durch Ausnutzung von Grenzflächen-Effekten auf die Richtcharakteristik und/oder gesamthaft abgestrahlte Leistung eines Dipols.

Die Fluoreszenz-Lebensdauern τ_F von Rhodamin-Farbstoffen (R110, R6G, R101 und SR101) in stark verdünnter Lösung (Konzentration $\leq 10^{-7}$ mol/l) wurden als Funktion der Brechungsindices n_0 der Lösungsmittel gemessen. Weil die Theorie eine Proportionalität zwischen der gesamthaft abgestrahlten Leistung eines elektrischen Dipols und der Brechzahl n_0 des umgebenden Mediums lieferte, wurde eine lineare Regression der gemessenen totalen Übergangsrate $A_{tot} = 1/\tau_F$ auf n_0 berechnet ($A_{tot} = n_0 A_{r,vac} + A_{nr}$), welche auch eine hohe Korrelation (>0.9) der Daten ergab, aber leider negative Werte für den Fit-Parameter A_{nr} (die strahlungslose Übergangsrate, im Gegensatz zur spontanen Emissionsrate A_r), welches ein physikalisch unmögliches Resultat darstellt. Die neue Relation $A_{tot} = \{3n_0^2/(2n_0^2 + 1)\}^2 n_0 A_{r,vac} + A_{nr}$ mit einer Lokalfeld-Korrektur für die Strahlungsleistung ergab ebenfalls eine gute Korrelation und diesmal positive A_{nr}. Aus den Regressionsparametern $A_{r,vac}$ und A_{nr} konnten Quantenwirkungsgrade zwischen 70 und 100 % berechnet werden.

Submonomolekulare Schichten der Farbstoffe R110, R6G, RB, SRB, R101, SR101, R700 und R800 mit Oberflächenkonzentrationen $\leq 10^{15}$ m^{-2} wurden mit einem Spin-coat Verfahren auf Glas mit Brechungsindex n_2 hergestellt. Deren Richtcharakteristiken zeigten, dass der mittlere Winkel zwischen der Oberflächennormalen und dem Emissionsdipolmoment der Moleküle $\theta = (77 \pm 2)°$ betrug, d.h. dass sie bevorzugt parallel zur Oberfläche orientiert waren. Die statische Depolarisation des Fluoreszenzlichtes zeigte, dass die Winkel zwischen Absorptions- und Emissionsdipolmoment der Farbstoffmoleküle kleiner als 15-25° sind.

Eine lineare Regression ($A_{tot}\,=\,l_\parallel(n_2)\,A_{r,vac} + A_{nr}$) der gemessenen Übergangsrate A_{tot} auf die berechnete abgestrahlte Leistung $l_\parallel(n_2)$ ergab hohe Korrelationen (>"0.9), aber negative Werte für A_{nr}. Eine Korrektur fürs lokale Feld wie oben war nicht anwendbar, stattdessen wurde ein Annäherungsexperiment durchgeführt, wo nur die optische aber nicht die chemische Umgebung der Moleküle verändert wurde (eine Glasplatte wurde gegen die Farbstoffschicht gedrückt und der Abstand kontinuierlich gemessen). Die totale Übergangsrate A_{tot} und die Fluoreszenzintensität änderten sich stetig, reversibel und mit einem qualitativen Verhalten wie vorhergesagt durch die Theorie. Leider erlaubte die Genauigkeit der Daten keine Bestimmung der Quantenwirkungsgrade.

Die unspezifische Adsorption eines Proteins aus einer Phosphatpufferlösung auf Glas wurde via die Lumineszenz eines Farbstoffes unter einem bestimmten Emissionswinkel beobachtet. Das Protein war rabbit-anti-human immunoglobulin (Gamma chains), markiert mit dem fluoreszierenden Farbstoff TRITC. Eine anfängliche Volumenkonzentration von $3\cdot10^{-6}$"mol/l ergab nach einigen Stunden eine Adsorbat-Oberflächenkonzentration von ≈"1"Molekül pro (7"nm)^2. Aus Richtcharakteristiken ergab sich eine Adsorbatfilmdicke von ≈"10"nm, eine Brechzahl von ≈"1.4 und eine isotrope Orientierung der Emitter. Unter der Annahme einer isotropen Orientierung berechneten wir eine Adsorbatschichtbrechzahl von 1.37"±"0.02 aus der Werten der Richtcharakteristiken beim Grenzwinkel der Totalreflexion.

Richtcharakteristiken des Lichtes gestreut durch Latex-Partikel auf Luft/Glas-Grenzflächen wurden gemessen. Die Latex-Schichten wurden mit einem Spin-coat Verfahren hergestellt. Aus dem Streuverhalten bestimmte mittlere Teilchenradien und Oberflächenkonzentrationen konnten durch Rasterelektronenmikroskopaufnahmen bestätigt werden.

1. INTRODUCTION

1.1. Object and Outline of this Work

The objects of this work were experimental investigations with and about the classical theory of electric dipole radiation near interfaces. In a first experiment (chapter 4) we tested experimentally the applicability of the theory to the fluorescence emission of excited molecules. We measured the emission of laser dyes in bulk solution to investigate local field effects and we measured the emission from submonomolecular layers on air/glass interfaces to study interface effects. In a second experiment (chapter 5) we used the fluorescence of dye-markers attached to proteins to monitor adsorption of protein-molecules on an interface. In a third experiment (chapter 6) we measured dipole scattering by dielectric particles on interfaces. The remaining sections of this chapter give an outline of this work. Note that the numbers and titles of the sections correspond to the numbers and titles of the following chapters. The sections contain a short summary and a pedagogical introduction into the subject of the corresponding chapter. Formulas are explicitly deferred to later chapters. Special emphasis was given to the introduction to the theory (section 1.2), the following sections were kept shorter.

1.2. Theory of Radiating Dipoles Near Interfaces

Chapter 2 recapitulates the formulas for the angular distribution of radiated power (radiation pattern $P(\alpha)$) and the total emitted power (L) of a single oscillating classical electric dipole near plane interfaces. Then we calculated distributions of emission dipole moments of fluorescent molecules near interfaces taking excitation into account. We give formulas to deduce orientation and quantum yield of the molecules from measurements of the fluorescence emission.

The angular distribution of radiated power in the far field ("radiation pattern") and the total emitted power of a classical oscillating electric (Hertz) dipole in free space are well known, cf. e.g. [1;2, p.465]. If the dipole is in a non-absorbing, homogeneous, and isotropic dielectric (1), and/or a plane boundary to a different (homogeneous and isotropic) medium (2) is placed close to the dipole, some distinct effects may occur. First calculations of such effects are from Sommerfeld [1;5]

for dipole antennas on the surface of the earth (1909). More recent contributions may be found in the reference list of [2;4] and of this work. Lukosz and Kunz [2;1-6] calculated those effects in a novel way by decomposing the field emitted by a dipole into plane and evanescent waves, analogous to the far and near field of a dipole, and solving the boundary problem for each wave separately.

a) effects on the emission of plane waves:

Angle dependent refraction and transmission at the interface 1/2 change the shape of the radiation pattern in medium 2. Radiation reflected at the interface 1/2 interferes with with radiation emitted in other directions in medium 1 and changes the shape of the radiation pattern in medium 1 ("wide angle interference", cf. fig. 1.1).

b) effects on the emission of evanescent waves:

The dipole's near field may reach to the interface and contribute to the radiated power by absorption in medium 2 or, if medium 2 is non-absorbing and optically denser than medium 1, by transmission and refraction into plane waves (visible above the critical angle of total internal reflection in medium 2, cf. fig. 1.2).
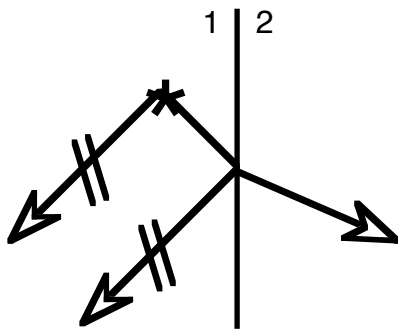
Fig. 1.1: Emission by plane waves, refraction and transmission in medium 2, wide angle interference in medium 1. * represents the emitting dipole.
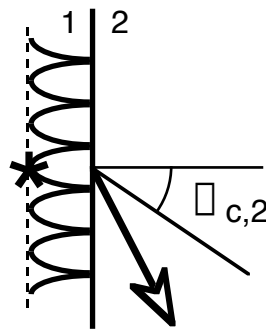
Fig. 1.2: Emission by evanescent waves, radiation visible above the critical angle of total internal reflection $\alpha_{c,2}$ in medium 2. * represents the emitter.

c) other effects:

The refractive index of medium 1 has an influence on the total radiated power because it changes the field generated by the dipole at its own location. Additionally the dipole is im-

mersed in the electromagnetic field reflected at the interface
which changes the total radiated power depending on the phase
shift upon reflection. Poynting's theorem shows that the total
radiated power is the negative of the work done per unit time
by the fields on the source. For an electric dipole the power
is proportional to the electric field component in direction of
the dipole axis which is 90° out of phase with the oscillating
dipole moment. [2;4, p. 1610]

Similar effects occur if the dipole is located not only in front
of a single interface but in a layer system. The strengths of
those perturbations depend on the dipole's orientation, dis-
tance to the interface in units of the wavelength λ, and on the
refractive indices of the media, i.e. they depend on the "opti-
cal environment". With "optical environment" we mean the re-
fractive indices of the media and their extent on a wavelength
scale in contrast to the "chemical environment", i.e. the mole-
cules, atoms or ions surrounding an emitting system on an
atomic scale.

Orientations of the dipoles with respect to the interface

radiation patterns for $n_2 = n_1$

radiation patterns for $n_2 = 1.5\, n_1$

Fig. 1.3: Polar plots of radiation patterns of electric dipoles
in medium 1 at a distance $z_0 = 0$ to the interface to medium 2;
$n_0 = n_1$, cf. chapter 2, fig. 2.1-3; arbitrary scales!

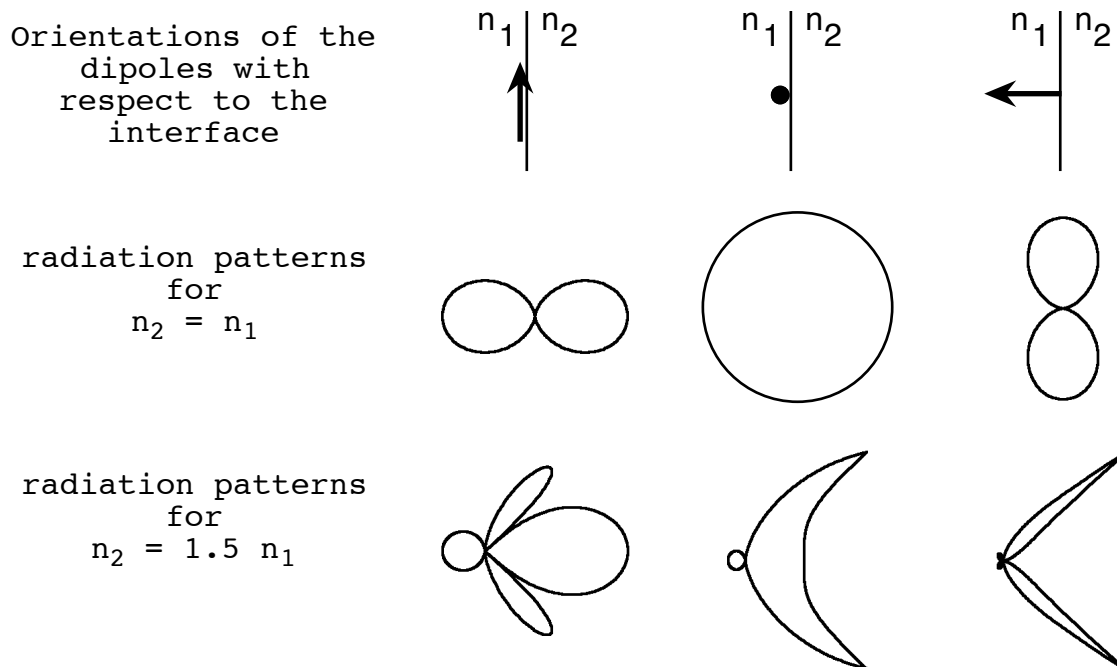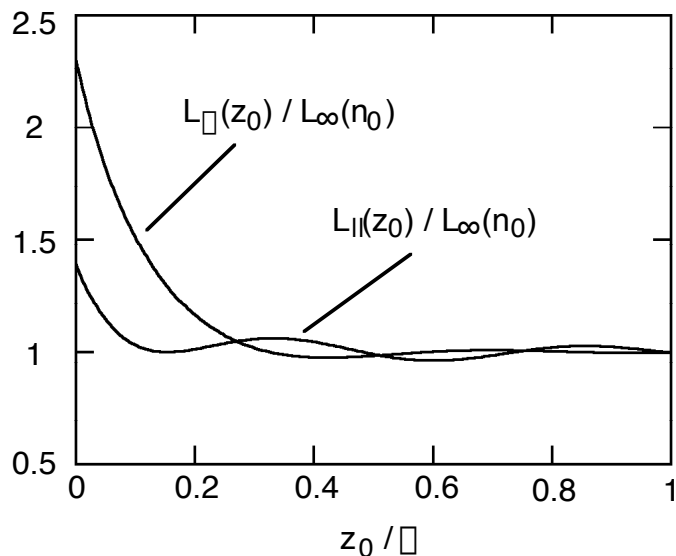Fig. 1.4: Normalized total radiated power of dipoles parallel $\{L_{\parallel}(z_0)\ /L_{\infty}(n_0)\}$ and perpendicular $\{L_{\perp}(z_0)/L_{\infty}(n_0)\}$ to an interface vs. distance z_0 to that interface. (parameters: $n_1" = n_0" =" 1$, $n_2" = 1.5$, $\lambda" =$ wavelength, cf. chapter 2)

1.3. Methods and Instrumentation

Chapter 3 gives a short description of the measuring apparatus and the methods used to analyze the data. The experimental setup was used to measure intensities, spectra, radiation patterns, and fluorescence lifetimes. A full description of the apparatus was given by Ch. Fattinger [3;1]. We developed the software to analyze radiation patterns and fluorescence lifetimes.

We used laser light to induce fluorescence or scattering. A stepper motor controlled turntable was used to record radiation patterns. Fluorescence lifetimes were measured by time-correlated single-photon-counting. The emitted radiation was detected with a photomultiplier. The measurements were transferred to and analyzed on a desktop computer.

1.4. Optical Environment Dependent Fluorescence of Laser Dyes

Chapter 4 presents the main results of this work. First, the fluorescence lifetimes of laser dyes in dilute solutions were measured. We investigated the influence of the refractive indices of the solvents on the lifetime (local field effects). Second, we measured radiation patterns and lifetimes of submonomolecular dye layers on different glass substrates. From the radiation patterns we determined the orientation of the molecules with respect to the surface. We also tried to determine the fluorescence quantum yield from the effect of the op-

tical environment on the fluorescence lifetimes and emitted intensities.

The fluorescence of laser dyes is an electric dipole transition. This quantum mechanical process corresponds to the radiation of a classical electric dipole, for details cf. section 2.2.3. The total radiated power corresponds to the spontaneous emission rate. The radiation pattern corresponds to the angular probability distribution to detect the emitted photon. From measurements of their radiation patterns, the orientations of the dye-molecules can be deduced. In addition to the classical dipole model, a molecule may undergo non-radiative transitions. Where the radiative transitions (spontaneous emission) depend on the optical environment, the non-radiative transitions depend on intrinsic parameters and the chemical environment. The different size of those two environments allows to change the optical environment in a controlled manner and leave the other unaltered. This can in principle be used to determine the non-radiative transition rate of a dye in a specific chemical environment. [4;12]

1.5. Adsorption of Proteins with a Fluorescent Label

Chapter 5 is an application of the fluorescence of dye molecules near interfaces. We monitored adsorption of protein molecules on an interface by means of fluorescent labels attached to the proteins. This is a method widely used in biochemistry [5;1-3]. Fluorescence was excited with an evanescent wave produced by total internal reflection at the interface. From the emitted intensity, the surface coverage of the protein was estimated. From the radiation pattern, the refractive index and thickness of the adsorbate layer was determined and the orientation of the marker molecules was deduced.

1.6. Rayleigh Scattering by Small Particles

Chapter 6 gives a short outlook to a different field where the theory is applicable: Dipole or Rayleigh scattering by small dielectric particles near interfaces. We measured the radiation patterns of the light scattered by latex particles on air/glass interfaces.

A small dielectric particle becomes polarized in a homogeneous electric field and the induced field outside the particle is

like the field of a dipole. This still holds when the field is not static but oscillating if the corresponding wavelength is much larger than the particle [1;2, p."485, 6;1-2]. The induced oscillating dipole radiates energy and the whole process is called Rayleigh scattering (dipole scattering). If the particle radiates like a dipole then the theory for dipole radiation near interfaces should hold too if the particle is not in an infinite medium but close to an interface.

2. THEORY OF RADIATING DIPOLES NEAR INTERFACES

The objects of this chapter are:

1) recapitulate and discuss a.) the formulas for the angular distribution of radiated power {radiation pattern $P(\alpha)$} and for the total emitted power {$L(z_0)$} of a single oscillating electric dipole between two interfaces (section 2.1.1.) and b.) the expressions for the radiation patterns from ensembles of dipoles (section 2.1.2.).

2) present a model of fluorescent molecules (absorption- and emission-dipole moments in sections 2.2.1-2, quantum efficiency in section 2.2.3.) and to investigate in theory the possibilities to measure orientation and quantum yield of those molecules in ensembles.

3) recollect the formulas for scattering by a small dielectric sphere in an infinite dielectric matrix (section 2.3.).

2.1. Radiation Pattern and Radiative Power
2.1.1. Single Electric Dipole

This section contains a compilation of the formulas for the radiation pattern $P^{(s,p)}(\alpha)$ and the total emitted power $L(z_0)$ of a single electric dipole from [2;1-6]. An oscillating electric dipole $\mathbf{D}$ with a dipole moment $\mathbf{p}_{em}$ is assumed to be located in a layer of a nonabsorbing medium 0 with refractive index n_0 and thickness d_0 between two media 1 and 2 (half spaces) with refractive indices n_1 and n_2, cf. fig. 2.1. Media 0, 1 and 2 are linear, nonmagnetic ($\mu = 1$), homogeneous, and isotropic. The dipole's distance to medium 2 is z_0 ($0 \leq z_0 \leq d_0$), its angle to the z-axis is ϑ, and its azimuth angle is φ ($\varphi=0$ if $\mathbf{D} \parallel$ x-axis, not shown in fig. 2.1). The Hertz dipole $\mathbf{D}$ is assumed to oscillate with angular frequency $\omega = 2\pi c/\lambda$, where c is the speed of light in vacuum and λ the corresponding vacuum wavelength. The values of n_0, n_1, n_2, z_0/λ, and d_0/λ determine the dipole's optical environment. The angular
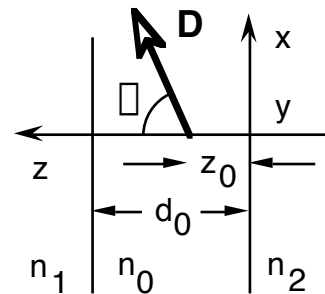

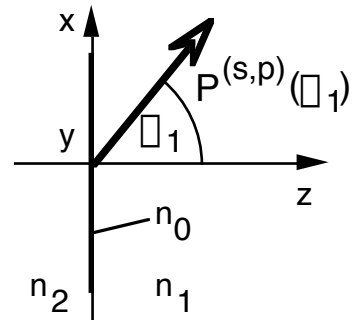Fig. 2.1: Electric dipole **D** in its optical environment

Fig. 2.2: Radiation pattern $P^{(s,p)}(\alpha_1)$

distribution of radiated power in the far field in medium 1 is $P^{(s,p)}(\alpha_1)$ where the superscripts s and p denote the polarization (s or TE polarization means **E** ∥ y-axis, p or TM means **H** ∥ y-axis, where **E** is the electric and **H** the magnetic field vector). The emission angle α_1 is measured in the (x,z)-plane, cf. fig. 2.2. Medium 1 must be nonabsorbing, if the radiation shall reach the far field on that side of the interface, i.e. $Im(n_1) = 0$ and $Re(n_1) \geq 1$, where Im() and Re() denote imaginary and real part of a complex number. (Analogously for medium 2). If one of the media outside the layer (n_0,d_0) is absorbing, then the dipole must be separated from it $(z_0 > 0$ or $d_0 - z_0 > 0)$ for that the total radiated power remains bounded. The radiation pattern $P^{(s,p)}(\alpha)$ and the total radiated power $L(z_0)$ of a dipole have been calculated by representing the dipole's near field as a superposition of s- and p-polarized plane and evanescent waves $\propto \exp(ik_x x + ik_y y + ik_z z)$.

The **light distribution in medium 1:**
$$Im(n_0) = Im(n_1) = 0 \qquad [2;1, p. 748]$$
The following symbols and relations are used:

$$n = n_1/n_0 \tag{2.1}$$
$$k_j = n_j \, 2\pi/\lambda_{vac} \; ; \; j = 0,1,2 \text{ (magnitude of wavevector)} \tag{2.2}$$
$$k_j^2 = k_x^2 + k_y^2 + k_{z,j}^2 \; ; \; (k_y = 0 \text{ in the (x,z)-plane}) \tag{2.3}$$
$$k_{z,j} = (k_j^2 - k_1^2 \sin^2\alpha_1)^{1/2} \text{ (real or complex)} \tag{2.4}$$
$$\text{(z-component of wavevector)}$$
$$k_0^2 \sin^2\alpha_0 = k_1^2 \sin^2\alpha_1 \; (= k_x^2) \text{ (Snell's law)} \tag{2.5}$$
$$\alpha_{c,j} = \arcsin(n_0/n_j) \text{ if } n_0 \leq n_j \tag{2.6}$$
$$\text{(critical angle of total internal reflection in medium } j)$$
$$\rho = 0 \text{ (if s-pol.) and } \rho = 1 \text{ (if p-pol.)} \tag{2.7}$$
$r_{0,j}^{(s,p)}$, $t_{0,j}^{(s,p)}$: Fresnel reflection and transmission coefficients (see below)

Emission by plane waves: for $0° \leq \alpha_1 \leq 90°$ (if $n_0 > n_1$) or $0° \leq \alpha_1 \leq \alpha_{c,1}$ (if $n_0 \leq n_1$). This part of the radiation pattern in medium 1 originates from the plane waves in the Fourier decomposition of the source field in medium 0. $(k_{z,0} = k_0 \cdot (1 - n^2 \cdot \sin^2\alpha_1)^{1/2}$ is a real number)

$$P^{(s,p)}(\alpha_1) = Q^{(s,p)}(\alpha_0) \, M^{(s,p)}(\alpha_0) \, T_{0,1}^{(s,p)}(\alpha_1) \tag{2.8}$$

where

$$Q^{(s)}(\alpha_0) = \frac{3}{8\pi}\ \sin^2\vartheta\ \sin^2\varphi\ W_+^{(s)}(\alpha_0) \tag{2.9}$$

$$Q^{(p)}(\alpha_0) = \frac{3}{8\pi}\ [\cos^2\vartheta\ \sin^2\alpha_0\ W_+^{(p)}(\alpha_0) \tag{2.10}$$

$$+\ \sin^2\vartheta\ \cos^2\varphi\ \cos^2\alpha_0\ W_-^{(p)}(\alpha_0)$$

$$-\ \sin(2\vartheta)\ \cos\varphi\ (1/2)\ \sin(2\alpha_0)\ (1 - |r_{0,2}^{(p)}|^2)]$$

$$W_\pm^{(s,p)} = |1 \pm r_{0,2}^{(s,p)}\ \exp(2ik_{z,0}z_0)|^2 \tag{2.11}$$

$$M^{(s,p)}(\alpha_0) = |1 - r_{0,1}^{(s,p)}\ r_{0,2}^{(s,p)}\ \exp(2ik_{z,0}d_0)|^{-2} \tag{2.12}$$

$$T_{0,1}^{(s,p)}(\alpha_1) = |t_{0,1}^{(s,p)}\ k_0/k_{z,0}|^2\ \cos^2\alpha_1\ n^{3-2\rho} \tag{2.13}$$

If all the media are nonabsorbing, and if $n_0 > n_1$ and $n_0 > n_2$, then the layer (n_0,d_0) may guide waves by total internal reflection. This case is not included in the formulas above because one possible mathematical formulation of the waveguiding criterion is $1/M^{(s,p)}(\alpha_0) = 0$ (2.14), M as in (2.12).

Emission by evanescent waves: for $\alpha_{c,1} \le \alpha_1 \le 90°$ (if $n_0 < n_1$). This part of the radiation pattern in medium 1 originates from the evanescent waves in the Fourier representation of the dipole's near field in medium 0. ($k_{z,0} = k_0 \cdot (1 - n^2\ \sin^2\alpha_1)^{1/2}$ is a purely imaginary number)

$$P^{(s,p)}(\alpha_1) = Q^{(s,p)}(\alpha_1)\ M^{(s,p)}(\alpha_1)\ T_{0,1}^{(s,p)}(\alpha_1)$$

$$\cdot \exp(-2|k_{z,0}|(d_0-z_0)) \tag{2.15}$$

where

$$Q^{(s)}(\alpha_1) = \frac{3}{8\pi}\ \sin^2\vartheta\ \sin^2\varphi\ W_+^{(s)}(\alpha_1) \tag{2.16}$$

$$Q^{(p)}(\alpha_0) = \frac{3}{8\pi}\ [\cos^2\vartheta\ n^2\sin^2\alpha_1\ W_+^{(p)}(\alpha_1) \tag{2.17}$$

$$+\ \sin^2\vartheta\ \cos^2\varphi\ (n^2\sin^2\alpha_1 - 1)\ W_-^{(p)}(\alpha_1)$$

$$-\ \sin(2\vartheta)\ \cos\varphi\ n\ \sin\alpha_1\ (n^2\sin^2\alpha_1 - 1)^{1/2}$$

$$\cdot 2\mathrm{Im}\{r_{0,2}^{(p)}(\alpha_0)\}\ \exp(-|k_{z,0}|z_0)]$$

$$W_\pm^{(s,p)}(\alpha_1) = |1 \pm r_{0,2}^{(s,p)}\ \exp(-2|k_{z,0}|z_0)|^2 \tag{2.18}$$

$$M^{(s,p)}(\alpha_1) = |1 - r_{0,1}^{(s,p)}\ r_{0,2}^{(s,p)}\ \exp(-2|k_{z,0}|d_0)|^{-2} \tag{2.19}$$

$$T_{0,1}^{(s,p)}(\alpha_1) = |t_{0,1}^{(s,p)}\ k_0/k_{z,0}|^2\ \cos^2\alpha_1\ n^{3-2\rho} \tag{2.20}$$

The **light distribution in medium 2** $P^{(s,p)}(\alpha_2)$ (2.21) is obtained from $P^{(s,p)}(\alpha_1)$ through the interchanges 1×2, $\vartheta \times 180°-\vartheta$, and $z_0 \times d_0-z_0$.

Normalization of the radiation pattern:

The integration of the radiation pattern $P^{(s,p)}(\alpha)$ over the solid angle $\Omega = 4\pi$ yields the normalized total power $L(z_0)$ (see below) radiated by the source into media 1 and 2:

$$\int_{\ }^{4\pi} [P^{(s)}(\alpha) + P^{(p)}(\alpha)]\, d\Omega \ = \ \frac{L(z_0)}{L_\infty(n_0)} \qquad (2.22)$$

(Waveguiding is not included in this formula and all the media must be nonabsorbing). Therefore $P^{(s,p)}(\alpha) \cdot L_\infty(n_0)/L(z_0)$ or short P/L is the angular probability distribution to detect the emitted light. Its normalization is

$$\int_{\ }^{4\pi} [P^{(s)}(\alpha) + P^{(p)}(\alpha)]\, \frac{L_\infty(n_0)}{L(z_0)}\, d\Omega \ = \ 1 \qquad (2.23)$$

The **Fresnel reflection and transmission coefficients** $r_{0,j}^{(s,p)}$ and $t_{0,j}^{(s,p)}$ for the amplitudes of plane, linear polarized, and monochromatic waves $\propto \exp(ik_x x \pm ik_z z)$ incident in medium 0 in the (x,z)-plane on a single interface (z = 0) to medium j (j = 1,2) are given below for the convenience of the reader. The media must be linear, nonmagnetic ($\mu = 1$), homogeneous, and isotropic. The waves may not only be homogeneous ($\mathrm{Re}(k_z) \neq 0$, $\mathrm{Im}(k_z) = 0$) but may be also evanescent ($\mathrm{Re}(k_z) = 0$, $\mathrm{Im}(k_z) \neq 0$) or inhomogeneous ($\mathrm{Im}(k_z) \neq 0$, $\mathrm{Re}(k_z) \neq 0$). If the polarization is s (TE, $\rho = 0$) then the coefficients are $r_{0,j}^{(s)} = E_{y,refl}/E_{y,in}$ and $t_{0,j}^{(s)} = E_{y,trans}/E_{y,in}$ where the E_y are the y-components of the incident, reflected or transmitted electric fields at the interface. If the polarization is p (TM, $\rho = 1$) then the coefficients are $r_{0,j}^{(p)} = H_{y,refl}/H_{y,in}$ and $t_{0,j}^{(p)} = H_{y,trans}/H_{y,in}$ where the H_y are the y-components of the magnetic fields at the interface; E_x and E_z can be calculated from H_y via the Maxwell equations.

$$r_{0,j}^{(s,p)} = \frac{k_{z,0}/n_0^{2\rho} - k_{z,j}/n_j^{2\rho}}{k_{z,0}/n_0^{2\rho} + k_{z,j}/n_j^{2\rho}} \qquad (2.24)$$

$$t_{0,j}^{(s,p)} = 1 + r_{0,j}^{(s,p)} = \frac{2\, k_{z,0}/n_0^{2\rho}}{k_{z,0}/n_0^{2\rho} + k_{z,j}/n_j^{2\rho}} \qquad (2.25)$$

The formulas for $P^{(s,p)}(\alpha_j)$ and for the total radiated power below remain valid, if the single interface between the two media 0,j is replaced by a planar stratified layer system and if the reflection and transmission coefficients are calculated accordingly [2;1, p. 753]. The coefficients $r_{abc}^{(s,p)}$, $t_{abc}^{(s,p)}$ for a three media (a,b,c) system are (for both polarizations):

$$r_{abc} = \frac{r_{ab} + r_{bc}\exp(2ik_{z,b}d_b)}{1 + r_{ab}r_{bc}\exp(2ik_{z,b}d_b)} \qquad (2.26)$$

$$t_{abc} = \frac{t_{ab}t_{bc}\exp(ik_{z,b}d_b)}{1 + r_{ab}r_{bc}\exp(2ik_{z,b}d_b)} \qquad (2.27)$$

For a system with more layers, those formulas have to be applied recursively, e.g. r_{abcd} is calculated from r_{ab}, $k_{z,b}$, d_b, and r_{bcd}. The reflectance $R_{a,...,e}^{(s,p)}$ and transmittance $T_{a,...,e}^{(s,p)}$ for a homogeneous plane wave in medium (a) incident on a layer system separating the half spaces (a) and (e) are:

$$R_{a,...,e}^{(s,p)} = \left| r_{a,...,e}^{(s,p)} \right|^2 \tag{2.28}$$

$$T_{a,...,e}^{(s,p)} = \frac{\mathrm{Re}(k_{z,e}/n_e^\rho)}{k_{z,a}/n_a^\rho} \left| t_{a,...,e}^{(s,p)} \right|^2 \tag{2.29}$$

regardless of the number of layers separating the media (a) and (e). The absorbance inside the layer system is $A = 1-R-T$.

The **total emitted power** of the oscillating electric dipole above is: [2;2, p. 3034]

$$L(z_0) = \cos^2\vartheta \, L_\perp(z_0) + \sin^2\vartheta \, L_\parallel(z_0) \tag{2.30}$$

$$\frac{L_\parallel(z_0)}{L_\infty(n_0)} = 1 + \tag{2.31}$$

$$\frac{3}{8(k_0)^3} \, \mathrm{Re}\left(\int_0^\infty \left[(k_{z,0})^2 \, r_-^{(p)} + (k_0)^2 \, r_+^{(s)} \right] (k_{z,0})^{-1} \, d(\kappa^2) \right)$$

$$\frac{L_\perp(z_0)}{L_\infty(n_0)} = 1 + \frac{3}{4(k_0)^3} \, \mathrm{Re}\left(\int_0^\infty r_+^{(p)} (k_{z,0})^{-1} \kappa^2 \, d(\kappa^2) \right) \tag{2.32}$$

where

$$\kappa^2 = (k_0)^2 - (k_{z,0})^2 \tag{2.33}$$

$$r_\pm^{(s,p)} = \{ 2 \, r_{0,1}^{(s,p)} \, r_{0,2}^{(s,p)} \exp(2i \, k_{z,0} \, d_0) \tag{2.34}$$
$$\pm r_{0,1}^{(s,p)} \exp(2i \, k_{z,0} \, (d_0-z_0))$$
$$\pm r_{0,2}^{(s,p)} \exp(2i \, k_{z,0} \, z_0) \} /$$
$$\{ 1 - r_{0,1}^{(s,p)} \, r_{0,2}^{(s,p)} \exp(2i \, k_{z,0} \, d_0) \}$$

(Emission into waveguide modes is not included, but absorption outside the layer (n_0,d_0) is. The symbols $\parallel$ and $\perp$ denote an orientation parallel or perpendicular to the interface.)

$$L_\infty(n_0) = n_0 \, L_{vac} \tag{2.35}$$

$$L_{vac} = \left| \mathbf{p}_{em} \right|^2 \omega^4 / 12\pi\hat{\varepsilon}_0 \, c^3 \tag{2.36}$$

If $n_0 = n_1$ then the following Taylor series approximates $L(z_0)/L_\infty(n_0)$ in the region $z_0 \ll \lambda/10$: [2;3, p. 197]

$$\frac{L(z_0)}{L_\infty(n_0)} = l^{(0)} + l^{(1)} (2k_1 z_0) + l^{(2)} \frac{(2k_1 z_0)^2}{2!} + .. \tag{2.37}$$

$$l^{(0)}_{\perp} = \frac{1}{n^2+1}\left\{2\frac{n^5-1}{n^2-1} - \frac{n^4}{n+1}\left(1 - \frac{3n}{n^2+1}\right)\right.$$
$$\left. - 3\frac{n^6 \ln[(\sqrt{n^2+1}-n)(\sqrt{n^2+1}+1)/n]}{(n^2+1)^{3/2}(n^2-1)}\right\} - 2 \qquad (2.38)$$

$$l^{(0)}_{\parallel} = \frac{1}{n^2+1}\left\{\frac{n^5-1}{n^2-1} + \frac{n^2}{2n+2}\left(1 - \frac{3n}{n^2+1}\right)\right.$$
$$\left. + \frac{3}{2}\frac{n^4 \ln[(\sqrt{n^2+1}-n)(\sqrt{n^2+1}+1)/n]}{(n^2+1)^{3/2}(n^2-1)}\right\} \qquad (2.39)$$

$$l^{(1)}_{\perp} = -\frac{3\pi}{16}n^2\frac{n^2-1}{n^2+1}\left(1 + \frac{4n^2}{(n^2+1)^2}\right) \qquad (2.40)$$

$$l^{(1)}_{\parallel} = \frac{1}{2}l^{(1)}_{\perp} - \frac{3\pi}{32}(n^2-1)\left(1 - \frac{4n^2}{(n^2+1)^2}\right) \qquad (2.41)$$

where $n = n_2/n_0$ and $\mathrm{Im}(n) = 0$.

Examples:

$n_0 = 1$	$n_2 = 1.46$	$l^{(0)}_{\parallel} = 1.34999$	$l^{(0)}_{\perp} = 2.20199$
		$l^{(1)}_{\parallel} = -0.4676$	$l^{(1)}_{\perp} = -0.8482$
$n_0 = 1.33$	$n_2 = 1.46$	$l^{(0)}_{\parallel} = 1.05567$	$l^{(0)}_{\perp} = 1.25029$
		$l^{(1)}_{\parallel} = -0.06624$	$l^{(1)}_{\perp} = -0.1314$
$n_0 = 1$	$n_2 = 1.88$	$l^{(0)}_{\parallel} = 1.77513$	$l^{(0)}_{\perp} = 3.19573$
		$l^{(1)}_{\parallel} = -1.2151$	$l^{(1)}_{\perp} = -1.9638$
$n_0 = 1.33$	$n_2 = 1.88$	$l^{(0)}_{\parallel} = 1.30674$	$l^{(0)}_{\perp} = 2.08249$
		$l^{(1)}_{\parallel} = -0.4027$	$l^{(1)}_{\perp} = -0.7402$
$n_0 = 1.46$	$n_2 = 1.88$	$l^{(0)}_{\parallel} = 1.19632$	$l^{(0)}_{\perp} = 1.75254$
		$l^{(1)}_{\parallel} = -0.2463$	$l^{(1)}_{\perp} = -0.4688$

The expression
$$\frac{L(z_0)}{L_\infty(n_0)} \approx 1 + (l^{(0)}-1)\exp\left(\frac{l^{(1)}(2k_1 z_0)}{l^{(0)}-1}\right) \qquad (2.42)$$
interpolates the radiated power between $z_0 = 0$ and $z_0 = \infty$. For $z_0 = 0$ it yields the correct slope, for $z_0 > 0$ it approximates $L(z_0)$ "without interference ripples" [2;4, p. 1612].

The formulas for the **radiation pattern** of a dipole in an **extremely thin layer** (n_0, d_0) (i.e. in the limit $n_0 d_0 \ll \lambda/10$, $n_0 \geq 1$) between two media with refractive indices n_1 and n_2 reduce to the formulas for the pattern of a dipole in medium 1 on

the interface $(z_0\,=\,0)$ to medium 2 but with different normalization: [2;1, p. 751]

$(P_{1,0,2})_\parallel\,=\,(n_1/n_0)(P_{1,2})_\parallel$ $(P_{1,0,2})_\perp\,=\,(n_1/n_0)^5(P_{1,2})_\perp$ (2.43-44)

$(L_{1,0,2})_\parallel\,=\,(L_{1,2})_\parallel$ $(L_{1,0,2})_\perp\,=\,(n_1/n_0)^4(L_{1,2})_\perp$ (2.45-46)

This means, that even an unphysically small layer has an influence on the radiation patterns via scaling factors which are functions of its refractive index. The scaling factors for dipoles parallel or perpendicular to the interface are not the same! In the experiments in section 4.2 the layers had thicknesses of $d_0\,\approx\,10^{-12}\,$m $(n_0 d_0/\lambda\,\approx\,10^{-5}..10^{-7})$ and in chapter 5 $d_0\,\approx\,10^{-8}\,$m $(n_0 d_0/\lambda\,\approx\,0.025)$. This imposed a difficulty on the determination of n_0, d_0 and orientation from measured radiation patterns. If the layer (n_0,d_0) containing the dipoles is extremely thin $(n_0 d_0\,\ll\,\lambda/10)$ then it is not possible to deduce n_0, d_0 and orientation independent of each others. The fits have to be done with a reasonable assumption about n_0, e.g. $n_0\,=\,n_1$, and then its possible to convert the measured orientation mathematically from $n_0\,=\,n_1$ to $n_0\,\neq\,n_1$. In the special case where the orientation is known, the refractive index n_0 may be deduced from a radiation pattern and vice versa, cf. (5.5).

2.1.2. Ensembles of Dipoles

We planned to measure radiation patterns of fluorescent molecules on interfaces and then in a second step to interpret those patterns physically. For the first part of this task a standard representation of the radiation patterns of ensembles of emitters was used (this section). In a second step (next section) we started with a theoretical distribution of molecules and calculated radiation patterns taking fixed-angle excitation into account. We had to take this route because the radiation pattern of an ensemble of incoherently emitting dipoles may be calculated from its distribution of emitters $G(z_0,\vartheta,\varphi)$, cf. section 2.2.1., but not vice versa because many different distributions may generate the same radiation pattern. I do not know whether it is possible to measure the distribution of the molecules if radiation patterns are measured as a function of variable-angle excitations.

We use two standard representations for the radiation pattern of ensembles with one or two degrees of freedom respectively to

fit measured (normalized) radiation patterns. To calculate them
we start with the radiation pattern $P^{(s,p)}(\alpha)$ of a single dipole,
cf. (2.8-20). If we multiply out the product $P^{(s,p)}(\alpha)$ with re-
spect to the summands in $Q^{(s,p)}(\alpha)$ and rename the terms properly
we get:

$$P^{(s,p)}(\alpha) = \sin^2\vartheta\cos^2\varphi \cdot P_x^{(p)}(\alpha) + \sin^2\vartheta\sin^2\varphi \cdot P_y^{(s)}(\alpha)$$
$$+ \cos^2\vartheta \cdot P_z^{(p)}(\alpha) + \sin(2\vartheta)\cos\varphi \cdot P_{xz}^{(p)}(\alpha) \qquad (2.50)$$

The radiation pattern of a single dipole is composed of the
patterns of the dipole-components parallel to the coordinate-
axes plus a "mixing term". This pattern has to be averaged over
an ensemble of incoherently emitting dipoles. We describe the
distribution of the emitting dipoles with a density- or weight-
function $G(z_0, \vartheta, \varphi)$. The last term on the right hand side in
equation (2.50) is the only one which can take on positive and
negative values, it's possible that it is averaged out. The
mathematical criterion for that is:

$$\int_0^{2\pi}\mathrm{d}\varphi\int_0^{\pi}\sin\vartheta\,\mathrm{d}\vartheta \; \sin(2\vartheta)\cos\varphi\, G(z_0, \vartheta, \varphi) = 0 \qquad (2.51)$$

(In our experiments it was possible to fulfill this condition
by selecting the excitation properly, cf. section 2.2.1. where
we calculate the effect of the excitation on an ensemble of
fluorescent molecules.) If criterion (2.51) is fulfilled, we
arrive after an average over the ensemble at the first standard
representation:

a) $P^{(s,p)}(\alpha) \propto g_x P_x^{(p)}(\alpha) + g_y P_y^{(s)}(\alpha) + g_z P_z^{(p)}(\alpha) \qquad (2.52)$

The measured radiation pattern is fitted with the weighted
sum of the patterns of dipoles parallel to the three coordinate
axes [4;10], cf. fig. 2.3. The weight-factors $g_{x,y,z}$ fulfil the
relations $0 \leq g_{x,y,z} \leq 1$ and $g_x + g_y + g_z = 1$ (2.53). If (2.51)
is not fulfilled, one "mixing term" $g_{xz} \cdot P_{xz}^{(p)}(\alpha)$ has to be in-
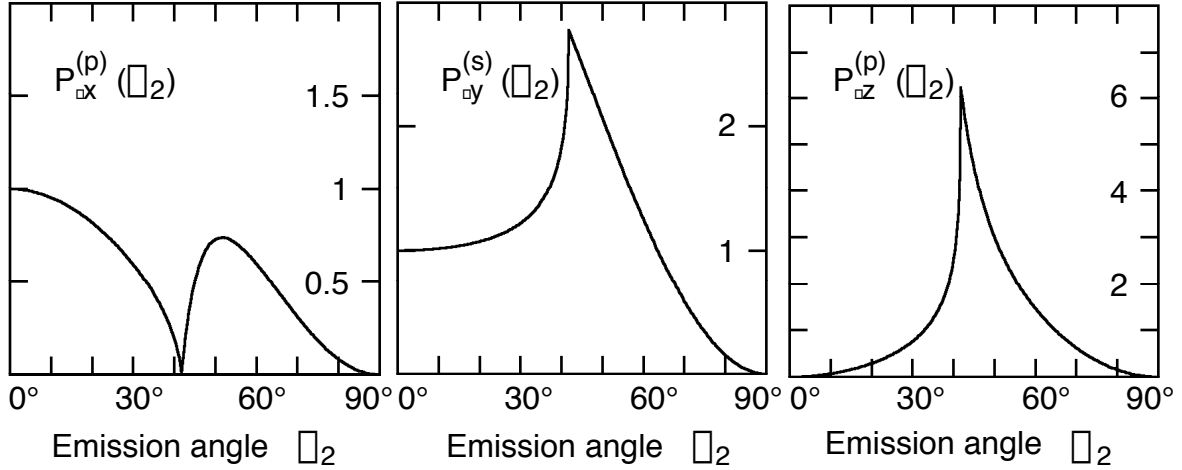troduced in the pattern.

Fig. 2.3: Radiation pattern $P_{(x,y,z)}^{(s,p)}(\alpha_2)$; parameters: $n_0" =" n_1" =" 1$, $n_2" =" 1.5$, $z_0" =" 0$; $P_x^{(s)}(\alpha_2)" =" P_y^{(p)}(\alpha_2)" =" P_z^{(s)}(\alpha_2)" =" 0$.

If the emitter-ensemble is rotationally isotropic with respect to the z-axis, then (2.51) is fulfilled and we arrive at the second standard representation:

b) $P^{(s,p)}(\alpha)" \propto" \sin^2\theta" P_\parallel^{(s,p)}(\alpha)" +" \cos^2\theta" P_\perp^{(p)}(\alpha)$ \hfill (2.54)

[2;1, p. 751] The measured radiation pattern is fitted with the weighted sum of the patterns of one dipole perpendicular to the interface ($\vartheta" =" 0°$) and a rotationally isotropic ensemble of dipoles parallel ($\vartheta" =" 90°$) to it (or alternatively an ensemble of incoherently radiating dipoles lying on a cone with half angle θ and rotationally symmetric with respect to the z-axis. This is an example of two different distributions which generate the same pattern).

$$P_\parallel^{(s,p)}(\alpha) \;=\; \frac{1}{2\pi} \int_0^{2\pi}" P^{(s,p)}(\alpha," \vartheta" =" 90°)" d\varphi \qquad (2.55)$$

$$P_\perp^{(s,p)}(\alpha) \;=" P^{(s,p)}(\alpha;" \vartheta" =" 0°) \qquad (2.56)$$

If the ensemble of emitters is not rotationally isotropic, then the angle θ is only a fit parameter for the measured pattern $P^{(p)}(\alpha)$ which remains to be interpreted.

Representation a) is related to b) because

$$P_\parallel^{(s,p)}(\alpha)" =" (P_x^{(s,p)}(\alpha)" +" P_y^{(s,p)}(\alpha))/2, \qquad (2.57)$$

$$P_\perp^{(s,p)}(\alpha)" =" P_z^{(s,p)}(\alpha) \;\text{and} \qquad (2.58)$$

$$2\cot^2\theta" =" g_z/g_x \qquad (2.59)$$

Representation a) and b) have the advantage that the measured and normalized pattern $P^{(p)}(\alpha)$ may be fitted with only one parameter (θ or g_z/g_x). If the symmetry condition (2.51) is not

fullfilled, then the fit has to be done with two parameters (g_z/g_x and g_{xz}/g_x) which complicates the task.

The z_0 dependence of the density function is treated by i) assuming a specific value for z_0 for all dipoles, e.g. $z_0 = 0$ in section 4.2, ii) averaging over the layer containing the dipoles (in chapter 5) or iii) taking a weighted mean of the dipoles with a weight e.g. proportional to the intensity ($\mathbf{E}^2(z_0)$) of the field which excites the emission process, in particular for evanescent wave excitation.

2.2. A Simple Model for Fluorescent Molecules

The object of this section is to present a classical, i.e. not quantum mechanical, model of fluorescent molecules which will be used to interpret data from measurements of ensembles of fluorescent dye molecules. The model describes radiation patterns from absorption and emission by electric dipole moments on an interface (section 2.2.1.), some depolarization effects (section 2.2.2.), and the quantum efficiency and its dependence on the optical environment (section 2.2.3.).

2.2.1. Absorption and Emission Dipole Moments

In the preceding sections we only dealt with emitters. In this section, we shall take the effect of the exciting field and the distribution of the fluorescent molecules into account. The weight-function $G(z_0,\vartheta,\varphi)$ of the emitters is calculated from the distribution (z_0) and orientation (ϑ,φ) of the molecules and from the exciting field. The probability that a molecule gets excited depends on the angle between its absorption dipole moment and the direction of the exciting field vector. We calculate in four examples the radiation patterns of four ensembles of molecules.

Each molecule is assumed to have an absorption ($\mathbf{p}_{abs}$) and an emission ($\mathbf{p}_{em}$) dipole moment fixed relative to its atomic structure with an angle ψ between them. All molecules are assumed to be identical. The probability to absorb energy from an electromagnetic wave (make an upward dipole transition) is proportional to the temporal average of $|\mathbf{p}_{abs}\mathbf{E}|^2$, where $\mathbf{E}$ denotes the electric field vector at the molecule's location. We suppress the

harmonic time dependence $\exp(-i\omega t)$ of **E** throughout this text.
The probability per unit time to make a downward transition is
A_{tot} (tot = abbrev. for total, confer section 2.2.3. for de-
tails) and to emit a photon A_r (r = abbrev. for radiative, A_r is
also called spontaneous emission rate). $\tau_F\ =\ 1/A_{tot}$ (F = abbrev.
for fluorescence) is the experimentally observed lifetime of
the upper state. The angular probability distribution to detect
the emitted photon is proportional to the radiation pattern P
of a classical electric dipole $\mathbf{p}_{em}$ in the same optical environ-
ment, and A_r is proportional to its radiative power L.

We characterize the orientations of the absorption-dipoles of an
ensemble by a density- or weight-function $G_{abs}(z_0,\vartheta,\varphi)\ \geq\ 0$. If we
know the exciting field $\mathbf{E}\ =\ (E_x,E_y,E_z)$ at the molecules' loca-
tion, and if we assume the quantum yield to be 100 % and $\mathbf{p}_{abs}\ \parallel$
$\mathbf{p}_{em}$, then we can calculate the weight-function $G(z_0,\vartheta,\varphi)$ of the
emitting dipoles $\mathbf{p}_{em}$:

$$G(z_0,\vartheta,\varphi)\ \propto\ G_{abs}(z_0,\vartheta,\varphi)\cdot|\mathbf{p}_{abs}(z_0,\vartheta,\varphi)\cdot\mathbf{E}|^2 \qquad (2.60)$$

The effect that the distribution of radiating dipoles depends
on the excitation is important for the determination of orien-
tations and transition rates. From the weight-function $G(z_0,\vartheta,\varphi)$
we can calculate the radiation pattern, i.e. we can calculate
the patterns $g'_x\cdot P_x^{(p)}(\alpha)$, $g'_y\cdot P_y^{(p)}(\alpha)$ and $g'_z\cdot P_z^{(p)}(\alpha)$ of the
dipol components parallel to the three coordinate axes thus im-
itating the standard representation (2.52). In the special case
$\mathbf{p}_{abs}\ \parallel\ \mathbf{p}_{em}$, i.e. $\psi\ =\ 0°$, the sum g'_j of the projections of all
the emission dipole moments $\mathbf{p}_{em}^2$ in an ensemble on the coordi-
nate axis $\hat{\mathbf{e}}_j$ (unit vectors, $j\ =\ x,y,z$) yields:

$$g'_j\ \propto\ \int dz_0\ \int_0^{2\pi}d\varphi\ \int_0^{\pi}\sin\vartheta\ d\vartheta\ \ (\hat{\mathbf{e}}_j\cdot\mathbf{p}_{em})^2\ G_{abs}\ |\mathbf{p}_{abs}\cdot\mathbf{E}|^2 \qquad (2.61)$$

We use $(\hat{\mathbf{e}}_j\cdot\mathbf{p}_{em})$ squared because the total radiated power L is
proportional to $|\mathbf{p}_{em}|^2$, cf. (2.36). If $\mathbf{p}_{em}$ and $\mathbf{p}_{abs}$ are not
parallel, then an additional step accounting for that has to be
applied in the calculation, cf. example 4 in this section. We
normalize the weight-factors $g'_{x,y,z}$ such that $0\ \leq\ g'_{x,y,z}\ \leq\ 1$
and $g'_x\ +\ g'_y\ +\ g'_z\ =\ 1$ (2.62). If the quantum efficiency is
100 %, then the weights $g'_{x,y,z}$ equal the weights $g_{x,y,z}$ in the
standard representation of a radiation pattern, see remark at
the end of this section.

It's assumed that we may calculate the distribution of emitters $G(z_0,\vartheta,\varphi)$ as in (2.60). Formula (2.51) is the criterion that the radiation pattern has no "mixing term" $g_{xz} \cdot P_{xz}$. The criterion is fulfilled if we excite fluorescence with a field parallel to one of the coordinate axes (cf. fig. 2.4) and restrict $G_{abs}(z_0,\vartheta,\varphi)$ on distributions which fulfill $G_{abs}(z_0,\vartheta,\varphi) = G_{abs}(z_0,\vartheta,\varphi+\pi)$ (2.63) or $G_{abs}(z_0,\vartheta,\varphi) = G_{abs}(z_0,\pi-\vartheta,\varphi)$ (2.64). Both are sufficient but not necessary. Both restrictions on $G_{abs}(z_0,\vartheta,\varphi)$ were almost certainly fulfilled in the experimental situations we encountered. E.g. condition (2.63) is fulfilled if the distribution of absorbers is rotationally isotropic with respect to the z-axis.
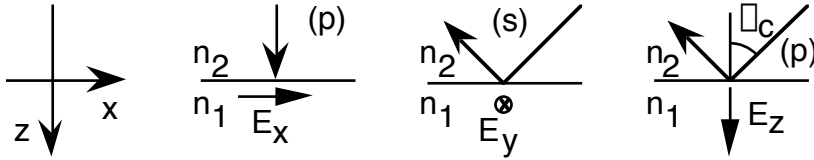

Fig. 2.4: Angles of incidence $\alpha_{e,2}$ and polarizations (s or p) of exciting radiation in medium 2 which are needed to produce in medium 1 electric field vectors parallel to the coordinate axes: Those are $\alpha_{e,2} = 0°$ and p-pol., $\alpha_{e,2}$ arbitrary and s-pol., and $\alpha_{e,2} = \alpha_c$ and p-pol.; n_1,n_2: refractive indices, $n_1 < n_2$.

Examples:

We assume ensembles of molecules distributed in a plane ($z_0 = 0$). Excitation is with a s-polarized plane or evanescent wave $\mathbf{E} = (E_x,E_y,E_z) = (0,E_y(z_0),0)$. The absorption dipole moments of the molecules shall be parallel to the emission dipole moments ($\mathbf{p}_{abs} \parallel \mathbf{p}_{em}$). The weights $g'_{x,y,z}$ of the emission dipole moments of the ensembles are assumed to be identical to the weights $g_{x,y,z}$ of their radiation patterns. By inserting in equation (2.61) we get:

$$g'_j \propto \int dz_0 \int_0^{2\pi} d\varphi \int_0^{\pi} \sin\vartheta \, d\vartheta \, (\hat{\mathbf{e}}_j \cdot \mathbf{p}_{em})^2 \, G_{abs} \, |\mathbf{p}_{abs} \cdot \mathbf{E}|^2 \qquad (2.65)$$

$$\propto \int_0^{2\pi} d\varphi \int_0^{\pi} \sin\vartheta \, d\vartheta \, (\hat{\mathbf{e}}_j \cdot \mathbf{p}_{em})^2 \, G_{abs}(\vartheta,\varphi) \, |\mathbf{p}_{abs} \cdot (0,E_y,0)|^2 \qquad (2.66)$$

$$\propto \int_0^{2\pi} d\varphi \int_0^{\pi} \sin\vartheta \, d\vartheta \, (\hat{\mathbf{e}}_j \cdot \mathbf{p}_{em})^2 \, G_{abs}(\vartheta,\varphi) \, |\sin\vartheta \, \sin\varphi|^2 \qquad (2.67)$$

Explicitly:

$$g'_x = b\int_0^{2\pi}d\varphi\int_0^{\pi}\sin\vartheta\,d\vartheta\,(\sin\vartheta\cos\varphi)^2\,G_{abs}(\vartheta,\varphi)\,|\sin\vartheta\sin\varphi|^2 \qquad (2.68)$$

$$g'_y = b\int_0^{2\pi}d\varphi\int_0^{\pi}\sin\vartheta\,d\vartheta\,(\sin\vartheta\sin\varphi)^2\,G_{abs}(\vartheta,\varphi)\,|\sin\vartheta\sin\varphi|^2 \qquad (2.69)$$

$$g'_z = b\int_0^{2\pi}d\varphi\int_0^{\pi}\sin\vartheta\,d\vartheta\,(\cos\vartheta)^2\,G_{abs}(\vartheta,\varphi)\,|\sin\vartheta\sin\varphi|^2 \qquad (2.70)$$

and for sake of completeness, cf. (2.50-52):

$$g'_{xz} = b\int_0^{2\pi}d\varphi\int_0^{\pi}\sin\vartheta\,d\vartheta\,(\sin2\vartheta\cos\varphi)\,G_{abs}(\vartheta,\varphi)\,|\sin\vartheta\sin\varphi|^2 \qquad (2.71)$$

where b is a constant such that $g'_x + g'_y + g'_z = 1$.

We now use the expressions developed above to calculate the effect of some especially important distributions $G_{abs}(z_0,\vartheta,\varphi)$ on the weight-factors in the standard representation (2.52).

1) The absorption dipole moments are assumed to be **isotropically distributed,** i.e. $G_{abs}(\vartheta,\varphi) = $ const. Inserting in (2.68-70) yields $g'_x = 1/5$, $g'_y = 3/5$, $g'_z = 1/5$ (2.72). A fit to a (sp)-radiation pattern of this ensemble gives $g_z/g_x = 1$ or $\theta = 54.74°$ (2.73). "(sp)"-radiation pattern means s-pol. excitation and p-pol. emission.

2) The absorption dipole moments are assumed to be **preferentially parallel** to the interface, distributed rotationally isotropic with respect to the z-axis, and scattered around $\vartheta = \pi/2$. We assume a Gaussian distribution in ϑ:

$$G_{abs}(\vartheta,\varphi) \propto \frac{1}{\sqrt{2\pi\sigma^2}}\,\exp\left(\frac{(\vartheta-\pi/2)^2}{2\sigma^2}\right) \quad \text{where } 0 \le \sigma \ll \pi/2 \qquad (2.74)$$

(σ in radians). From that follows by inserting in (2.68-70):

$$g'_x = b\int_0^{2\pi}\sin^2\varphi\,\cos^2\varphi\,d\varphi\int_0^{\pi}d\vartheta\,\frac{\sin^5\vartheta}{\sqrt{2\pi\sigma^2}}\,\exp\left(\frac{(\vartheta-\pi/2)^2}{2\sigma^2}\right) \qquad (2.75)$$

$$\approx b\,\pi/4\int_{-\infty}^{+\infty}d\vartheta\,\frac{\cos^5\vartheta}{\sqrt{2\pi\sigma^2}}\,\exp\left(\frac{\vartheta^2}{2\sigma^2}\right) \qquad (2.76)$$

$$= b\,\pi/4\,\frac{1 + 5\,\exp(8\sigma^2) + 10\,\exp(12\sigma^2)}{16\,\exp((25/2)\sigma^2)} \qquad (2.77)$$

$$g'_y = 3\,g'_x \qquad (2.78)$$

$$g'_z" = b\int_0^{2\pi}" \sin^2\varphi" \, d\varphi" \int_0^{\pi}" d\vartheta"" \frac{\sin^3\vartheta" \cos^2\vartheta"}{\sqrt{2\pi\sigma^2}}! \exp\left(\frac{(\vartheta-\pi/2)^2}{2\sigma^2}\right) \qquad (2.79)$$

$$" \approx b"\pi \int_{-\infty}^{+\infty}" d\vartheta" \frac{\cos^3\vartheta" \sin^2\vartheta}{\sqrt{2\pi\sigma^2}}! \exp\left(\frac{\vartheta^2}{2\sigma^2}\right) \qquad (2.80)$$

$$= b \, \pi"" \frac{2" \exp(12\sigma^2)" -" \exp(8\sigma^2)" -" 1}{16" \exp((25/2)"\sigma^2)} \qquad (2.81)$$

A fit to a (sp)-radiation pattern of this ensemble gives values as listed in table 2.1 and shown in fig. 2.5.

Fig. 2.5: Calculated weights g_z/g_x and θ vs. the width σ of a Gaussian distribution of emitters around $\vartheta" = 90°$ (parallel to the interface)
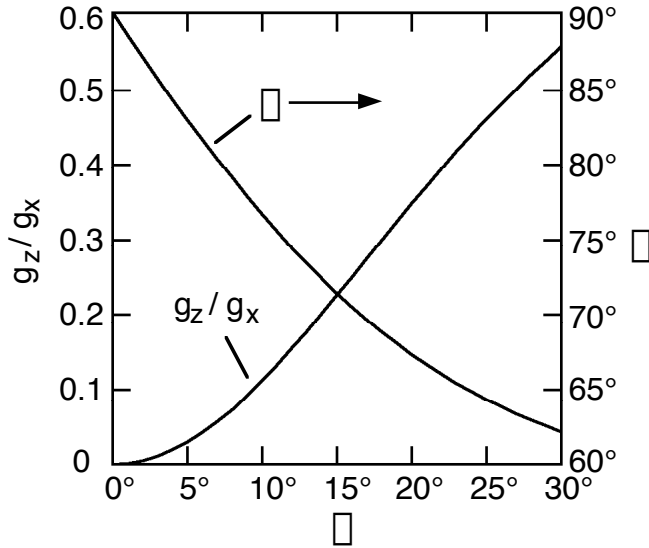
σ [°]	g_z/g_x	θ [°]
0	0	90
2.5	.007572	86.48
5	.029776	83.04
7.5	.065129	79.77
10	.111346	76.72
15	.224836	71.46
20	.347004	67.39
25	.460334	64.37
30	.556491	62.19

T a b l e   2 . 1 : Calculated weights resulting from   a Gaussian   distribution of   dipoles   near $\vartheta" =" 90°$.

3) The absorption dipole moments are assumed to lie on a cone with half angle θ_0 and symmetrical to the z-axis, i.e. $G_{abs}(\vartheta,\varphi) \propto \delta(\vartheta-\theta_0)$ (2.82) where $\delta(*)$ is the Dirac delta-distribution. We selected this weight-function because of its relationship to the standard representation (2.54). The result after inserting in (2.68-70) is $g'_x" = (1/4)\cdot\sin^2\theta_0$, $g'_y" = (3/4)\cdot\sin^2\theta_0$, $g'_z" = \cos^2\theta_0$ (2.83). A fit to the (sp)-radiation pattern of this ensemble gives $g_z/g_x" = 2" \cot^2\theta" = 4" \cot^2\theta_0$ (2.84). In this example an "isotropic ensemble" of absorption dipole moments $\{\cos^2\theta_0" =$

$1/3$, $\sin^2\theta_0 = 2/3 \Rightarrow \theta_0 = 54.74°$ (2.85)} yields a fit parameter $\theta = 45°$ (2.86).

Note that for all three examples $g_x/g_y = 1/3$ (2.87), which is a consequence of our choice that $\mathbf{p}_{abs} \parallel \mathbf{p}_{em}$. This need not be the case for real molecules!

4) We shall now drop the assumption that absorption- and emission dipole moments are parallel to each other, but instead it is assumed that the absorption- and emission dipole moments are isotropically distributed in the plane $z_0 = 0$ with an angle ψ between $\mathbf{p}_{abs}$ and $\mathbf{p}_{em}$, i.e. $G_{abs}(\vartheta,\varphi) \propto \delta(\vartheta-\pi/2)$ (2.88). Both orientations $(+|\psi|$ and $-|\psi|)$ shall be isotropically distributed. By inserting in equation (2.61) we get:

$$g'_x = b \int_0^{2\pi} d\varphi \; \cos^2(\varphi \pm \psi)^2 \sin^2\varphi = (2-\cos2\psi)b\pi/2 \qquad (2.89)$$

$$g'_y = b \int_0^{2\pi} d\varphi \; \sin^2(\varphi \pm \psi)^2 \sin^2\varphi = (2+\cos2\psi)b\pi/2 \qquad (2.90)$$

and $g'_z = 0$, where b is a normalizing factor. We get therefore the ratio

$$\frac{g'_x}{g'_y} = \frac{g_x}{g_y} = \frac{2-\cos2\psi}{2+\cos2\psi} = \frac{3-2\cos^2\psi}{1+2\cos^2\psi} = \frac{3-2\cos^2\psi}{3-2\sin^2\psi} \qquad (2.91)$$

which can in principle be used to determine the angle ψ.

Remark concerning the connection between $g'_{x,y,z}$ and $g_{x,y,z}$: A question still open is the connection between the weights g_x, g_y, g_z deduced from an experimental radiation pattern and the weight-factors g'_x, g'_y, g'_z calculated from a weight-function $G(z_0,\vartheta,\varphi)$ of the radiating dipoles, because in the representation $P^{(s,p)}(\alpha) \propto g_x P_x^{(p)}(\alpha) + g_y P_y^{(s)}(\alpha) + g_z P_z^{(p)}(\alpha)$ the patterns P_x and P_z do not have exactly the same normalization ($L_\parallel/L_\infty$ vs. $L_\perp/L_\infty$, cf. formula 2.22). The component perpendicular to the interface (g'_z) radiates with another power than the components parallel to the interface ($g'_{x,y}$). But if the quantum efficiency η is independent of the radiative power, cf. section 2.2.3. for details, then the normalization of the radiation patterns is such that this difference in radiative power is compensated, i.e. if $\eta = 100\%$ then $g'_{x,y,z} = g_{x,y,z}$. If the quantum yield depends on the radiative power then the equation $g'_{x,y,z} = g_{x,y,z}$ is only approximative ($g'_z < g_z$ if $L_\parallel < L_\perp$). Such an effect on

the shape of the radiation pattern could in principle be used to determine the quantum yield.

2.2.2. Radiative Lifetime and Depolarization

Until now we have regarded the dipoles as fixed in space, but real molecules in a solution may rotate, which has an influence on the angular distribution of emitters. Care has to be taken to exclude those rotational diffusion effects from measurements of the fluorescence lifetime τ_F of dyes in solution. The independent dye molecules are assumed to form an ensemble with isotropically orientated absorption and emission dipole moments $\mathbf{p}_{abs}$ and $\mathbf{p}_{em}$ with an angle ψ between the moments. An ensemble of molecules excited with a short pulse of linearly polarized light emits immediately afterwards partially polarized light, but then the molecules may undergo Brownian rotational diffusion in the solution and the degree of polarization of the emitted fluorescence decreases further. If the fluorescence lifetime τ_F is not much shorter than the so called rotational diffusion time τ_R, then Brownian rotational diffusion destroys this initial polarization of the ensemble. Perrin [4;1] described this effect for cw excitation and measurement:

$$\left(\frac{1}{\wp} - \frac{1}{3} \right) = \left(\frac{1}{\wp_0} - \frac{1}{3} \right) \left(1 + \frac{\tau_F}{\tau_R} \right) \quad (2.92); \qquad \wp = \frac{I_\parallel - I_\perp}{I_\parallel + I_\perp}$$

$$(2.93)$$

where $\wp$ is the degree of polarization of the fluorescence and $\wp_0$ is the limiting degree of polarization ($\tau_R \gg \tau_F$). $I_\parallel$ and $I_\perp$ are the irradiances of light emitted in a direction perpendicular to the exciting field vector and polarized parallel ($\parallel$) or perpendicular ($\perp$) to it. An order of magnitude estimate of the rotational diffusion time is $\tau_R \approx \eta v/k_B T$ (2.94) where T = temperature, k_B = Boltzmann constant, η = viscosity of solvent, and v = "effective" volume of a dye molecule [4;1, 3;2-3]. If, for example, $T = 300$ K, $v = (1 \text{ nm})^3$, $\eta = 10^{-3}$ Pa·s, and $k_B = 1.381 \cdot 10^{-23}$ J/K, then $\tau_R = 0.24$ ns.

If rotational diffusion is absent ($\tau_F \ll \tau_R$), then $\wp = \wp_0$ and

$$\wp_0 = \frac{3 \cos^2\psi - 1}{\cos^2\psi + 3} \qquad (2.95)$$

If $\tau_F \gg \tau_R$ then $\wp = 0$ (2.96) [4;1].

If we assume an exponential transition from $\wp\,"="\,\wp_0$ to $\wp\,"="\,0$ after a delta-pulsed excitation [3;2], then we can construct the following model for the fluorescence response:

$$I_\parallel(t)\ \ =\ I_0\ \{1/3\ +\ a_\parallel\ \exp(-t/\tau_R)\}\ \exp(-t/\tau_F) \qquad (2.97)$$

$$I_\perp(t)\ \ =\ I_0\ \{1/3\ +\ a_\perp\ \exp(-t/\tau_R)\}\ \exp(-t/\tau_F), \qquad (2.98)$$

where I_0 is a constant and the ratio $a_\parallel/a_\perp\,"="\,-2$ (2.99) holds independent of ψ. It follows that $I_\parallel(t)\,"+"\,2I_\perp(t)\ =\ I_0\,"\,\exp(-t/\tau_F)$ (2.100) is free from rotational effects. If $\psi\,"="\,0°$, i.e. $\mathbf{p}_{abs}\,"\,\|$ $\mathbf{p}_{em}$, then we get from (2.93,95) that $a_\parallel\,"="\,4/5$ and $a_\perp\,"="\,-2/5$ (2.101).

Formula (2.95) for the depolarization if rotational diffusion is absent ($\tau_R\,"\,»\,"\,\tau_F$) has also a two dimensional version (cf. example $"\,4$ in section 2.2.1.): If the absorption and emission dipole moments are distributed isotropically in a plane ($z_0\,"="\,0$, $g_z\,"="\,0$) and excitation is s-pol., then we get from (2.91):

$$\tan^2\psi\,"="\,\frac{3(g_x/g_y)\,"\,-1}{3"\,-"\,(g_x/g_y)} \qquad (2.102)$$

where g_x, g_y and g_z are the weights of the radiation pattern of the ensemble defined in section 2.1.2.

2.2.3. Quantum Efficiency

«The spontaneous emission rate A_r times the photon energy $E\,"=\,\hbar\omega$ is equal to the expectation value L of the energy emitted in unit time per excited system: $\hbar\omega\cdot A_r\,"="\,L$. In other words, L is the total power radiated by a transition dipole. According to the correspondence principle L will be given by the expression for the total power radiated by a classical dipole in which the classical dipole moment has to be replaced by the transititon dipole moment.» [2;2, p. 3031], symbols changed by the autor. We now want to use this relation to determine in theory the quantum efficiency. The ratio $\eta\,"="\,A_r/A_{tot}$ (2.105) of the numbers of radiative to all downward transitions of an excited molecule is called quantum efficiency, the probability that a molecule which has absorbed an excitation photon emits a fluorescence photon is called quantum yield [4;12, p. 4814]. We will not distinguish between this two quantities in this text. The total transition rate A_{tot} comprises radiative (A_r) and non-radiative (A_{nr}) transition rates, the non-radiative transition rate A_{nr} summarizes thermal and all other non-radiative relaxations, i.e. $A_{tot}\,"="\,A_r+A_{nr}$ (2.106). The spontaneous emission-

rate A_r is proportional to the total emitted power of a classical electric dipole in the same optical environment: $A_r \propto L$ (2.107). The ratio of the spontaneous emission rates of a molecule in two different optical environments is equal to the ratio of the total radiated powers of a classical electric dipole in the same environments $A_{r,1}/A_{r,2} = L_1/L_2$ (2.108), provided that the size of the dipole moment and the non-radiative transition rate A_{nr} do not change. We use ratios of spontaneous emission rates and radiative powers for that the absolute sizes of the dipole moments do not matter. Because $A_{tot} = A_r + A_{nr}$ and $A_r \propto L$, the quantum yield $\eta = A_r/A_{tot} = A_r/(A_r + A_{nr})$ (2.109) depends on the optical environment. We assume that the strength of the emission diople moments do not depend on the optical environment. The total transition rate is the reciprocal of the fluorescence lifetime measured in an experiment: $A_{tot} = 1/\tau_F$ (2.110).

The conventional way to determine the quantum yield of a dye is to measure the number of photons absorbed in a sample at the excitation wavelength and to compare this to the number of photons reemitted into the solid angle 4π at the fluorescence wavelength [4;2], see table 4.6 for examples. The difficulties are to measure low absorbances accurately and to detect all the photons emitted into the solid angle 4π.

An alternative way is to construct an experimental situation where A_{nr} (depends on the chemical environment on an atomic scale) remains constant and A_r (depends on the optical environment on a wavelength scale) is variable [4;12, p. 4817]. By measuring the fluorescence lifetimes τ_1, τ_2 in two different optical environments and calculating the corresponding radiative powers L_1, L_2 (which ought to be different), the quantum yields η_1 and η_2 can in principle be determined:

$$\frac{1}{\eta_1} - 1 = \frac{L_2}{L_1}\left(\frac{1}{\eta_2} - 1\right) , \qquad\qquad (2.111)$$

$$\eta_1 = \frac{1 - \tau_1/\tau_2}{1 - L_2/L_1} \quad (\eta_2 \text{ analogous}) . \qquad\qquad (2.112)$$

The optical environment can be varied by e.g. changing d_0 and/or n_1 (cf. fig. 2.1 and fig.4.11; "optical contact experiment").

Another (new) way to determine η is to measure its effect on the emitted intensity while the optical environment is changed. The intensity I_F observed in an experiment is

$$I_F \propto E^2(z_0,..) \, \eta(z_0,..) \, P(z_0,..) \, \frac{L_\infty(n_0)}{L(z_0,..)} \qquad (2.113)$$

where $E^2(z_0,..)$ is the time averaged squared exciting electric field at the molecule's location, η is its quantum yield and the last factors are the radiation pattern normalized as in (2.23). P is proportional to the emitted power, P/L is proportional to the emitted irradiance of an ensemble. By measuring two intensities I_1, I_2 in two different optical environments and calculating the corresponding E^2, P, and L, one obtains in principle the quantum yield:

$$\eta_1 = \frac{1 - \dfrac{I_1 \, E_2^2 \, P_2}{I_2 \, E_1^2 \, P_1}}{1 - \dfrac{L_2}{L_1}} \qquad (\eta_2 \text{ analogous}) \, . \qquad (2.114)$$

Equations (2.112, 114) for η have the structure $\eta_1 = \dfrac{1-\gamma}{1-L_2/L_1}$ (2.115) where γ is τ_1/τ_2 or $I_1 \, E_2^2 \, P_2 / I_2 \, E_1^2 \, P_1$, so we can do a combined error analysis:

$$\Delta\eta \approx \left| \frac{1}{1 - L_2/L_1} \right| \, \Delta\gamma, \qquad (2.116)$$

where we assume L_2/L_1 to be exact. In our experiments, the first factor in (2.116) was about five, cf. sections 2.1.1. and 4.2. To achieve an accuracy of 5 % in η, $\gamma = \tau_1/\tau_2$ or $I_1 \, E_2^2 \, P_2 / I_2 \, E_1^2 \, P_1$ has to be determined to $\pm$ 1 %! The most critical part in those last two procedures is to determine the optical environment accurately, i.e. to determine n_0, n_1, n_2, z_0, d_0, and ϑ for the calculation of $E^2(z_0,..)$, $L(z_0,..)$ and $P(z_0,..)$.

2.3. Rayleigh Scattering

The object of this section is to present a process different from fluorescence to which the theory of dipole radiation near interfaces is applicable: Dipole- or Rayleigh-scattering by dielectric particles [6;1-2]. A small particle in an electric field $\mathbf{E}_0$ gets polarized and a dipole moment $\mathbf{p}_0 = \alpha \, \mathbf{E}_0$ is induced, where α is the polarizability of the particle. If the electric field oscillates, so does the induced dipole moment and it emits (scatters) radiation. Formulas are given below for

the case of dielectric spherical particles embedded in a homogeneous dielectric matrix [1;2, p.174, 485]. If such a dipole-scatterer is close to an interface, then its radiation should be subject to interface effects [2;4, p. 1613]. A rigorous solution to the mathematical problem of scattering by a sphere near or on an interface was given by Bobbert and Vlieger [6;2].

A dielectric sphere (refractive index n_s, radius a) in an infinite dielectric matrix with refractive index n_0 reacts to an external homogeneous static electric field $\mathbf{E}_0$. The resultant field is homogeneous inside the sphere and outside that of a dipole $\mathbf{p}_0$ (plus the field $\mathbf{E}_0$). If the field $\mathbf{E}_0$ is not static but oscillating with angular frequency $\omega = 2\pi c/\lambda$, then the statement above is still valid if $2a\cdot(2\pi/\lambda)\cdot(n_s/n_0 - 1) \ll 1$ (2.120, the Rayleigh-Gans criterion) is fulfilled, i.e. if the diameter of the sphere is much smaller than the wavelength (and electrostatics is still applicable). The induced electric dipole $\mathbf{p}_0$ is located at the center of the sphere and parallel to $\mathbf{E}_0$. Its size in SI units is:

$$\mathbf{p}_0 = 4\pi\hat{\varepsilon}_0 \ a^3 \, n_0^2 \ \left(\frac{n_s^2 - n_0^2}{n_s^2 + 2n_0^2} \right) \ \mathbf{E}_0 \qquad (2.121)$$

The homogeneous field $\mathbf{E}_s$ inside the sphere is:

$$\mathbf{E}_s = \left(\frac{3 \, n_0^2}{2n_0^2 + n_s^2} \right) \mathbf{E}_0 \qquad (2.122)$$

(we used $\varepsilon_i = n_i^2$ (2.123) at optical frequencies, ε_i = dielectric constant). The dipole oscillates in phase with the applied field and radiates. If the field $\mathbf{E}_0$ is a homogeneous, plane, linear polarized wave (irradiance I_0), then the scattered irradiance I_{scat} and total power L_{scat} radiated by the sphere are:

$$I_{scat}(\gamma,r) = (2\pi)^4 \left| \frac{n_s^2 - n_0^2}{n_s^2 + 2n_0^2} \right|^2 \frac{a^6}{\lambda^4} \frac{\sin^2\gamma}{r^2} \ I_0 \qquad (2.124)$$

$$L_{scat} = \sigma \ I_0 \ , \qquad \sigma = \frac{4}{3} \ (2\pi)^5 \left| \frac{n_s^2 - n_0^2}{n_s^2 + 2n_0^2} \right|^2 \frac{a^6}{\lambda^4} \qquad (2.125)$$

where σ is a scattering cross section, γ is the angle between $\mathbf{E}_0$ and the direction of observation, and r is the distance to an observer. If the spheres are homogeneously dispersed in a solvent with (small) concentration c_{sol} then they have an extinction $I(d) = I_0 \exp(-c_{sol} \, \sigma \, d)$ (2.126) where d is the distance light travels in the dispersion.

Example:

The scattering cross section σ for a latex particle in ethanol is $\sigma = 2.8\cdot10^{-16}\,m^2$ (parameters: $n_0 = 1.36$, $n_s = 1.6$, $a = 70\,nm$, $\lambda = 514.5\,nm$, cf. chapter 6). For comparison with the fluorescence experiments: Garoff et al. [4;9] report an absorption cross section of $1.8\cdot10^{-20}\,m^2$ for rhodamine 6G in solution and $2.1\cdot10^{-20}\,m^2$ for rhodamine B at their respective absorption maxima.

2.4. Summary

Regarding the radiation patterns, the theory fitted very well to the experiments, i.e. for every measured pattern we found a set of parameters such that the calculated pattern coincided almost completely with it. One problem was that the radiation pattern is not a bijective function of the distribution of emitters, i.e. the pattern may be calculated from the distribution but not vice versa. We had to assume a suitable model-distribution and find values for its free parameters. Another problem was the exact determination of the optical constants of the film containing the dipoles from a measured pattern. In the limit of extremely thin layers a determination of the optical constants of the film is impossible and in our experiments we were always near that limit. This implied that an orientation could be fitted from the patterns only with suitable assumptions about the refractive index of the layer.

Regarding the total radiated power, the predictions of the theory were qualitatively observed, but the extreme sensitivity on the optical environment prohibited any quantitative analysis. E.g. for a dipole in front of an interface, the power changed noticeably on a $\lambda/100$ scale!

3. METHODS AND INSTRUMENTATION

The object of this chapter is to give a short description of a.) the measuring apparatus and b.) of the methods used to analyze the data (correcting and fitting procedures). A full description of the measuring apparatus was given by Ch. Fattinger in [3;1]. In the next section we give a summary of the experimental setup. The remaining sections show how we measured fluorescence intensities, spectra, radiation patterns, and fluorescence lifetimes. My own contribution was the software to analyze time and angle resolved measurements (deconvoluting and correcting algorithms).

3.1. Short Description of the Measuring Apparatus

We used an air-cooled Ar^+ laser (ILT) tunable to λ_e = 514.5 or 488 nm as a light source for cw measurements and a Spectra Physics Mod. 3000 frequency doubled Nd:YAG laser (λ_e = 532 nm, pulse length < 85 ps) as a light source for time resolved measurements. Their light was guided by several mirrors to a turntable with the sample, cf. fig. 3.1 and 3.2.
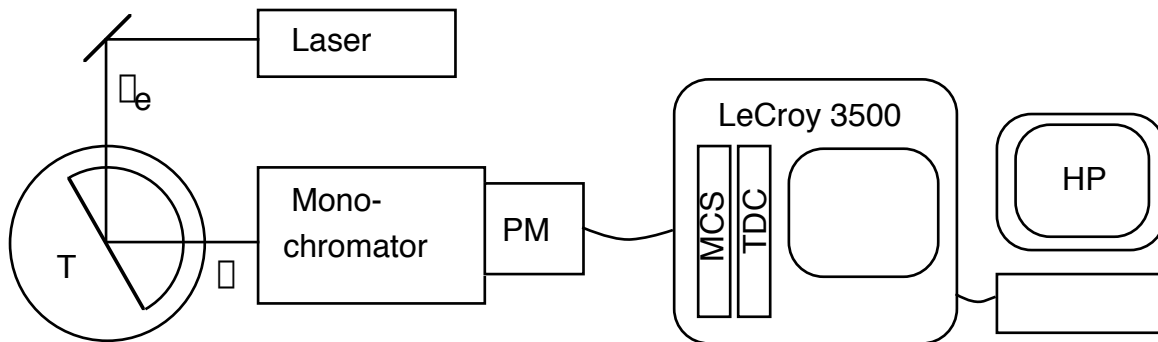

Fig. 3.1: Schematic drawing of experimental setup: Laser with wavelength λ_e, turntable T with hemicylindrical prism, emission at wavelength λ, monochromator, photomultiplier PM, multichannel analyzer LeCroy 3500 with multichannel scaling module MCS and time to digital converter TDC, desktop computer HP 217.

Before illuminating the sample the exciting light (irradiance ≈ 1 mW) passed through a polarizer to get a pure s- or p-polarization state. The dyes were in a glass or PMMA cuvette for the measurements in section sections 4.1., on a microscope slide or the plane face of a hemicylindrical glass prism for the measurements in section sections 4.2., or in a thin film cuvette attached to a hemicylindrical prism for the measure-

ments in chapter 5. The hemicylindrical glass prisms (radius = height = 2.5 cm) had polished microscope slides of the same glass type optically contacted to the plane face, cf. fig. 3.2; this simplified the maintainance of the optical quality of the plane face of the prism.

The emitted light passed through a second polarizer, called analyzer, which polarized it to s or p. A combination of spherical and cylindrical lenses collimated the light on the entrance slit of a double prism monochromator (Carl Leiss, Berlin-Steglitz). The light was detected by a photomultplier (PRA 1551) operating in photon-counting mode. The counts were displayed on a LeCroy 3500 multichannel analyzer with a built in multichannel scalar (MCS) module for quasi cw measurements and a time to digital converter (TDC) module for time resolved measurements. Then we
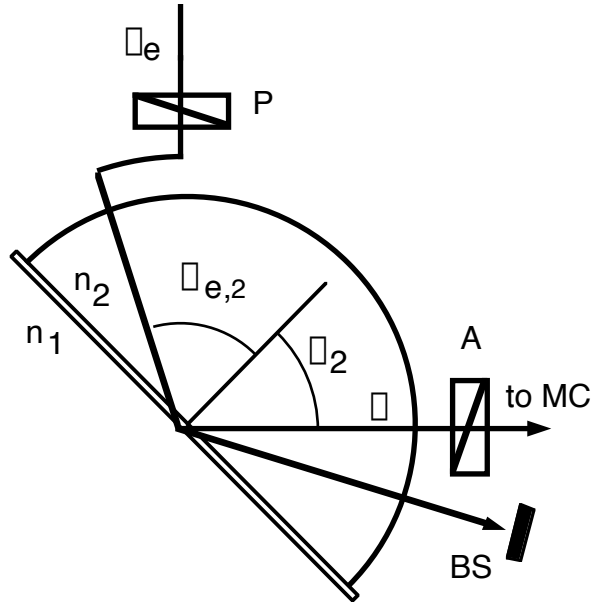

Fig.3.2: Hemicylindrical prism on turntable. λ_e: excitation wavelength, P: polarizer, $\alpha_{e,2}$: excitation angle, $n_{1,2}$: refractive indices, α_2: emission angle, λ: emission wavelength, A: analyzer, BS: beam stopper, MC: monochromator

transferred the histogram files to a HP 217 personal computer to correct and analyze them.

3.2. Measuring Intensities

Fluorescence was excited with a cw argon-laser. The laser had an intensity noise < 1% and irradiated the dye-sample with approximately 1 mW. The dyes sometimes bleached out because of light induced chemical reactions or oxidation, but the degradation-times depended on the paricular dye used and were between days and minutes, cf. section 4.2. The weakly luminescent substrate (or dirt on the substrate) supporting the dye-sample contributed a background signal which had to be measured separately and subtracted afterwards. From the samples point of

view the entrance pupil of the light collecting lens sytem sub-
tended a solid angle of 0.0079"sr (0.0625"% of the full solid
angle 4π). The monochromator had a transmission of 10^{-5} for
light outside the transmission band and 10% on the average in-
side the transmission band. The transmission depended on polar-
ization and wavelength. The photomultiplier (PM) was Peltier-
cooled to -"20°"C to ensure a dark count rate below five counts
per second. The detection quantum efficiency of the PM was ca.
10% in the visible and droped to zero above 800"nm. The LeCroy
3521 MCS module had dwelltimes between 1"μs and 4296"s and an
interchannel deadtime of 5"ns. A limiting factor for measuring
intensities was the dynamic range of the counter of the MCS
module (16383 counts per run and channel), but severel runs
could be added. To avoid counter-overflow errors, neutral den-
sity filters were used to set the irradiance of the exciting
laser light to an appropriate level.

3.3. Measuring Spectra

The system was not intended for spectroscopy, the mono-
chromator rather served as tunable filter to seperate excita-
tion and emission wavelengths. But to find appropriate mono-
chromator settings or to check for unexpected effects, spectra
had to be measured.
a) Emission spectra: The sample was mounted in front of the
monochromator and excited with an argon laser. The fluorescence
transmitted through the monochromator was recorded while a
stepper motor slowly increased the monochromator's transmission
wavelength, then the photon counts were displayed on the multi-
channel analyzer. The spectral resolution was 12 nm (FWHM @
589"nm) with a slit width of 1.5"mm.
b) Absorption spectra: The spectrum of an incandescent lamp was
measured with (1) and without (2) a sample in front of it. Af-
terwards spectrum (1) was numerically divided by (2) and the
result subtracted from one.

3.4. Measuring and Analyzing Angle-Resolved Radiation Patterns

A hemicylindrical glass prism with a fluorescent or scat-
tering film on the plane face was mounted on a stepper motor
controlled turntable, cf. fig. 3.1-2. The motor slowly and con-
tinuously turned it with respect to the detection system. The

detection system recorded the emitted intensity during such an angular scan. The angle of incidence α_e of the light exciting the fluorescence was held constant with respect to the sample. A scan of the emission angle from 0° to 90° and a scan from 90° to 0° were added to eliminate bleaching-effects (to first order in time). Both scans together took 132 sec (0.52 sec per channel), several scans could be added. The measured angular resolution was < 1°. The multichannel analyzer displayed 2.5 channels per degree. Separately recorded backgrounds were subtracted from the measured radiation patterns (if possible) which were then transferred to a HP 217 personal computer. Corrections for reflections inside the hemicylindrical prism and for the aperture of the detection system (see below) were applied and the patterns were normalized to 1 at emission angle 0°. These patterns were superimposed on calculated radiation patterns and the best fit was visually determined.

The **corrections** to the measured "raw" radiation patterns $P^{(s,p)}_{raw}(\alpha_2)$ were modeled by two functions $K_R^{(s,p)}(\alpha_2)$ and $K_A(\alpha_2,\sigma)$ (see below). The "raw" pattern had to be divided by these angle dependent functions:

$$P^{(s,p)}_{corr}(\alpha_2) = P^{(s,p)}_{raw}(\alpha_2)/\{K_R^{(s,p)}(\alpha_2)\cdot K_A(\alpha_2,\sigma)\} \qquad (3.1)$$

The division was carried out numerically on the computer. Typical values of those corrections at $\alpha_2 = 0°$ are listed in table 3.1-2. Both corrections tend to lower the ratio $P(\alpha_{c,2})/P(0°)$ of the raw pattern.

a) We had to correct for angle dependent reflections of the emitted light inside the hemicylindrical prisms. We modeled the correction with the function $K_R^{(s,p)}(\alpha_2)$:

$$K_R^{(s,p)}(\alpha_2) = \frac{1 - R_0}{1 - R_0 R^{(s,p)}(\alpha_2)} \qquad (3.2)$$

$$R_0 = \left(\frac{1-n_2}{1+n_2}\right)^2 \qquad (3.3)$$ is the normal-incidence reflectance at the air/prism interface and $R^{(s,p)}(\alpha_2) = |r^{(s,p)}_{201}|^2$ (2.28) is the reflectance at the n_2-n_0-n_1 interface (n_2: refractive index of hemicylindrical prism at the emission wavelength, n_0: index of layer containing the emitters, n_1: index of medium adjacent to the plane face of the prism; adjacent to the cylindrical face of the hemicylindrical prism was air, cf. fig. 2.1 and 3.2). The mechanism responsible for this pertubation worked in the following way (cf. fig. 3.3): Radiation emitted in the di-

rection $-\alpha_2$ was partially retro-reflected at the prism/air interface, then partially reflected at the n_2-n_0-n_1 layer system, then partially transmitted through the prism/air interface at $+\alpha_2$ and partially retro-reflected, etc. We implicitely used the fact that our radiation patterns $P^{(s,p)}(\alpha_2)$ were symmetrical with respect to $\alpha_2 = 0°$, i.e. $P^{(s,p)}(\alpha_2) = P^{(s,p)}(-\alpha_2)$. The function $K_R^{(s,p)}(\alpha_2)$ is equal to 1 for $\alpha_2 \geq \alpha_{c,2}$ (critical angle of total internal reflection in medium 2).
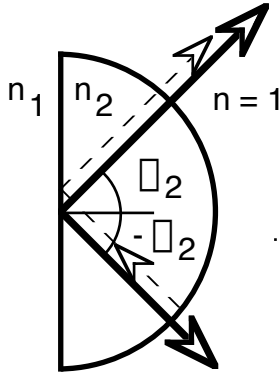

Fig. 3.3: Reflections inside a hemicylindrical prism. $n_{1,2}$: refractive indices, $\pm\alpha_2$: emission angles. Radiation emitted under the angle $-\alpha_2$ is partially retroreflected and emitted under $+\alpha_2$, etc.
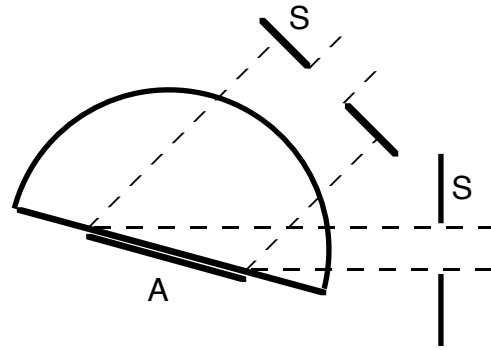
Fig. 3.4: Angle dependent cut-off by the entrance slit S of the monochromator. The size of the projection of the fluorescent area A on the slit varies with the emission angle. Drawings not to scale!

b) The finite aperture of the monochromator (1.5 mm slit) was responsible for a small distortion of the radiation pattern if the spot illuminated by the laser was large. We developed a simple, one-free-parameter model to compensate this effect and we kept the spot small (≈ 1 mm diameter) to decrease the size of this pertubation. The function describing this correction was $K_A(\alpha_2, \sigma)$ with the parameter σ:

$$K_A(\alpha_2, \sigma) = \int_{-1}^{1} \frac{d\xi}{\sqrt{2\pi\Sigma^2}} \exp\left(\frac{-\xi^2}{2\Sigma^2}\right) \quad , \text{ where } \Sigma = \sigma \cos(\alpha_2) \quad (3.4)$$

The sample was illuminated with a (centered) Gaussian laser beam. The entrance slit of the monochromator was rectangular and had a width much smaller than its length. $K_A(\alpha_2, \sigma)$ describes an angle dependent cut-off by this slit, cf. fig. 3.4. The parameter σ is a measure for the ratio of the diameter of

the illuminated area to the width of the slit. Because the radiation patterns $P^{(s)}(\alpha_2)$ are completely determined by theory for $\alpha_2 \leq \alpha_{c,2}$, we were able to fit for σ in that region. σ was usually ≤ 0.5 in our experiments.

n_2	$n_1 = n_0$	$K_R(0°)$
1.46	1	0.96622
1.46	1.33	0.96511
1.88	1	0.91461
1.88	1.33	0.90913

σ	$K_A(0°,\sigma)$
0	1
0.1	1
0.25	0.99994
0.4	0.98758
0.5	0.95451
0.6	0.90443
1	0.68270

Table 3.1-2: Corrections for the measured raw radiation patterns at $\alpha_2 = 0°$. $P^{(s,p)}{}_{corr}(\alpha_2) = P^{(s,p)}{}_{raw}(\alpha_2)/\{K_R{}^{(s,p)}(\alpha_2) \cdot K_A(\alpha_2,\sigma)\}$

3.5. Measuring and Analyzing Fluorescence Lifetimes

The light source was a mode-locked and frequency-doubled Nd:YAG laser which emitted 85 ps pulses of green light with 82 MHz repetition frequency. A cavity dumper, installed externally, lowered the pulse repetition frequency to 820 kHz. We used an EG&G ortec 583 constant fraction differential discriminator module together with a LeCroy 4201 time to digital converter module with a channel-width of 78 ps for recording histograms of fluorescence photon arrival times. The count rate was held far below 1 MHz to avoid dead time errors of the PM. The apparatus response function was recorded by scattering the laser pulses from a small aluminium rod. One measurement took one to ten minutes. The background was negligible. The measured apparatus response functions (M_A) and fluorescence response functions (M_F), both arrays of integers, were transferred to a BASIC-programmable HP 217 computer. A single exponential decay (3.5), with a fluorescence lifetime τ_F as parameter, was numerically convoluted (3.6) with the apparatus response function M_A:

$$(1/\tau_F)\cdot\exp(-t/\tau_F) \text{ for } t \geq 0 \text{ and zero for } t < 0 \qquad (3.5)$$

$$C(i) \propto \sum_{j=0}^{j\_max} M_A(i-j)\cdot\exp(-j\cdot 78 \text{ ps}/\tau_F)/\tau_F \qquad (3.6)$$

The result C(i) was shifted in time to compensate for differences in optical path lengths. (When fluorescence was measured, the light passed trough a glass hemicylinder, but when the ap-

paratus response funcion was measured, it passed this distance
through air.) The shifts were between 0 and 2 channels corre-
sponding to 0-2·78" ps delay or 0-44" mm optical path difference.
They were calculated in advance and not a fit-parameter. Then
the amplitude of C(i-Shift) was fitted to the fluorescence re-
sponse function, i.e. the constant A was determined such that

$$\sum_{j=j\_min}^{j\_max} {}''[M_F(j)" -"A\cdot C(j-Shift)]^2 = Minimum \qquad (3.7)$$

The fit {A·C(i-Shift)}, fluorescence response function {$M_F(i)$}
and the residuum {log(M_F)"- log(fit)} were graphically dis-
played, cf. fig. 3.5. This procedure was repeated for several
trial τ_F until the best fit, i.e. with the smallest χ^2 and best
visual appearance, was found on the fit-intervall choosen. We
determined the best τ_F usually with a resolution of 10" ps yield-
ing an accuracy of 0.05-0.1" ns, depending on the experiment.
The fit-intervalls usually began 10 to 30 channels after the
maximum of the fluorescence response function and reached over
100 channels, longer fit-intervall were possible but too time
consuming on our computer. This fitting strategy had been cho-
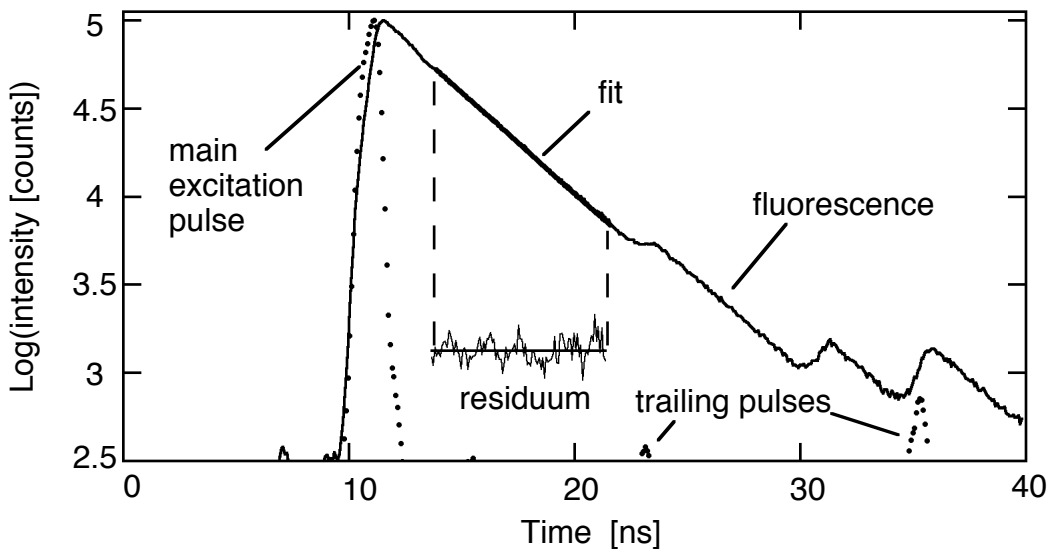sen because it proofed to be robust even at high noise levels.

Fig. 3.5: Measured apparatus response to the excitation pulses
(dots), fluorescence response (solid line) and calculated fit
(dots between dashed lines). The residuum {log(fluorescence)-
log(fit), vertically 13 times enlarged} is shown as inset. The
measurement is from rhodamine" 6G in ethanol at a concentration
<" 10^{-6}" mol/l, the fit for a fluorescence lifetime of 3.722" ns,
cf. section 4.1.2. The trailing pulses originated from the la-
ser system, the first was suppressed more than the second due
to properties of the cavity dumper's timing technique.

4. OPTICAL ENVIRONMENT DEPENDENT FLUORESCENCE OF LASER DYES

The object of this chapter is to present studies of the fluorescence of laser dye molecules, namely measurements of molecular parameters such as quantum yield and orientation with respect to an interface. We investigated two systems: dilute homogeneous dye solutions and extremely thin dye layers on glass. They represented especially simple arrangements where a comparison with the classical theory of dipole radiation (chapter 2) was straightforward.

4.1. Fluorescence of Dilute Dye Solutions

We used this system to investigate the influence of the refractive index of the solvent on the fluorescence lifetime. The theory of chapter 2 predicts that the spontaneous emission rate depends linearly on the refractive index of the solvent. This first approximation was not satisfactory. Combining this result with the known concept of the local field we arrived at an improved theory.

4.1.1. Sample Preparation and Preparatory Measurements

Solutions of eight rhodamine dyes in ethanol with concentrations $c_{sol} \leq 10^{-6}$ mol/l have been prepared, cf. table 4.1. We measured emission spectra (cf. section 3.3., excitation wavelength $\lambda_e = 514.5$ nm) to obtain the monochromator settings for highest photon count rates which were used later in the measurements of radiation patterns and lifetimes.

dye	abbrev.	MM [g/mol]	λ_F [nm]
rhodamine 110	R110	366.80	526
rhodamine 6G	R6G	479.02	554
rhodamine B	RB	479	569
sulforhodamine B	SRB	558.66	573
rhodamine 101	R101	591	586
sulforhodamine 101	SR101	607	594
rhodamine 700	R700	538	674
rhodamine 800	R800	495.52	702

Table 4.1: Fluorescence emission maxima (λ_F) of dilute solutions of rhodamine dyes in ethanol ($\lambda_e = 514.5$ nm), MM: molar mass.

To be sure that the monochromator setting is not a critical parameter for the determination of the transition rates, a meas-

urement of the fluorescence lifetime τ_F versus the emission wavelength λ for SR101 in ethanol was performed, cf. fig. 4.1. No significant deviation of the lifetime from the value measured at the emission maximum λ_F occurred.
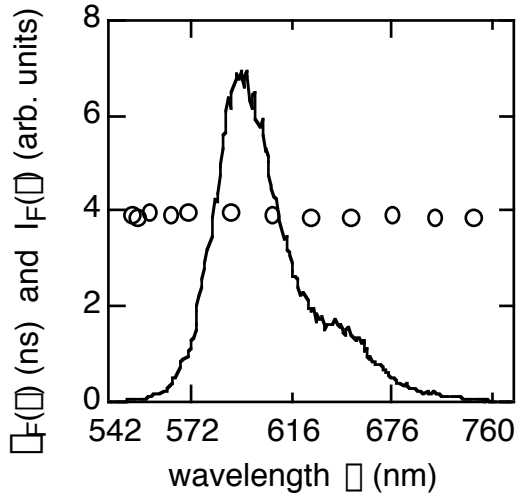

Fig. 4.1: Emission spectrum $I_F(\lambda)$ [arb. units] of SR101 in ethanol, $\lambda_e = 514$ nm, and fluorescence lifetime $\tau_F(\lambda)$ [ns], $\lambda_e = 532$ nm, versus emission wavelength λ.

4.1.2. Dependence of the Fluorescence Lifetime on the Refractive Index of the Solution

Solutions of dyes in various solvents (listed in table 4.2) have been prepared such that no coloration was visible at daylight illumination, i.e. concentration $\leq 10^{-6}$ mol/l. This to exclude absorption and reemission of fluorescence.

Pos.	Solvent	n_D
1	1,1,1,3,3,3-hexafluoro-2-isopropanol	1.2752
2	2,2,2-trifluoroethanol	1.285
3	methanol	1.33
4	water	1.33
5	acetone	1.36
6	ethanol	1.36
7	ethylene glycol	1.43
8	glycerol	1.47
9	dimethyl sulfoxide (DMSO)	1.48
10	benzyl alcohol	1.54
11	diiodopropane	1.64
12	diiodomethane	1.74

Table 4.2: Solvents used for the experiments; n_D: refractive index at $\lambda_D = 589$ nm.

The fluorescence lifetimes τ_F were measured at the emission max-
imum, cf. table 4.3. (The τ_F of R110 was measured at λ = 545 nm
because the emission maximum was too close to the excitation
wavelength of λ_e = 532 nm). Effects of rotational diffusion
have been eliminated by the method mentioned in section 2.2.2,
formula (2.100). The refractive indices of the solvents at the
emission wavelengths of the dyes were calculated from
dispersion formulas. These were extracted from measurements of
the refractive indices with an Abbé refractometer.

Solvent	R110	R6G	RB	SRB	R101	SR101	R700	R800
1	4.53	4.06	3.94	3.76	4.79	*4.54*	4.08	*2.05*
2	4.33	4.03	3.41	3.33	4.73	4.77	3.65	*2.04*
3	3.93	3.87	2.26	2.31	4.16	4.23	*2.39*	*1.67*
4	4.01	3.90	1.48	1.44	4.03	4.00	*1.30*	*0.79?*
5	3.69	3.76	1.93	2.80	4.31	4.11	2.90	2.35
6	3.77	3.72	2.76	2.78	4.13	4.18	2.64	1.94
7	3.45	3.48	2.75	2.74	3.92	3.90	2.12	*1.50?*
8	3.33	3.27	3.15	3.28	*3.49*	3.69	*2.16*	*1.31*
9	3.19	3.37	*2.26*	2.32	3.80	3.80	2.32	*1.79*
10	3.28	3.24	3.11	3.14	3.66	3.59	*2.86*	*2.02*
11	*1.59*	*1.29*	*1.83*	2.34	*2.70*	*2.41*	2.73	2.46
12	*2.20*	*1.53*	*1.67*	*1.80*	*2.00*	*2.05*	*2.40*	*2.04*

Table 4.3: Fluorescence lifetimes [ns] of dyes in various sol-
vents (listed in table 4.2); accuracy ≤ 0.05 ns for values set
in normal style and ≈ 0.1 ns for values in *italic*.

The theory states that the radiated power $L_\infty(n_0)$ of an electric
dipole in an unbounded medium (0) is proportional to the refrac-
tive index n_0 of that medium, cf. formula (2.35). If this is
still true for the radiative transition rate of fluorescent
molecules in a solution then the following equations hold for
the transition rates of the molecules:

$$L_\infty(n_0)/L_{vac} = n_0 \quad (2.35) \qquad A_{tot} = A_r + A_{nr} \quad (2.106)$$
$$A_r = A_{r,vac} L_\infty(n_0)/L_{vac} \text{ (from 2.108)} \qquad (4.1)$$
$$\Rightarrow A_{tot} = A_{r,vac} n_0 + A_{nr} \qquad (4.2)$$

where $A_{r,vac}$ is the radiative transition rate in a medium with
refractive index 1 (called "vacuum"). If the non-radiative tran-
sition rate A_{nr} is independent of the solvent-material, then the
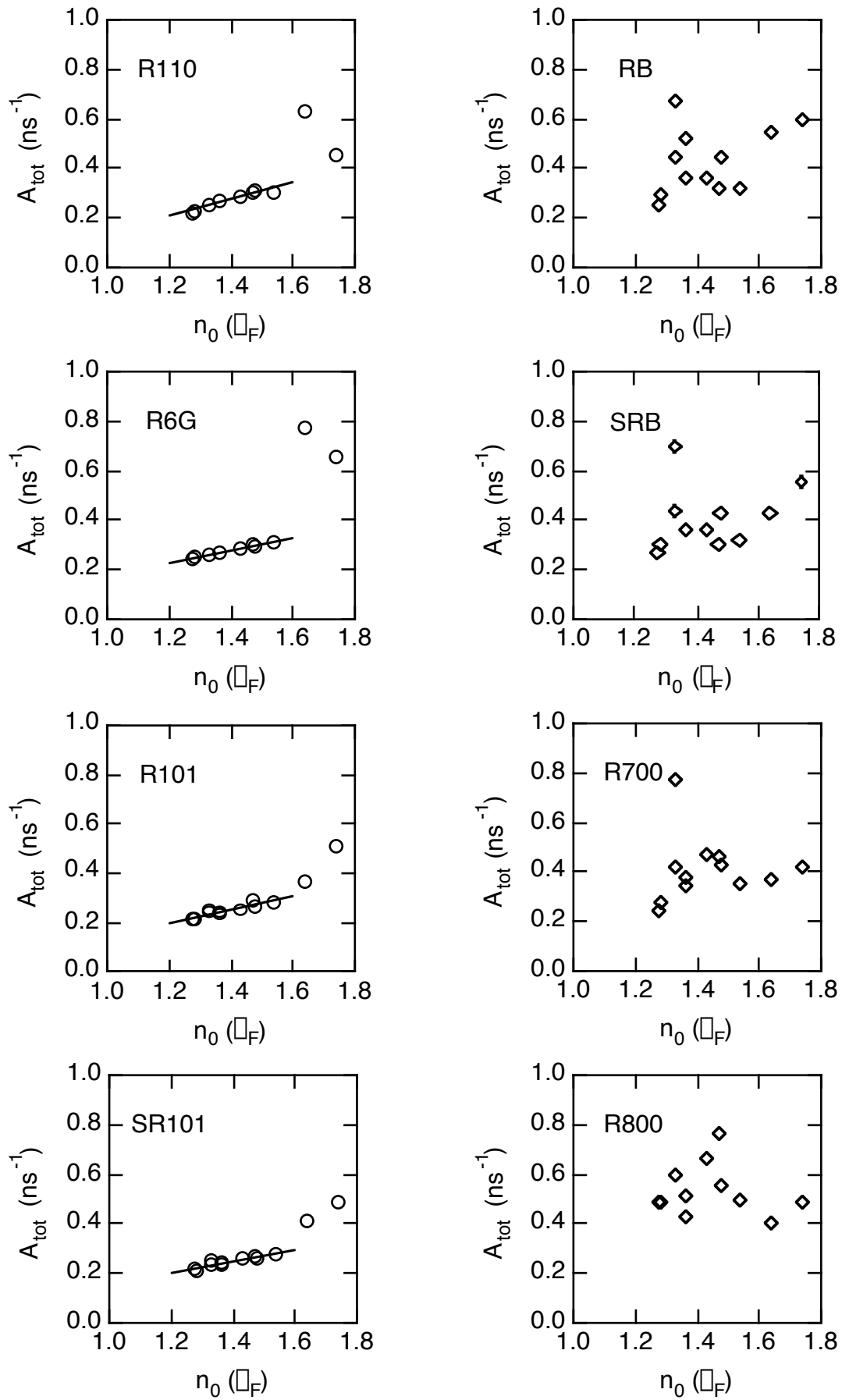graph of the function $A_{tot}(n_0)$ is a straight line, cf. fig. 4.2.

Fig. 4.2: Measured emission rate $A_{tot}" = 1/\tau_F$ (ns^{-1}) vs. the refractive index of the solvent $n_0(\lambda_F)$, data taken from table 4.3.

The correlations between $A_{tot} = 1/\tau_F$ and $n_0(\lambda_F)$ are high for the dyes R110, R6G, R101, and SR101, but low for RB, SRB, R700, and R800. (The fluorescence efficiency of RB is strongly dependent on solvent and temperature. This has been attributed to some kind of torsion or rotation of its amino groups occurring in the excited state. In R101 this mobility is prevented by its chemical structure, cf. [4;5]). For R110, R6G, R101, and SR101 the correlation coefficients [1;4] were evaluated and the $A_{r,vac}$ and A_{nr} were determined by linear regression, cf. table 4.4. The negative values obtained for A_{nr} show that something with this approximation must be wrong.

Dye	$A_{r,vac}$ [ns^{-1}]	A_{nr} [ns^{-1}]	CC
R110	0.33796	−0.19874	0.9512
R6G	0.26103	−0.08799	0.9841
R101	0.25448	−0.10671	0.9038
SR101	0.23228	−0.07526	0.9425

Table 4.4: Result from linear regression of $1/\tau_F$ on n_0 for the model $1/\tau_F = A_{r,vac}\, n_0 + A_{nr}$, CC = correlation coefficient.

The problem may be that in the derivation of the formula $L_\infty(n_0) = n_0 L_{vac}$ (2.35) the summarized description $\mathbf{D} = \varepsilon_0\, \hat{\varepsilon}_0\, \mathbf{E}$ (4.3) of the interaction of the electric field with matter in the Maxwell equations was used (ε_0: specific inductive capacity or dielectric constant of medium 0, $\hat{\varepsilon}_0$: permittivity of the vacuum; $\varepsilon_0 = n_0^2$ at optical frequencies). But this averaged description is not valid any more if we look at the electric field at the molecule's location on an atomic scale. «To estimate the difference [between effective and mean field], consider a particular molecule and imagine it to be surrounded by a small sphere whose radius is nevertheless large compared with its linear dimensions. We shall consider separately the effects on the central molecule produced by the matter outside and inside this sphere. In determining the effect of the matter *outside* the sphere we may clearly neglect the molecular structure and treat the substance as continuous. We may then assume that, outside the sphere, the polarization $\mathbf{P}$ produced by the mean electric field is constant. Concerning the effect of the molecules *inside* the sphere we shall assume, as may be shown for a number of important special cases, including that of random distribution, that they do not produce any resulting field at the cen-

tral molecule. Hence we may regard the molecule as being situated in a spherical region, inside which there is vacuum and outside which there is a homogeneously polarized medium.», from [1;1, p.85]. In section 2.3 we gave equation (2.122) for the field inside a sphere. From that we get for the local field $\mathbf{E}_{local}$ inside a hollow sphere (n_s = 1) immersed in a medium with refractive index n_0 the expression

$$\mathbf{E}_{local} = \left(\frac{3\,n_0^2}{2n_0^2 + 1} \right) \mathbf{E}_0 \qquad (4.4)$$

where $\mathbf{E}_0$ is the homogeneous electric field in the surrounding medium (0) far from the sphere. By "local" or "effective" field we mean the field at the molecule's location taking the atomic structure of matter into account. The "near" field is the field in the immediate vincinity, i.e. at distances r « λ, of the dipole in the continuum approximation. The electric field at the molecule's location is enhanced by the factor $3\,n_0^2/(2n_0^2 + 1)$ (4.5). In the emission-process, the radiated power is proportional to the fields squared, i.e. enhanced by $\{3\,n_0^2 / (2n_0^2 + 1)\}^2$ (4.6). The enhancement (4.6) is also present in the absorption-process, but this does not manifest itself in a measurement of the spontaneous emission rate. If the emitted (time averaged) intensity is measured, the factor (4.6) manifests itself via absorption but not via the spontaneous emission rate. Together with (4.6) we get in analogy to the formulas (4.1-2):

$$L_\infty(n_0) = n_0 \left(\frac{3\,n_0^2}{2n_0^2 + 1} \right)^2 L_{vac} \qquad (4.7)$$

$$\Rightarrow A_{tot} = A_{r,vac}\, n_0 \left(\frac{3\,n_0^2}{2n_0^2 + 1} \right)^2 + A_{nr} \qquad (4.8)$$

Least squares fits with this "corrected" model have been applied to the same set of data as in table 4.4 and the result is listed in table 4.5. The fits are not better regarding the correlation coefficients, but the non-radiative transition rates obtained are now all positive and of reasonable size yielding quantum efficiencies in the range 70 - 100 %. The non-radiative transition rates measured in this way are averaged over many solvents, i.e. over many different chemical environments. For comparison with the quantum yields in table 4.5 we give some quantum efficiencies from Schäfer and Drexhage [4;2]. The quantum yield depends on n_0, because the transition rates depend on the optical environment. From (2.109) we get $\eta = (A_{tot}-A_{nr})/A_{tot}$ where we use (4.8) to calculate A_{tot}. Beside this section, the

factor (4.6) was used in the calibration procedures for the surface coverages in sections 4.2.1. and 5.2., but nowhere else in this text.

Dye	$A_{r,vac}$ [ns^{-1}]	A_{nr} [ns^{-1}]	CC	η(1.36)	η(1.43)
R110	0.13304	0.008478	0.9515	0.967	0.970
R6G	0.10238	0.072721	0.9833	0.727	0.745
R101	0.09914	0.051254	0.8934	0.786	0.801
SR101	0.09072	0.068397	0.9357	0.716	0.734

Table 4.5: Result from linear regression for the corrected model (equation 4.8), CC = correlation coefficient, $\eta(n_0)$ = quantum yield calculated for n_0 = 1.36 and n_0 = 1.43.

dye	solvent	η	remarks
R6G	ethanol	95 %	
R110	ethanol	85 %	25° C
R101	ethanol	100 %	
RB	ethanol	40 %	25° C
RB	glycerol	100 %	

Table 4.6: Quantum yield η of some dyes (accuracy ca. 5 %), from [4;2]

Onsager has calculated a refinement to expression (4.4) for the local field. He calculated $\mathbf{E}_{local}$ by assuming a molecule to be embedded in a spherical cavity [4;6]. The diameter 2 a of the cavity is assumed to be of molecular size. The molecule's dipole moment $\mathbf{p}$ is assumed to be an idealized point dipole at the center of the cavity with the dipole moment $\mathbf{p} = \mathbf{p}_{em} + \alpha \cdot \mathbf{E}_{local}$ (4.9), where α is the molecules polarizability and $\mathbf{p}_{em}$ its fixed dipole moment. (From [4;7, 4;2] we know that rhodamine dyes have no static dipole moment in the ground or excited state, i.e. $\mathbf{p}_{em}$ is really only the transition dipole moment.) Onsager determined the field at the center of the cavity using $\mathbf{p}_{em} \neq 0$ and $\alpha \neq 0$. We have converted Onsager's formulas to SI-units and to our notation. We get for the local field:

$$\mathbf{E}_{local} = \frac{\dfrac{3n_0^2}{2n_0^2 + 1}\, \mathbf{E}_0 + \dfrac{2(n_0^2 - 1)}{2n_0^2 + 1}\, \dfrac{\mathbf{p}_{em}}{4\pi\, \hat{\varepsilon}_0\, a^3}}{1 + \dfrac{2(n_0^2 - 1)}{2n_0^2 + 1}\, \dfrac{\alpha}{4\pi\, \hat{\varepsilon}_0\, a^3}} \qquad (4.10)$$

A fit analogous to (4.8) with this refined model for the local field gave higher correlations, positive non-radiative transi-

tion rates A_{nr} and higher quantum yields as in table 4.5, but the improvement over model (4.4) was not significant. The results were ambiguous because they depended on the parameter a^3 which is not well defined. We have not attempted to extend (4.10) to an elliptical cavity.

If we assume the dye molecules to be non-polarizable ($\alpha \varnothing 0$) and if we neglect effects of the emission dipole moment ($\mathbf{p}_{em}$ small) and/or if the cavity (dye molecule) has a large radius a, then (4.10) leads back to (4.4). On the other hand, if we assume the local field to be the same as for the solvent molecules, cf. [1;1-3], then we arrive at the expression

$$\mathbf{E}_{local} = \frac{n_0^2 + 2}{3} \mathbf{E}_0 \tag{4.12}$$

for the local field [4.6]. Eq. (4.12) is used in the derivation of the Lorentz - Lorenz law. In analogy to (4.4-8) a linear regression of the measured total transition rates A_{tot} on the calculated radiative power (4.13) has been made according to the following model (4.14):

$$L_\infty(n_0) = n_0 \left(\frac{n_0^2 + 2}{3} \right)^2 L_{vac} \tag{4.13}$$

$$\Rightarrow A_{tot} = A_{r,vac} n_0 \left(\frac{n_0^2 + 2}{3} \right)^2 + A_{nr} \tag{4.14}$$

The results of these least sqares fits are presented in table 4.5a. The correlation coefficients (CC) are lower than in table 4.5, but not significantly. (The standard deviations of the CC are 0.01-2.) The quantum efficiencies η are in the 90 - 100 % range which compares favourably with the values reported by Schäfer [4.2], cf. table 4.6, and they are higher than the η's in table 4.5. But a decisive conclusion whether (4.14) is superior to (4.8) may not be drawn.

Dye	$A_{r,vac}$ [ns^{-1}]	A_{nr} [ns^{-1}]	CC	$\eta(1.36)$	$\eta(1.43)$
R110	0.06259	0.1193	0.9302	0.949	0.956
R6G	0.04917	0.1557	0.9778	0.935	0.944
R101	0.04743	0.1321	0.8862	0.944	0.952
SR101	0.04361	0.1419	0.9303	0.940	0.948

Table 4.5a: Result from linear regression for the corrected model (equation 4.14), CC = correlation coefficient, $\eta(n_0)$ = quantum yield calculated for $n_0 = 1.36$ and $n_0 = 1.43$.

4.2. Fluorescence of Sub-Monomolecular Dye Layers

We prepared dye layers on glass substrates with surface concentration $\leq 10^{15}\,m^{-2}$ so that the mean intermolecular distance is $\geq 30\,nm$. Then energy transfer between the molecules can be neglected. We measured in such systems a) the angular radiation patterns from which we determined the orientation of the molecules' emission dipole moments with respect to the interface, b) the fluorescence lifetime as a function of the substrate's refractive index, and c) we measured the changes in fluorescence lifetimes as a function of the gap width between the fluorescent layer and a second glass plate.

4.2.1. Sample Preparation and Preparatory Measurements

The preparation of a dye layer started from a solution of a laser dye with concentration c_{sol} in ethanol. We used ethanol because it is a good solvent, non poisonous, well wetting, has a high vapor pressure, and rhodamine dyes have a high quantum yield when they are dissolved in it [4;2]. The glass substrates were microscope slides or hemicylindrical glass prisms. Each slide was cleaned for five minutes in an ultrasonic bath filled with Contrad™ at room temperature, subsequently for five minutes in an ultrasonic bath filled with deionized water, and then dried with nitrogen. The hemicylindrical prisms were wiped several times with acetone and methanol moistened Kodak lens cleaning paper; this cleaning procedure was not good enough to exclude effects on the measured fluorescence lifetimes, but the shapes of the radiation patterns were not affected. A Convac spincoater was used to deposit the thin dye layers on glass substrates. A few drops ($\approx 0.1\,ml$) of the solution were given on the slowly (120 rpm) spinning cleaned glass substrate, which was then within 2 seconds accelerated to 3000 rpm. After 5 s the solvent had evaporated and the process was finished. The surface coverage of the substrate produced in this way was quite uniform and reproducible to $\pm 10\%$. The layers were visually clear for $c_{sol} \leq 10^{-4}\,mol/l$. For $c_{sol} \geq 10^{-3}\,mol/l$ microcrystals had formed and the films scattered light. The surface concentration c_{sur} of the dye layer was estimated by comparing its fluorescence emission to the emission of a dye solution of known dye concentration which was excited by an evanescent wave, cf. fig. 5.4. A spincoat solution of $c_{sol} = 10^{-6}\,mol/l$ yielded a surface concentration of $c_{sur} = 10^{15}\,m^{-2}$ (accuracy $\approx 50\%$). This

is much less than a monomolecular layer with $c_{mono} \approx 10^{18}$ m^{-2} (rhodamine molecules are about 10^{-9} m long), therefore we named them "sub-monomolecular" layers. The surface coverage was proportional to the concentration of the spincoat solution: $c_{sur} \approx c_{sol} \cdot 10^{21}$ m^{-2} l/mol (4.15). From the result of this calibration procedure we concluded that the molecules on the substrate were isolated if $c_{sol} \leq 10^{-6}$ mol/l (no Förster-energy transfer from molecule to molecule and to nonluminescent traps [4;1, 4;9]).

Measurements of fluorescence intensity (I_F) and lifetime (τ_F) of the molecules in the layer as a function of the concentration of the spincoat solution c_{sol} showed that this goal was achieved, cf. fig. 4.4. The mean intermolecular distance in a solution with bulk concentration c_{bulk} = 10^{-6} mol/l is 120 nm and for a thin layer with c_{sur} = 10^{15} m^{-2} it is 32 nm. The intermolecular distance where bulk energy-transfer starts to dominate is $\leq$ 10 nm [4;1-2], this corresponds to a bulk concen-

Fig. 4.4: Normalized fluorescence intensity (I_F/c_{sol} for R6G on Pyrex) and lifetime (τ_F for SR101 on Pyrex) vs. concentration of spincoat solution c_{sol}.

tration c_{bulk} = $1.7 \cdot 10^{-3}$ mol/l and a surface concentration c_{sur} = 10^{16} m^{-2}. The stability of the thin dye layers in ambient air at room temperature depended on the particular dye used. The fluorescence intensity from, e.g., R6G on Pyrex decreased 5 % per minute with an excitation intensity of 20 mW/mm^2 at 514 nm. Other dye layers (R700, R800) bleached even without being illuminated, just by being exposed to air, which was not the case for the stable dyes R6G, R101, and SR101, indicating an influence of the oxygen in the air. For the following experiments with submonomolecular dye layers in air, the exciting irradiance was held below 1 mW/mm^2 to minimize bleaching and to ensure that only a small fraction of the
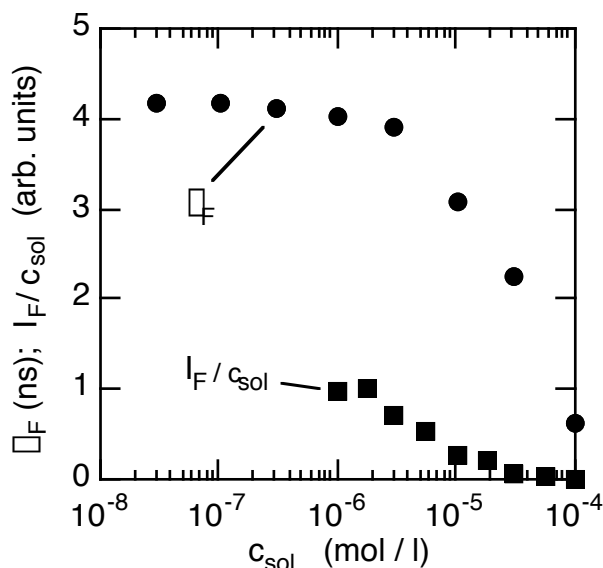
molecules were excited (no effects from saturation of the upper
level).

4.2.2. Emission Radiation Patterns

Radiation patterns of the dyes, applied as submonomolecu-
lar layers in ambient air on the plane face of a fused silica
hemicylindrical prism, were recorded and fits for the orienta-
tions were carried out. The fits were usually very good, exam-
ples are shown in fig. 4.5-7. Excitation was s-pol. at $\lambda_e =$
514.5 nm and $\alpha_{e,2} =$ 70° with an irradiance $\leq$ 1 mW/mm^2. The spin-
coat solution had a concentration of 10^{-6} mol/l, except for R700
and R800, where it was considerably higher to compensate bleach-
ing in air. A fit to the (sp)-radiation pattern (s-pol. excita-
tion, p-pol. emission) yielded $\theta =$ (77 $\pm$ 2)° for all dyes. With
(2.59) we get $g_z/g_x =$ 0.107 $\pm$ 0.034 and together with (2.53,87)
we get $g_z =$ 0.034. In the other extreme ($g_x/g_y =$ 3) we get $g_z =$
0.074. The weights g_x, g_y, g_z, and θ are defined in section
2.1.2, and for an interpretation cf. example 2 in section
2.2.1..
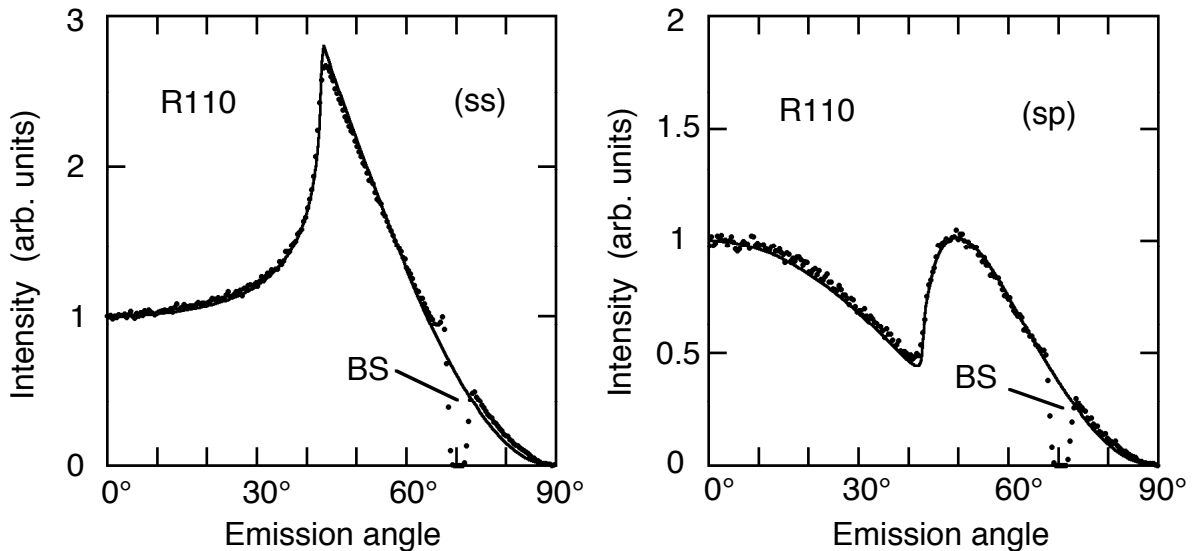
Fig. 4.5: Measured (ss)- and (sp)-radiation patterns (dots) of
R110 submonomolecular layers on fused silica hemicylinders com-
pared with calculated radiation patterns (solid lines); parame-
ters: $n_0 = n_1 =$ 1, $n_2(\lambda_F) \approx$ 1.46, and $z_0 =$ 0; fit parameter: $\theta =$
77° $\pm$ 2°; BS = beam stopper, $\alpha_{e,2} =$ 70°, $\lambda_e =$ 514.5 nm.
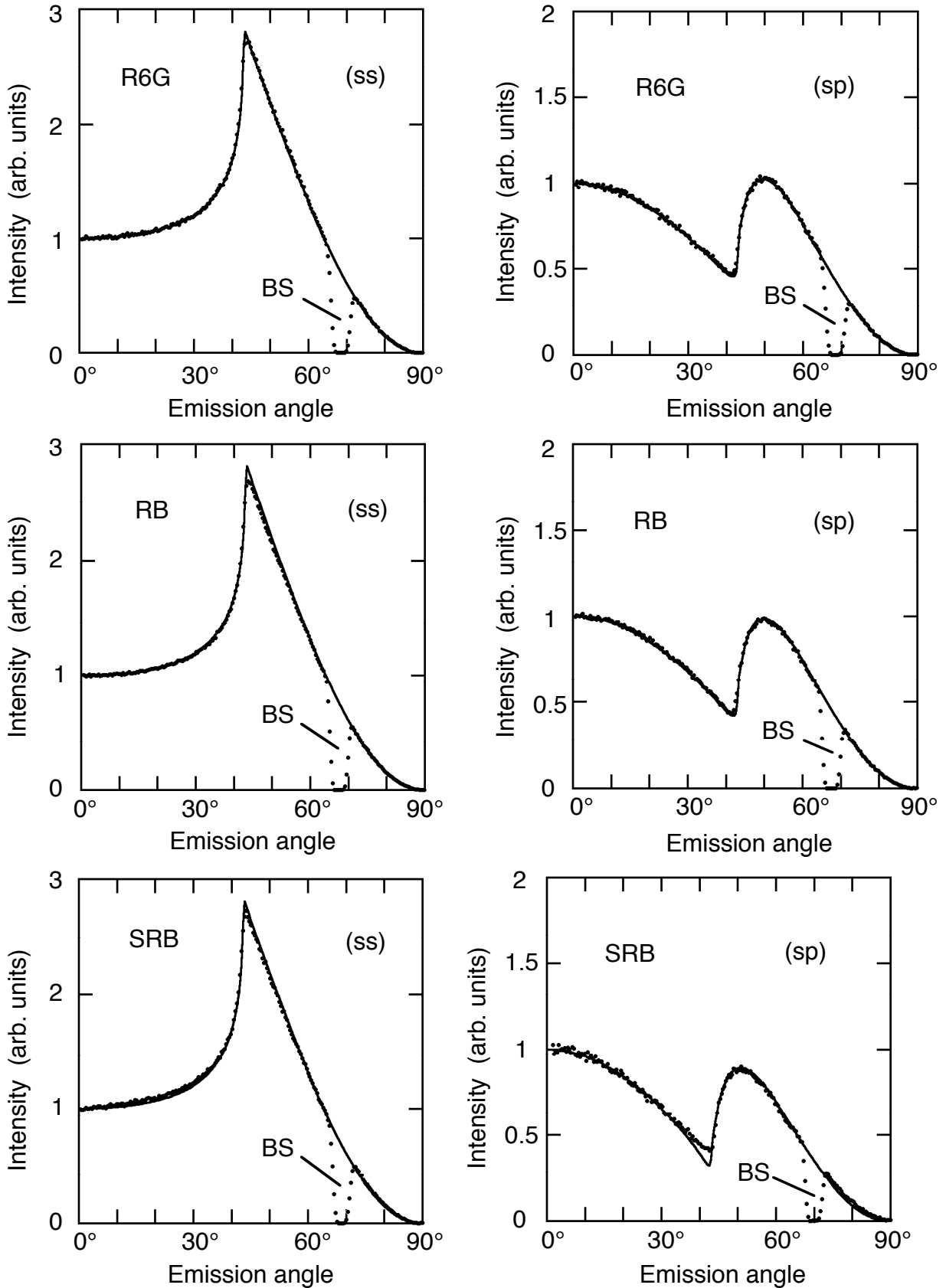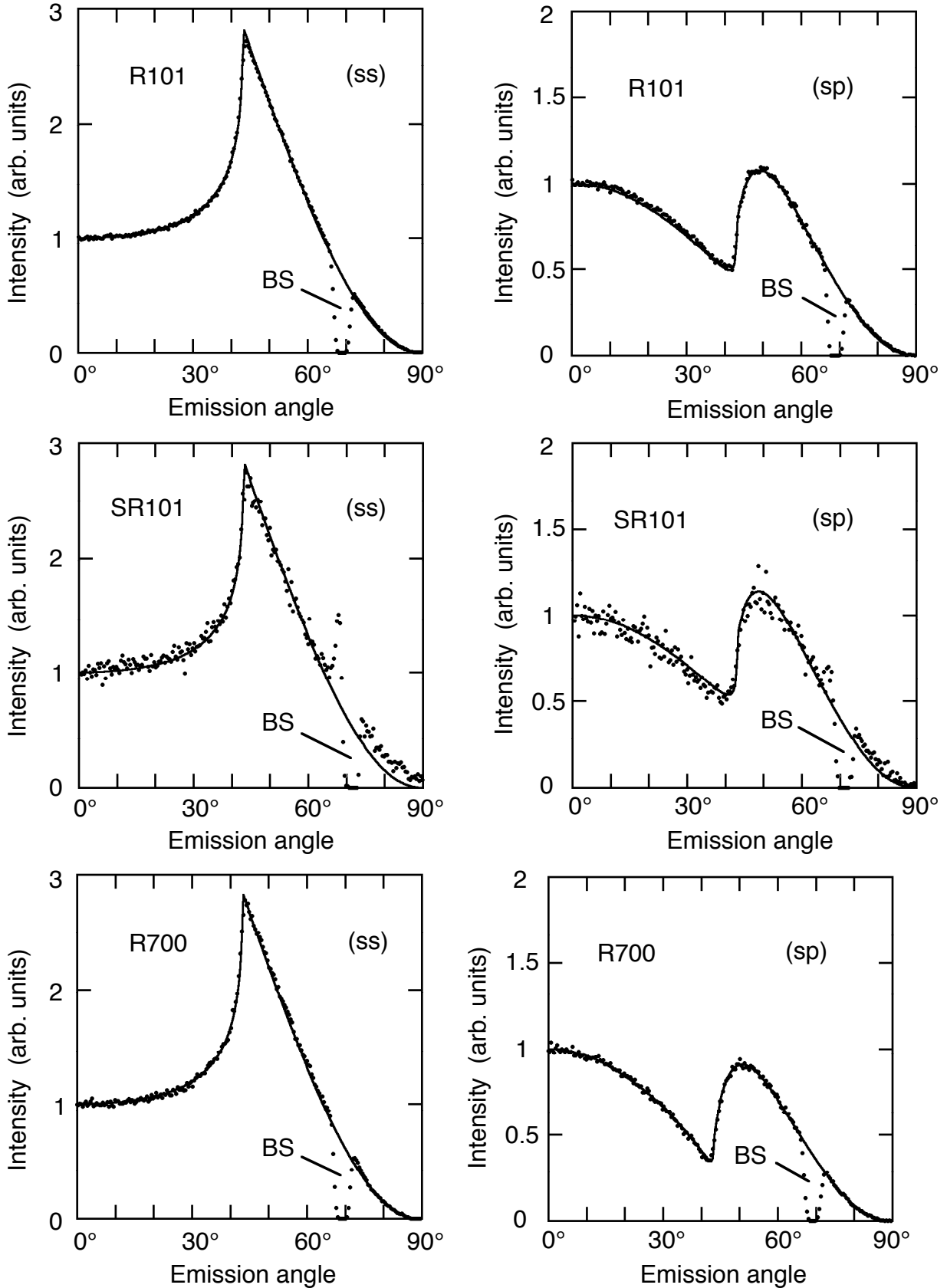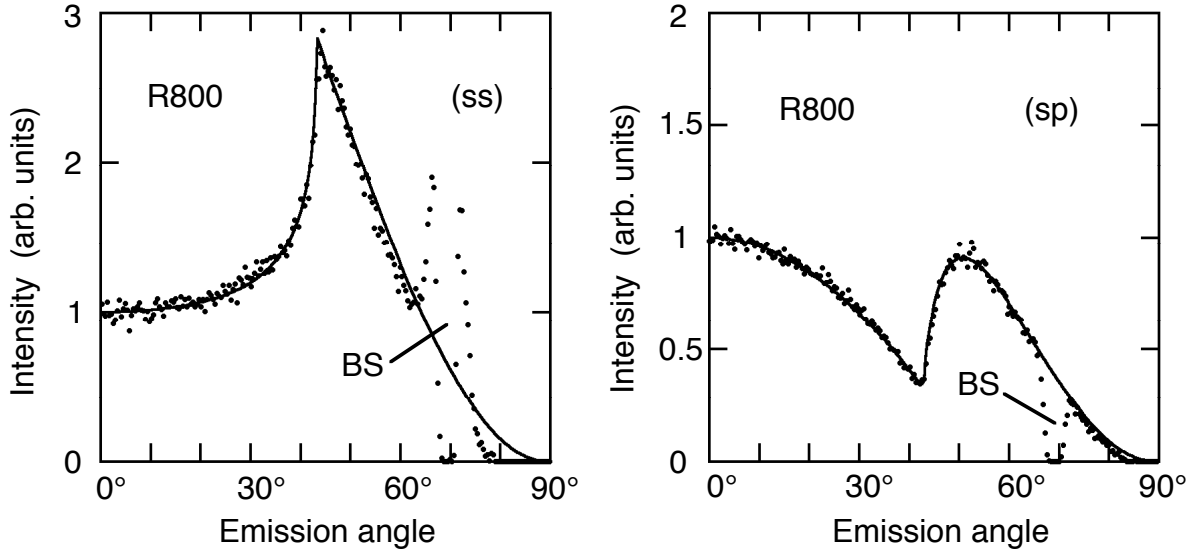
Fig. 4.6: Measured (ss)- and (sp)-radiation patterns (dots) of R6G, RB and SRB submonomolecular layers on fused silica hemi-cylinders compared with calculated radiation patterns (solid lines); parameters: $n_0" ="n_1" =" 1$, $n_2(\lambda_F)" \approx" 1.46$, and $z_0" =" 0$; fit parameter: $\theta!=!77°!\pm!2°$; BS!= beam stopper, $\alpha_{e,2}!=!70°$, $\lambda_e!=!514.5!nm$.

Fig. 4.7: Measured (ss)- and (sp)-radiation patterns (dots) of R101, SR101 and R700 submonomolecular layers on fused silica hemicylinders compared with calculated radiation patterns (solid lines); parameters: $n_0 = n_1 = 1$, $n_2(\lambda_F) \approx 1.46$, and $z_0 = 0$; fit parameter: $\theta = 77° \pm 2°$; BS = beam stopper, $\alpha_{e,2} = 70°$, $\lambda_e = 514.5$ nm.

Fig. 4.7a: Measured (ss)- and (sp)-radiation patterns (dots) of R800 submonomolecular layers on fused silica hemicylinders compared with calculated radiation patterns (solid lines); parameters: n_0 $=$ n_1 $=$ 1, $n_2(\lambda_F)$ $\approx$ 1.46, and z_0 $=$ 0; fit parameter: θ $=$ $77°$ $\pm$ $2°$; BS $=$ beam stopper, $\alpha_{e,2}$ $=$ $70°$, λ_e $=$ 514.5 nm.

Measurements of the emitted (ss)- and (sp)-intensity for α_e $\approx$ α $\approx$ $0°$ were made to determine the static depolarization g_x/g_y (g_z $=$ 0 assumed) and from that the angle ψ between the dipole moments $\mathbf{p}_{abs}$ and $\mathbf{p}_{em}$, cf. formula (2.102). Results are listed in table 4.7. They represent upper limits because measurement errors tend to degrade the degree of polarization [4;13, p.743].

Dye	g_x/g_y	angle ψ [°]
R110	0.417	17.3 $\pm$ 2
R6G	0.468	21.8 $\pm$ 2
RB	0.451	20.4 $\pm$ 2
SRB	0.434	18.9 $\pm$ 2
R101	0.504	24.8 $\pm$ 2
SR101	0.457	20.9 $\pm$ 2
R700	*0.939*	*43.2*
R800	*0.805*	*38.8*

Table 4.7: Static depolarization g_x/g_y and angle ψ between $\mathbf{p}_{abs}$ and $\mathbf{p}_{em}$ for dyes on fused silica substrates.

The measurements are for a concentration of the spincoat solution of 10^{-6} mol/l, except for R700 and R800 where the concentration was considerably higher to compensate for low fluorescence intensity. The high values measured for their g_x/g_y indicate nearly complete depolarization due to energy transfer between dye molecules. Complete depolarisation (g_x/g_y $=$ 1) would

give an angle $\psi = 45°$. We assumed that rotational diffusion of the excited molecules in those submonomolecular dye-layers on glass in air was negligible.

4.2.3. Dependence of Fluorescence Lifetimes on the Refractive Index of the Substrate

Submonomolecular dye layers on different glass substrates have been prepared. The concentration of the spincoat solution was 10^{-7} mol/l. This guaranteed that the molecules on the substrates were independent of each others. Polished "microscope" slides (Fisba Optik AG, St. Gallen, Switzerland) of the glass types listed in table 4.8 were used. Pyrex is a trademark of Corning, Suprasil of Heraeus, all other glasses of Schott.

Pos.	Glass Name	n_D	Glass Type
1	AF45	1.526	alkali free glass
2	F14	1.601	opt. glass
3	K11	1.500	opt. glass
4	LaSFN9	1.850	opt. glass
5	LaSFN15	1.878	opt. glass
6	LLF7	1.549	opt. glass
7	Pyrex	1.472	borosilicate glass
8	SF2	1.648	opt. glass
9	SF15	1.699	opt. glass
10	SF63	1.748	opt. glass
11	SFL6	1.805	opt. glass
12	Suprasil 2	1.458	fused silica

Table 4.8: Glass types used in the measurements; n_D: refractive index at $\lambda_D = 589$ nm.

In table 4.9 the measured fluorescence lifetimes of sub-monomolecular dye layers on different glasses in ambient air are shown. $\lambda_e = 532$ nm, $\alpha_e \approx 0°$, $\alpha \approx 0°$. For all lifetime measurements we chose the wavelength λ at the fluorescence maximum, with the exception of R110 (measured at 545 nm), because it had the emission maximum too close to λ_e. In fig. 4.8 two typical measurements of the fluorescence response on the exciting laser pulses are shown: R6G on the glasses with the lowest and the highest refractive indices used in this experiment (fused silica resp. LaSFN15).
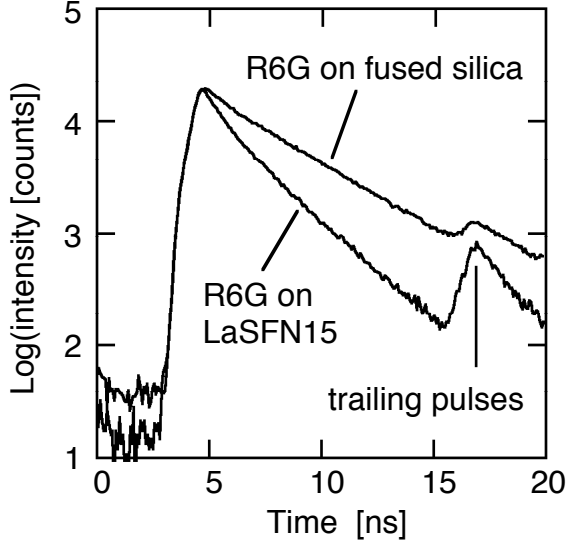
Fig. 4.8: Fluorescence response of a submonomolecular rhodamine 6G layer in ambient air on fused silica (n = 1.46) and on LaSFN15 (n = 1.88). The trailing pulses are artifacts of the lasersystem.

Glass	R110	R6G	RB	SRB	R101	SR101	R700	R800
AF45	3.637	3.632	3.573	3.447	3.770	3.947	2.983	1.790
F14	2.933	2.975	2.653	2.635	2.945	3.085	2.233	1.188
K11	3.383	3.282	3.175	3.155	3.183	3.66	2.628	1.523
LaSFN9	2.237	2.247	2.425	2.187	2.405	2.545	2.272	1.343
LaSFN15	2.183	2.083	2.243	2.062	2.312	2.358	2.037	1.388
LLF7	2.900	3.222	2.863	3.033	3.025	3.530	2.460	1.398
Pyrex	3.690	3.532	3.367	3.300	3.665	3.772	2.743	1.530
SF2	2.783	3.001	2.735	2.697	2.973	3.285	2.438	1.328
SF15	2.537	2.642	2.563	2.657	2.670	3.135	2.345	1.395
SF63	2.700	2.270	2.688	2.303	2.843	2.257	2.435	1.130
SFL6	1.683	1.623	1.703	1.695	1.76	1.942	1.835	1.262
Silica	3.593	3.667	3.385	3.480	3.590	4.132	2.800	1.557

Table 4.9: Fluorescence lifetimes [ns] of extremely thin dye-layers on glass substrates, accuracy ca. 0.05 ns.

Analogously to section 4.1.2. we obtain equations (4.16-18) for the total ($A_{tot} = 1/\tau_F$), radiative (A_r), and non-radiative (A_{nr}) transition rates of molecules in an extremely thin layer on an interface ($z_0 = 0$). The emission dipoles were assumed to be parallel to the interface, i.e. $L(z_0) = L_\parallel(z_0)$, and in air ($n_1 = n_0 = 1$).

$$A_{tot} = A_r + A_{nr} \quad (2.106)$$
$$A_r = A_{r,vac} L_\parallel(n_1,n_2,z_0)/L_{vac} \quad \text{(from 2.108)} \quad (4.16)$$
$$L_\parallel(n_1,n_2,z_0=0)/L_{vac} = l^{(0)}_\parallel \quad \text{(from 2.35,37-39,45-46)} \quad (4.17)$$
$$\Rightarrow A_{tot} = A_{r,vac} l^{(0)}_\parallel + A_{nr} \quad (4.18)$$

where $A_{r,vac}$ is the radiative transition rate in an infinite medium with refractive index 1 (called "vacuum") and $l^{(0)}{}_{\parallel}$ is the zero order term in the Taylor series for $L(z_0)/L_\infty(n_0)$, cf. formula (2.37). If the non-radiative transition rate A_{nr} is independent of the substrate-material, then the graph of the function $A_{tot}\{l^{(0)}{}_{\parallel}\}$ is a straight line, see fig. 4.9.

The results of a linear regression [1;4] of $A_{tot} = 1/\tau_F$ from table 4.9 on the calculated $l^{(0)}{}_{\parallel}$ are presented in table 4.10. The measurement on the glass SFL6 have been omitted because they showed too high transition rates for all dyes to fit into this model. The refractive indices of the glasses at the emission wavelengths of the dyes have been calculated with dispersion formulas given by Schott.

Fig. 4.9: Measured transition rates ($A_{tot} = 1/\tau_F$) for R6G vs. the calculated total radiated power $l^{(0)}{}_{\parallel}$ on glass substrates.

Although the correlations are quite high, the negative values for the non-radiative transition rates indicate that something in the model must be wrong. A correction analogous to section 4.1.2 is not as straightforward because the environment of the molecules was not isotropic. A correction for the local field analogous to (4.4) with $n_0 = 1$ (molecules in air) or $n_0 = 1.33$ (molecules embedded in 3-10 monolayers of water which are
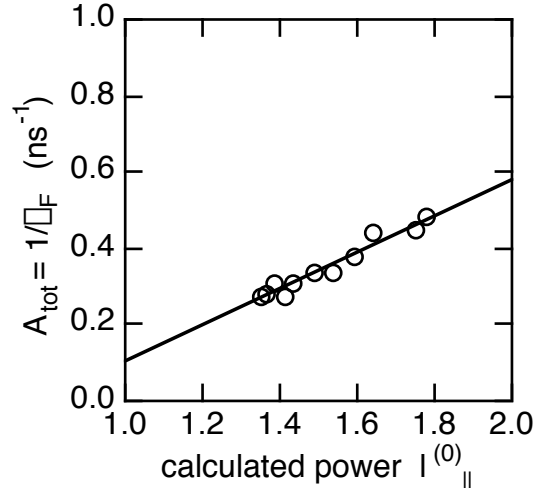
Dye	$A_{r,vac}$ [ns^{-1}]	A_{nr} [ns^{-1}]	CC
R110	0.4197	-0.2906	0.9634
R6G	0.4778	-0.3764	0.9732
RB	0.3232	-0.1371	0.9214
SRB	0.4444	-0.3093	0.9734
R101	0.3452	-0.1869	0.9402
SR101	0.4254	-0.3257	0.9115
R700	0.2530	-0.0236	0.8237
R800	0.3225	-0.2295	0.5139

Table 4.10: Result from linear regression of $1/\tau_F$ on $l^{(0)}{}_{\parallel}$ for the model $1/\tau_F = A_{r,vac} l^{(0)}{}_{\parallel} + A_{nr}$, CC = correlation coefficient.

always present in ambient air) would not have any effect on the calculated A_{nr} because it does not depend on n_2.

We measured the fluorescence lifetime of a thin SR101 dye layer on a fused silica hemicylindrical prism as a function of the emission angle α_2. We found no significant variation of τ_F for s-pol. excitation and s-pol. emission, cf. fig. 4.10. This assured that the emission angle is not a critical parameter if polarizations are (ss).

Fig. 4.10: Lifetime τ_F vs. emission angle for SR101 in air on a fused silica hemicylindrical prism for (ss)- and (sp)-polarization.

The measurements in this and the following sections were (ss). For the (sp)-case a variation was measured. The critical angle of total internal reflection $\alpha_{c,2}$, where measurements for (sp)-emission were difficult, was $\alpha_{c,2}$" $= 43°19'$, α_e" $= 60$ or $70°$.

4.2.4. Dependence of the Fluorescence Lifetimes and Intensities on the Optical Environment

The refractive indices and extents of the materials surrounding the emitters constitute the "optical environment" whereas the neighbouring molecules of the emitting molecules constitute the "chemical environment". Measurements of the fluorescence lifetime τ_F as a function of the optical/chemical environment have already been performed. In [4;14, 4;16] fatty acid monolayers served as spacers between a layer of fluorescent molecules and an interface. This method has the drawback that for each spacer thickness a new dye layer has to be produced, and that the chemical environments of the dye molecules are not the same for all measurements. We devised an experiment, where the optical environment was reversibly changed with the very same ensemble of molecules (A new variant of the "optical contact experiment", [4;12]).

A submonomolecular dye layer was deposited on the plane face of a fused silica ($n_2 = 1.46$) hemicylindrical prism. A glass plate of refractive index $n_1 = 1.88$ (LaSFN15) was pressed against it in such a way that just a small air gap ($n_0 = 1$, $d_0 = 0 .. \lambda/3$) between the two remained, cf. fig. 4.11, "optical contact experiment". The cylindrical glass plate (diameter 2.5 cm, thickness 1 mm) was glued on the opening of a tube. The tube was pressurized which bent the glass plate towards the hemicylindrical prism. The pressure was 0-700 mbar, adjustable to ± 1 mbar with a precision reducing valve. The gap was

Fig. 4.11: "Optical contact experiment"; n_1 = glass plate, n_2 = hemicylindrical prism, D = diode, λ_e = excitation wavelength, d_0 = gap width, p = pressure.

continuously monitored by recording the intensity of the reflected exciting laserbeam ($\lambda_e = 532$ nm, $\alpha_{e,2} = 70° > \alpha_{c,2} = 43°$). The laserbeam experienced frustrated total internal reflection at the n_2-(n_0,d_0)-n_1 layer system; the reflectance depended sensitively on the gap width d_0. Absorption of the exciting radiation by the dye layer was neglected. (Schäfer et al. [4;2] report an absorption cross section σ of about 10^{-20} m^2 for rhodamine dyes, cf. also the example in section 2.3.. Therefore a submonomolecular layer with surface coverage $c_{sur} = 10^{15}$ m^{-2} absorbs approximately the fraction $\sigma \cdot c_{sur} \approx 10^{-5}$ of the exciting radiation). From the measured reflectance $R^s(d_0)$ (2.28) the gap width was calculated with a resolution of ≤ 2 nm, but the absolute accuracy was much worse (± 30 nm for time resolved and ± 10 nm for cw experiments below, probably originating from beam-pointing instabilities of the laser and/or drifts in the electronics). A measurement of $1/\tau_F$ vs. d_0 (ss-pol, $\alpha_2 = 0°$) for RB is shown in fig. 4.12 and juxtaposed to the calculated total radiated power of an electric dipole parallel to the interface. The resemblance between the two plots is obvious. Analogously to (4.16-18) we obtain the following equations for the total ($A_{tot} = 1/\tau_F$), radiative (A_r), and non-radiative (A_{nr}) transition rates of molecules in this layer system:

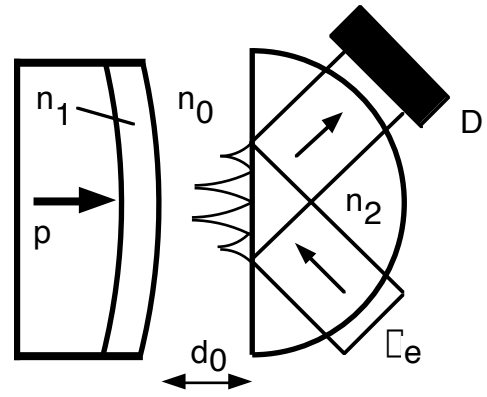$A_{tot}" =" A_r" +" A_{nr}$ (2.106)

$A_r" = A_{r,vac}" L(d_0,..)/L_{vac}$ (from 2.108)   (4.19)

$\Rightarrow" A_{tot}" = A_{r,vac}" L(d_0,..)/L_{vac}" +" A_{nr}$ (4.20)

where $A_{r,vac}$ is the radiative transition rate in an infinite medium with refractive index 1. The emission dipoles are assumed to be in air, parallel to (i.e. $L(*)" = L_\parallel(*)$) and directly on ($z_0" =" 0$) the interface. The graph of the function $A_{tot}\{L(d_0,...)\}$ should be a straight line. Unfortunately the measurement of the gap width d_0 was not accurate enough to permit a determination of the non-radiative transition rate or the quantum yield, but the reversibility of this process could be demonstrated and the qualitative behaviour of the lifetime was as expected.
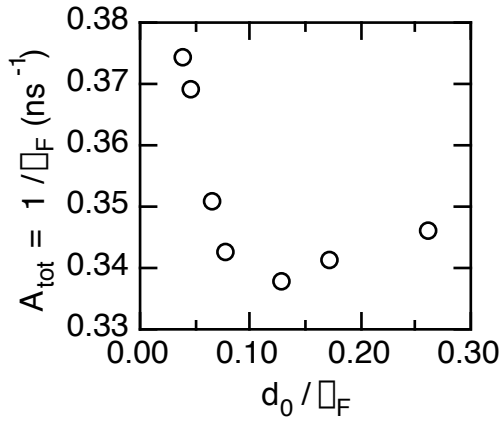
Fig. 4.12: $A_{tot} = 1/\tau_F$ vs. d_0/λ_F for RB on fused silica
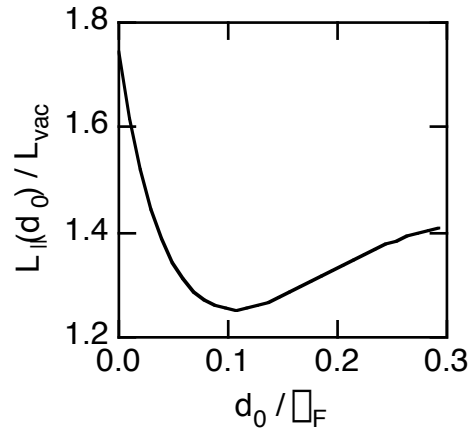
Fig. 4.13: Calculated power $L_\parallel/L_{vac}$ vs. gap width d_0/λ_F

Measurements of the emitted **fluorescence intensity vs. d_0** suffered from the same disadvantages as the measurement above: They were not accurate enough to allow the determination of a quantum yield, but the emitted intensity changed reversibly as a function of the gap width d_0 and its qualitative behaviour was as expected, cf. fig. 4.14. According to section 2.2.3. the following equations hold between emitted intensity I_F and intensity of the exciting field $E^2(d_0,...)$, quantum yield $\eta(d_0,...)$, radiation pattern $P(d_0,...)$, and total emitted power $L(d_0,...)$:

$I_F" = A" E^2" \eta" P" /" L$ (from 2.113)   (4.21)

from (2.109) and (2.107):

$\eta" = A_r/(A_r+A_{nr})" = B \cdot L/(B \cdot L+A_{nr})" =" L/(L" +" A_{nr}/B)$ (4.22)

$\Rightarrow" L" = A \cdot E^2 P/I_F" -" A_{nr}/B$ (4.23)

(A, and B are constants). I_F is measured directly and the E^2, P, and L are calculated from the measured d_0. Equation (4.23) is adapted to linear regression of L on E^2P/I_F.

A plot of $I_{calc} = E^2 \cdot P/L_\parallel$ vs. I_F is shown in fig. 4.14, the dye was R101, $\lambda_e" = 514"nm$, $\alpha_{e,2} = 70°$, $\alpha_2" =" 0°$, polarizations (ss). $I_{calc} = E^2 \cdot P/L_\parallel$ is proportional to the intensity emitted by an ensemble of dipoles orientated parallel to the surface and with quantum yield unity. Measured and calculated intensities correlate well, but for small gap widths d_0 (low fluorescence intensity) a systematic error occurs.
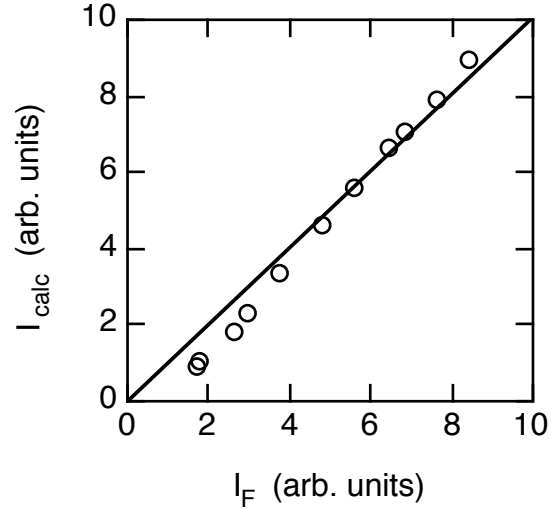
Fig. 4.14: Calculated intensity $I_{calc} = E^2(d_0)\ P(d_0)/L_\parallel(d_0)$ vs. measured $I_F(d_0)$.

4.3. Summary

For emission from dilute dye solutions, an increase of the total emission rate with increasing refractive index of the solvent was observed. In a first approximation, theory predicted an exactly linear increase of the spontaneous emission rate with the refractive index. This assumption led to physically impossible results, i.e. negative non-radiative transition rates. The next approximations, which included corrections for the local field, gave physically reasonable results.

For emission from submonomolecular dye layers, an increase of the total transition rate with increasing refractive index of the substrate was observed. The correlation between observed transition rates and calculated total radiative power was very high, but the lack of a theoretically founded local field theory prevented us from determining the quantum efficiencies quantitatively. The measured radiation patterns showed that the dye molecules' emission dipole moments had a mean angle $\theta = 77°$ $\pm 2°$ with respect to the surface normal, i.e. were orientated

preferencially parallel to the surface. To avoid a change of
the chemical environment of the dye molecules, an optical con-
tact experiment was designed. A glass plate was pressed against
the layer which changed the width of the remaining air gap in
steps of $\approx"\lambda/100$. The transition rates and emitted intensities
behaved qualitatively as expected, but the inability to measure
the gap width with sufficient precision prevented a numerical
determination of the quantum efficiency.

5. ADSORPTION OF PROTEINS WITH A FLUORESCENT LABEL

The object of this chapter is to show the connection between the theory of dipole radiation near interfaces and one important application of fluorescence. Luminescent markers have been used for a long time in biochemistry to monitor protein adsorption and desorption processes from specially prepared interfaces [5;1-3]. An example is the binding of a labelled antibody to an antigen. The following sections show a variant of this experiment: Unspecific adsorption to the bare substrate material, i.e. the surface is not covered with an antigen.

5.1. Sample Preparation and Preparatory Measurements

We used rabbit anti-human immunoglobulin (Gamma chains) of which 40"% are labelled with tetramethylrhodamine isothiocyanate, isomer R (supplied by Dakopatts, Glostrup, Denmark) dissolved in a phosphate buffer solution (pH"7.4, supplied by Roche, Basel) at a concentration of 0.45 mg/ml = 3"μmol/l. This corresponds to a concentration of $1.2\cdot10^{-6}$"mol/l of
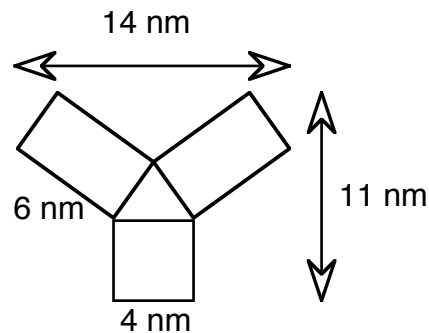

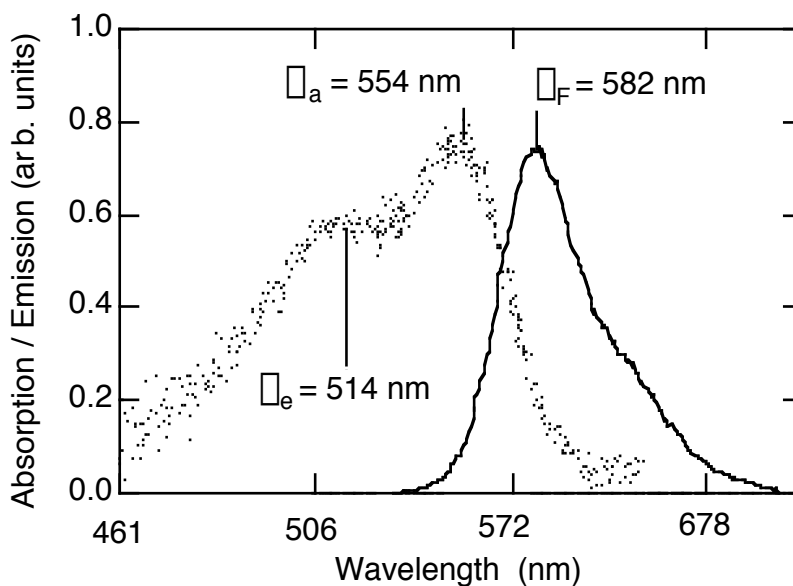
Fig. 5.1: Approximate shape and size of an IgG-molecule.

Fig. 5.2: Absorption (dots) and emission- (solid line) spectra of TRITC in PBS (arb. units). Excitation wavelength λ_e, absorption maximum λ_a and emission maximum λ_F are indicated.

fluorescent molecules, abbrev. IgG-TRITC in PBS. The molecular mass of IgG, cf. fig. 5.1, is 150'000"g/mol. Absorption and

emission spectra of the dye in PBS were measured, cf. section 3.3, and the absorption and emission maxima determined to be $\lambda_a = 554$ nm and $\lambda_F = 582$ nm; $\lambda_e = 514.5$ nm, cf. fig. 5.2. For these measurements, we used the dye tetramethylrhodamine B isothiocyanate, isomer mixture (supplied by Fluka AG, Buchs, Switzerland). The spectra of those two dyes are very similar to the spectrum of rhodamine B, cf. chapter 4.

5.2. Monitoring Protein Adsorption via the Fluorescence Intensity of a Dye Marker

We measured the unspecific adsorption of IgG-TRITC in PBS on the plane face of a TiO_2/SiO_2-covered LaSFN15 hemicylindrical prism, on Schott glass LaSFN15 ($n_2 = 1.87866$) alone, and on a fused silica ($n_2 = 1.458662$) hemicylindrical prism. The TiO_2/SiO_2-layer was fabricated with a dip-coating technique. Its optical constants ($d = 178$ nm, $n = 1.765$ at $\lambda = 582$ nm) were determined from a waveguiding reference layer on a Pyrex substrate produced in the same run. The waveguiding criterion depends sensitively on the parameters n and d of the waveguiding film and can be used to determine n and d precisely. The protein solutions were filled in black anodized aluminium cuvettes attached to hemicylindrical prisms, cf. fig. 5.4. The cuvettes were either 10 μm or 1 mm deep and had diameters of 2 or 1 cm. They were several times flushed with methanol, deionized water and PBS before the measurement and kept under methanol afterwards to prevent biological contamination. Fluorescence was excited with an evanescent wave ($\lambda_e = 514.5$ nm, $\alpha_{e,2} = 65°$) and the emission detected at $\lambda = 582$ nm, $\alpha_2 = 50°$. The size of the illuminated spot on the interface was ≤ 1 mm^2 and the 1/e penetration depth of the exciting intensity was 230 nm (for $n_2 = 1.46$, $n_1 = 1.335$). The 1/e penetration depth Δz of the exciting evanescent field $\mathbf{E}(z) \propto \exp(-z \cdot |k_{z,1}|)$ is defined as $\Delta z = 1/|k_{z,1}| = (\lambda_e/2\pi)|n_1^2 - n_2^2 \sin^2\alpha_e|^{-1/2}$ (5.1), cf. also (2.4). The penetration depth of the corresponding intensity ($\mathbf{E}^2(z)$) is half of that. The result of a typical measurement is shown in fig. 5.3.
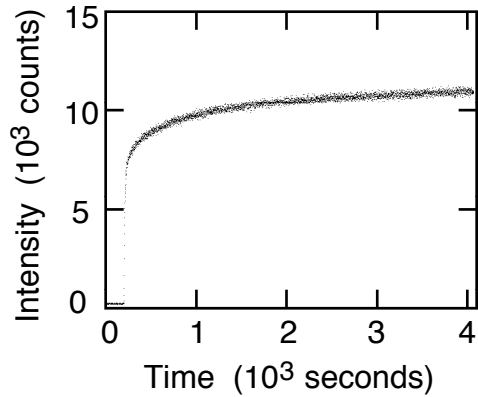
Fig. 5.3: Fluorescence intensi-
ty vs. time for unspecific ad-
sorption of IgG-TRITC in PBS on
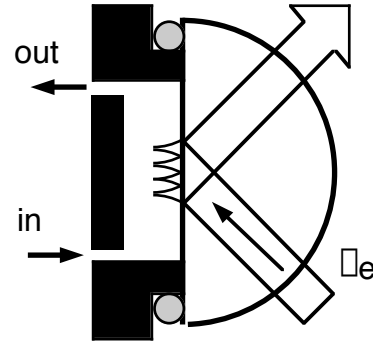a TiO_2-SiO_2 layer on LaSFN15,
dwelltime 1" s/channel.

Fig. 5.4: Schema of cuvette
on hemicylindrical prism,
excitation with evanescent
wave, λ_e" = wavelength of
exciting radiation.

As long as the cuvette was filled with PBS, only constant back-
ground fluorescence ($\approx$" 200 counts/s) was detected, cf. fig. 5.3.
As soon as the protein solution was filled in, the signal in-
creased ($\approx$" 200 counts/s) due to emission from dye-tracer-mole-
cules within the penetration depth of the exciting light, but
the main contribution to the signal ($\approx$" 10000 counts/s) came af-
ter the filling procedure had been completed due to adsorption
to the interface. (The concentration in the adsorbate layer,
0.5" $\mu g/cm^2$ in a $\approx$" 10" nm layer, was about 1000 times higher than
the bulk concentration!) Because adsorption started right at
the beginning of the filling procedure, the increase due to
bulk emission in fig. 5.3 is masked by emission from the grow-
ing adsorbate layer.

The calibration of the surface concentration yielded $8.2 \cdot 10^{15}$
dye-molecules/m^2 (accuracy ca. 30" %) after several hours of ad-
sorption of IgG-TRITC in PBS on a TiO_2/SiO_2-covered LaSFN15
hemicylindrical prism with an initial IgG bulk concentration of
0.45 mg/ml ($3 \cdot 10^{-6}$" mol/l). This corresponds to $2 \cdot 10^{16}$ IgG-mole-
cules/m^2 (labelled plus unlabelled) or a mass density of 0.5
$\mu g/cm^2$ or (7" nm)^2/molecule, i.e. about one monolayer. In the
calibration procedure we compared the emission of the IgG-TRITC
layer to the emission of a homogeneous TRITC solution of known
concentration adjacent to the same interface under the assump-

tion that the orientation was isotropic, cf. next section, and that the quantum yield was the same in both cases.

The biosensor group in our laboratory made adsorption experiments with human Immunoglobulin G (abbrev. h-IgG) on a TiO_2/SiO_2 waveguide surface [5;4-5]. The values measured with the input grating coupler for an initial bulk concentration of 5 mg/ml were $d_{F'} = 7.7$ nm for the adsorbate film thickness and $n_{F'} = 1.44$ for its refractive index. The surface coverage was calculated by means of the empirical relation $n_{F'} = n_{PS} + c_{F'} \cdot dn_{PS}/dc$ (5.2) with $dn_{PS}/dc = 0.188$ ml/g (5.3), where n_{PS} = refractive index of the protein solution ($\approx n_{PBS}$) and $c_{F'}$ = protein concentration in the adsorbate layer. From that the surface coverage Γ was calculated to be $\Gamma = c_{F'} \cdot d_{F'} = [(n_{F'} - n_{PS})/(dn_{PS}/dc)] \cdot d_{F'} = 0.45$ $\mu g/cm^2$ (5.4). An analogous calculation of Γ from a radiation pattern ($n_{F'} = n_0 = 1.4$, $d_{F'} = d_0 = 10$ nm, $n_{PS} = n_1 = 1.335$) yielded $\Gamma = 0.35$ $\mu g/cm^2$ which is in agreement with the results above within the quite large error limits of the values deduced from radiation patterns (cf. next section) and regarding the fact that our initial concentration was lower.

5.3. Radiation Patterns of Dye Tracers in Adsorbed Protein Layers

We measured (ss)- and (sp)-radiation patterns of the adsorbed IgG-TRITC layers described in section 5.2., cf. fig. 5.5-7. "(sp)" means s-pol. excitation and p-pol. emission, analogous for "(ss)". From a comparison of the measured and calculated radiation patterns we conclude that emission came from a homogeneous layer of thickness $n_0 d_0 \approx \lambda/40$ (or that the patterns do at least not contradict this assumption). The contribution from light emitting molecules in bulk solution near the interface but not adsorbed to it was negligible because the ratio of the emitted intensity from bulk molecules excited by the evanescent wave to the intensity emitted by the adsorbed layer was very small (≤ 2 %).
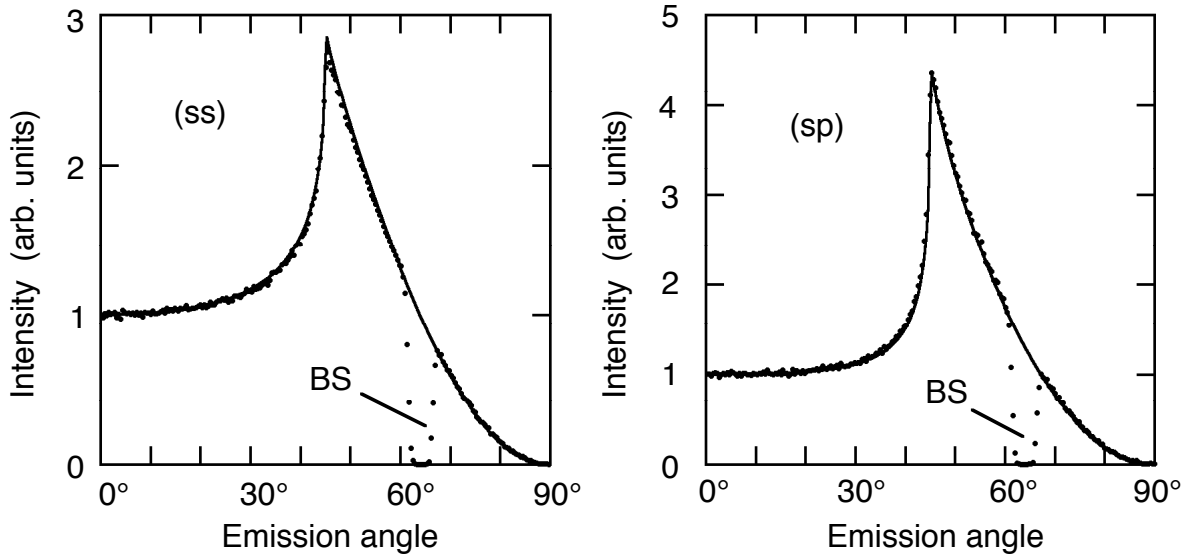
Fig. 5.5: Measured (ss)- and (sp)-radiation patterns (dots) for IgG-TRITC in PBS adsorbed to a LaSFN15 hemicylindrical prism compared with calculated patterns (solid lines); parameters: n_1 = 1.335, $n_2 = 1.879$, $\lambda = 582$ nm; fit parameters: $n_0 = n_1$, $d_0 = 10$ nm, $\theta = 58°$; BS = beam stopper, $\alpha_{e,2} = 65°$, $\lambda_e = 514.5$ nm.
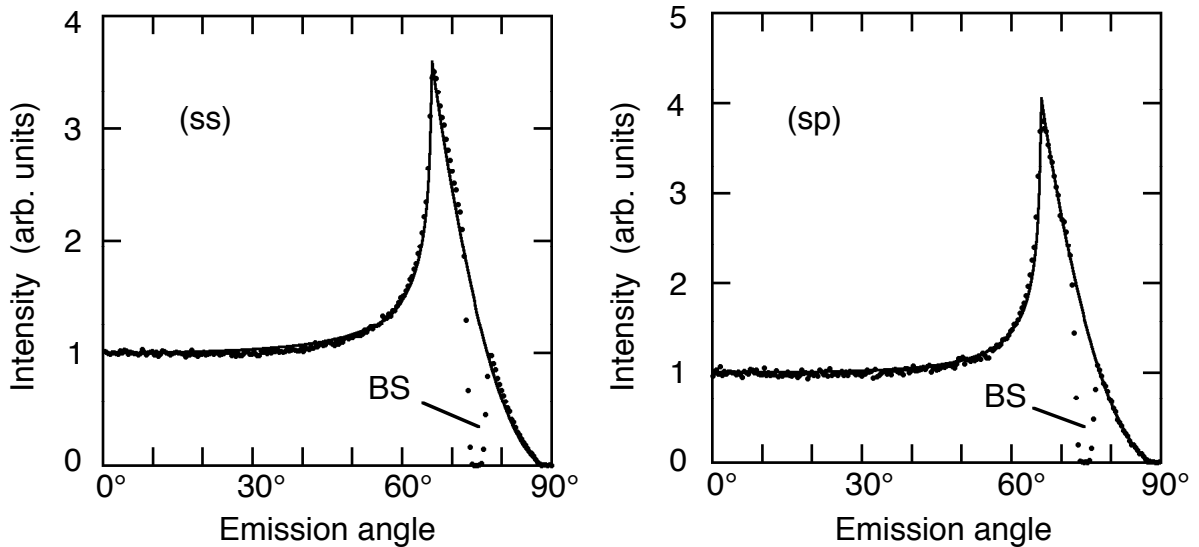

Fig. 5.6: Measured (ss)- and (sp)-radiation patterns (dots) for IgG-TRITC in PBS adsorbed to a fused silica hemicylinder compared with calculated patterns (solid lines); parameters: $n_1 = 1.335$, $n_2 = 1.459$, $\lambda = 582$ nm; fit parameters: $n_0 = n_1$, $d_0 = 10$ nm, $\theta = 55.5°$; BS = beam stopper, $\alpha_{e,2} = 65°$, $\lambda_e = 514.5$ nm.
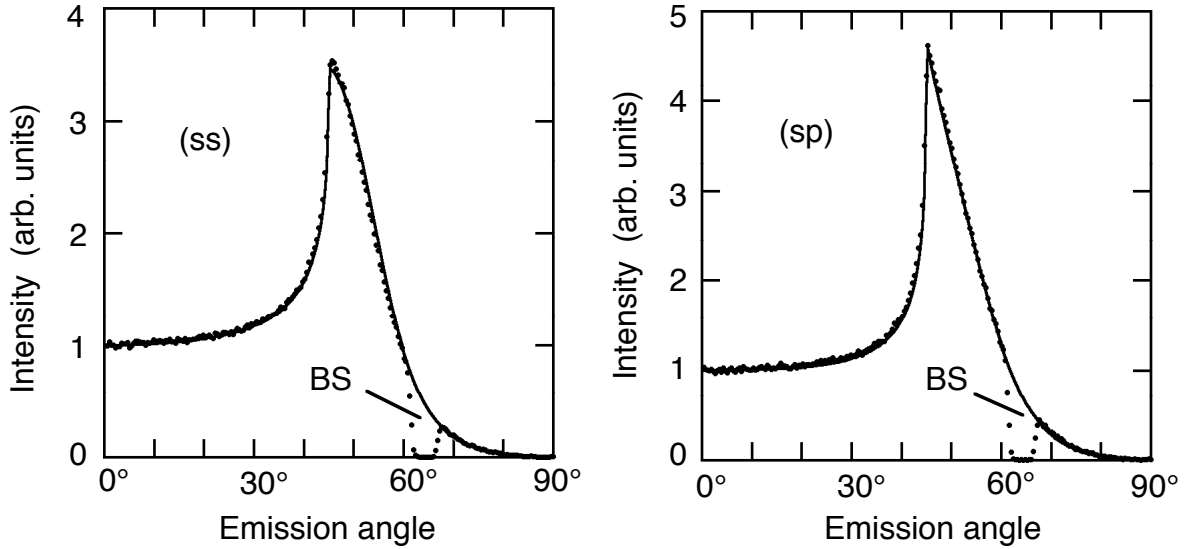
Fig. 5.7: Measured (ss)- and (sp)-radiation patterns (dots) for IgG-TRITC in PBS adsorbed to a TiO_2/SiO_2-covered LaSFN15 hemicylinder compared with calculated patterns (solid lines); parameters: $n_1 = 1.335$, TiO_2/SiO_2-layer: $n = 1.765$, $d = 178$ nm; $n_2 = 1.879$, and $\lambda = 582$ nm; fit parameters: $n_0 = n_1$, $d_0 = 10$ nm, $\theta = 57.9°$; BS = beam stopper, $\alpha_{e,2} = 65°$, $\lambda_e = 514.5$ nm.

We determined refractive index and thickness of adsorbate layers on fused silica, on LaSFN15, and on a TiO_2/SiO_2-layer on LaSFN15 from the radiation patterns. The refractive indices of the media at $\lambda = 582$ nm were: $n_1 = 1.335$ (PBS), $n_2 = 1.458662$ (fused silica) or 1.87866 (LaSFN15) and $n = 1.765$, $d = 178$ nm (TiO_2/SiO_2-layer). We determined n_0 and d_0 from a fit to the (ss)-radiation pattern for $\alpha > \alpha_c$, cf. fig. 5.5-7, which yielded for a protein layer adsorbed on LaSFN15:

$n_0 = n_1 \Rightarrow d_0 = 10$ nm (best fit),
$n_0 = 1.4 \Rightarrow d_0 = 20$ nm,
$n_0 = 1.5 \Rightarrow d_0 \geq 30$ nm,

for a protein layer adsorbed on fused silica:

$n_0 = n_1 \Rightarrow d_0 = 0..20$ nm,
$n_0 = 1.4 \Rightarrow d_0 = 0..20$ nm,

and for a protein layer adsorbed on a TiO_2/SiO_2 layer on LaSFN15:

$n_0 = n_1 \Rightarrow d_0 = 10$ nm (best fit),
$n_0 = 1.4 \Rightarrow d_0 = 10..20$ nm.

Although a fit for (n_0, d_0) was possible, the results were not very accurate because $n_0 \cdot d_0$ was smaller than $\lambda/10$, cf. (2.43-44).

When the values for (n_0, d_0) were known, the fit parameter θ in (2.54) could be determined from the (sp)-radiation pattern, which yielded for a protein layer adsorbed on LaSFN15:

$$n_0 = n_1, \quad d_0 = 10 \text{ nm} \qquad \Rightarrow \theta = 58°,$$
$$n_0 = 1.4, \quad d_0 = 20 \text{ nm} \qquad \Rightarrow \theta = 56°,$$

for a protein layer adsorbed on fused silica:

$$n_0 = n_1, \quad d_0 = 10 \text{ nm} \Rightarrow \theta = 55.5°,$$
$$n_0 = 1.4, \quad d_0 = 10 \text{ nm} \qquad \Rightarrow \theta = 53°,$$

and for a protein layer adsorbed on TiO_2/SiO_2:

$$n_0 = n_1, \quad d_0 = 10 \text{ nm} \Rightarrow \theta = 57.9°,$$
$$n_0 = 1.4, \quad d_0 = 10 \text{ nm} \qquad \Rightarrow \theta = 55°.$$

An isotropic orientation of emitters yields $\theta_{iso} = 54.73°$, cf. (2.73). It seems that the emission dipole moments of the marker molecules were orientated slightly parallel to the interface because $\theta \gtrsim \theta_{iso}$, but this tendency is not significant because the errors in the determination of θ were about 3°, i.e. the ensemble may be regarded as isotropic. For interpretations of the fit parameter θ confer example 1 of section 2.2.1.

From the measured emitted intensities (both polarizations) at the critical angle of total internal reflection α_c and the assumption that the ensemble of emitters was isotropically orientated we determined the refractive index of the adsorbate layer on fused silica and LaSFN15 [5;6]:

$$n_0 = \sqrt[4]{(n_1 n_2)^2 \, \frac{I^{(s)}(\alpha_c)}{I^{(p)}(\alpha_c)}} = 1.37 \pm 0.02 \qquad (5.5)$$

where $I(\alpha) = P(\alpha)/P(0°)$ is the emitted intensity normalized to 1 at emission angle 0°.

5.4. Summary

Unspecific adsorption to a liquid-glass interface of rabbit-anti-human immunoglobulin (Gamma chains) labelled with the fluorescent dye TRITC in phosphate buffer solution was observed. The radiation patterns showed that the fluorescent labels were isotropically orientated with respect to the interface and that emission came from a homogeneous layer of thickness ≈ 10 nm and refractive index ≈ 1.4. For an initial bulk concentration of $3 \cdot 10^{-6}$ mol/l or 0.45 mg/ml we measured after 1 hour a surface concentration of $1/(7 \text{ nm})^2$ or 0.5 $\mu g/cm^2$.

6. RAYLEIGH SCATTERING BY SMALL PARTICLES

The object of this chapter is to give an example for electric dipole radiation near interfaces different from fluorescence and to verify in part a prediction from [2;4, p. 1613] which states that light scattering by small particles (i.e. Rayleigh- or dipole scattering, cf. [6;1-2] and section 2.3.) is also subject to interface effects.

6.1. Sample Preparation and Preparatory Measurements

We used latex (Dow Chemicals), dissolved a small quantity in ethanol, filtered it with Millipore 0.2 µm filters, and used the resulting suspension with concentration c_{sol} for the spincoat process described in section 4.2.1. The substrate was a fused silica hemicylindrical prism. The surface coverage of the latex particles c_{sur} was estimated by assuming that the proportionality constant between c_{sur} and c_{sol} was the same as for the dye molecules in formula (4.15). The estimate yielded 1 particle per $(3\,\mu m)^2$. The concentration c_{sol} of the spincoat suspension was deduced from the measured extinction coefficient in bulk solution under the assumption that extinction resulted from scattering by equally sized small spheres, cf. eq. (2.126). The values used for that calculation were: refractive index of the spheres $n_s = 1.6$ (latex), sphere radius $a = 70\,nm$ (cf. next section), refractive index of ethanol $n_0 = 1.36$, and the (vacuum) wavelength of the incident and scattered light $\lambda = 514.5\,nm$.

6.2. Radiation Patterns of Small Latex Particles On Interfaces

We measured (ss)- and (pp)-radiation patterns of thin layers of latex particles prepared as in the foregoing section and compared them with calculated ones, cf. fig. 6.1-2. "(ss)" means s-pol. excitation and s-pol. scattering, analogously for "(pp)". The fits to the measured radiation patterns were not particularly good compared to the ones in the foregoing chapters because of the high background levels ($\approx 20\,\%$ in the better half of the patterns, i.e. for $\alpha_2 \geq \alpha_{c,2}$), but the fits were acceptable for angles above the critical angle of total internal reflection $\alpha_{c,2} \approx 43°$. For angles near the angle of incidence of the exciting radiation $\alpha_{e,2}$ ($= 0°$ in this experiment) strong scattering by dust particles, scratches or other unwanted objects in the direction of the optical path of the exciting radiation occurred. This scattered light had to be blocked off by

a large beam stopper in order to prevent damage of the photo-multiplier tube. The monochromator did not block straylight as in the fluorescence experiments because excitation and emission wavelengths coincided.
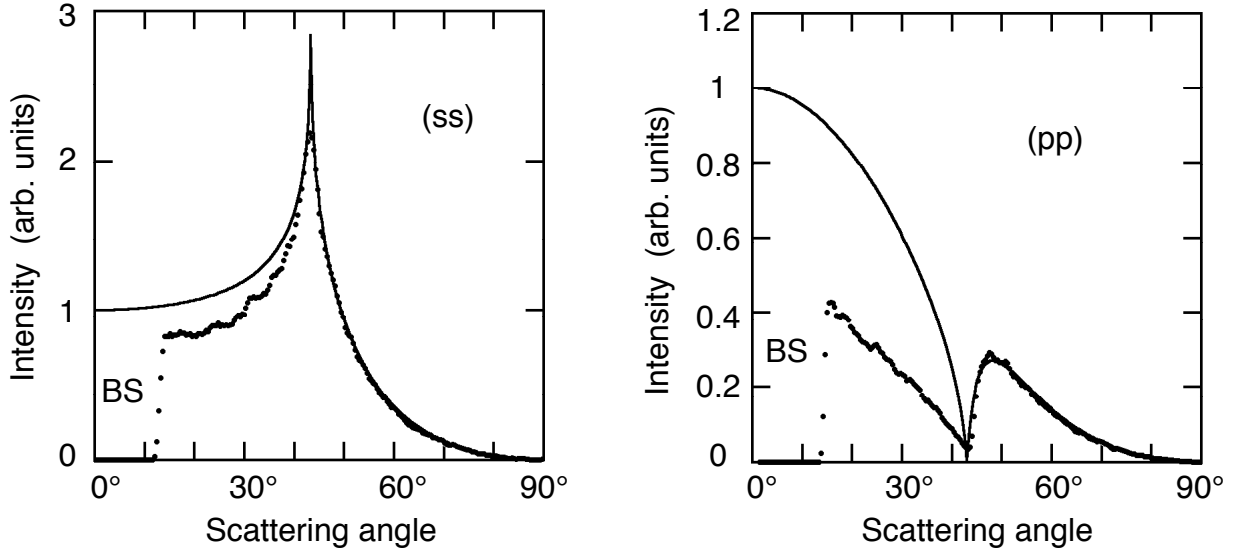

Fig. 6.1: Measured (ss)- and (pp)-radiation pattern (dots) for latex particles in air on fused silica compared with calculated patterns (solid lines); parameters: $n_1" =" 1$, $n_2" =" 1.462$ and $\lambda" = \lambda_e" = 514.5" nm$ (argon laser); fit parameters: $n_0" =" n_1$, $z_0" = 75" nm$ and $\theta" = 90°$; BS" = beam stopper, $\alpha_{e,2}" =" 0°$.
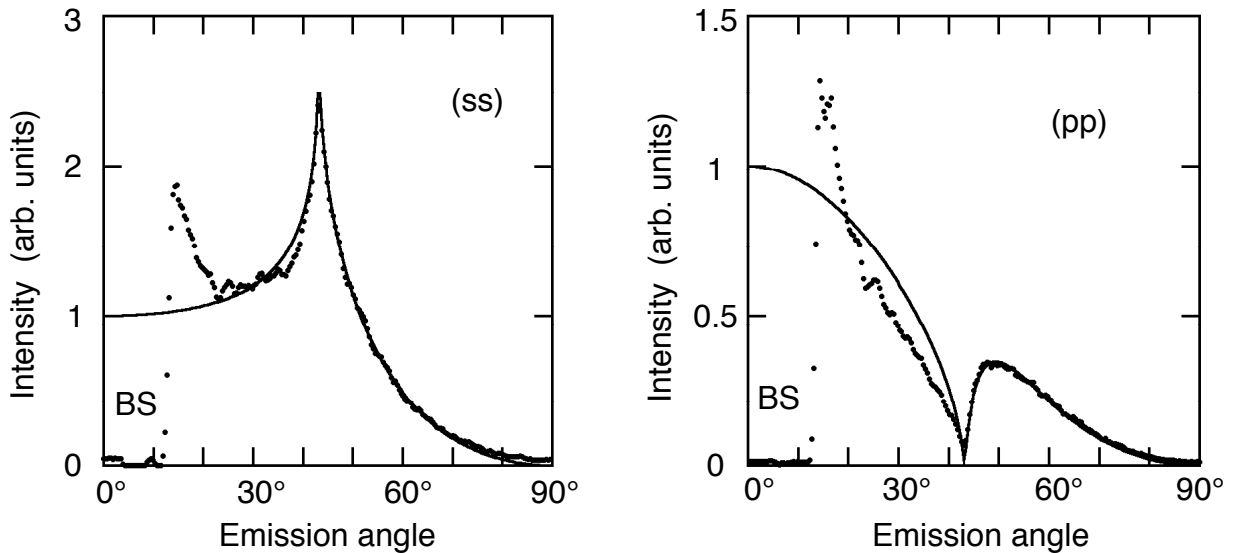

Fig. 6.2: Measured (ss)- and (pp)-radiation pattern (dots) for latex particles in air on fused silica hemicylinders compared with calculated patterns (solid lines); parameters: $n_1" =" 1$, $n_2" = 1.457$ and $\lambda" = \lambda_e" = 632.8" nm$ (He-Ne laser); fit parameters: $n_0" = n_1$, $z_0" = 65" nm$ and $\theta" = 90°$; BS" = beam stopper, $\alpha_{e,2}" =" 0°$.

Best fits to the (pp)- and (ss)-radiation pattern were for an ensemble orientation of $\theta = (90 \pm 5)°$ and $z_0 = (70 \pm 10)$ nm with parameters $\lambda_e = \lambda = 514.5$ nm or 632.8 nm, $n_0 = n_1 = 1$, $n_2(514.5$ nm$) = 1.4616$, $n_2(632.8$ nm$) = 1.4570$; $\alpha_{e,2} = 0°$. Measurements with crossed polarizers yielded much less detected scattered light (≈ 1 % of that with parallel ones). Our expectation in the (pp)-case was, that the exciting electric field and hence the induced dipoles were parallel to the interface (cf. fig. 2.4), i.e. $g_x = 1$, $g_y = g_z = 0$, $\theta = 90°$. The measurements yielded $g_z/g_x \approx 0.015$ and $g_y/g_x \approx 0.01$. If we assume that the latex particles were spherical with radius $a = z_0 = 70$ nm, then they fulfilled the Rayleigh-Gans criterion $2a (2\pi/\lambda) (n_s/n_0 - 1) = 0.3 < 1$ (2.120) and thus our assumption of the dipolarity of the scattering process was justified. An estimate of surface coverage and particle diameter from a few raster electron micrographs of a latex covered glass slide yielded $c_{sur} = (0.85 \pm 0.1)$ particles per $(3\ \mu m)^2$ and $2 a = (180 \pm 66)$ nm which is in agreement with the values deduced from the scattering experiments.

6.3. Summary

The Rayleigh scattering of small latex-particles in air on a glass surface was observed. The measured radiation patterns were within the error limits identical with the patterns of dipoles at a distance equal to the particle radius from the interface. The biggest problem was the huge background near the excitation angle (perhaps from strong forward or backward scattering by dust particles in the path of the exciting laser beam or a similar process). It remains to be shown that not only the shape of a radiation pattern but also the total radiated power depends on the optical environment as predicted by theory.

REFERENCES

1;1 M. Born and E. Wolf, "Principles of Optics",
     6th edition, Pergamon Press (1984)
1;2 J.D. Jackson, "Klassische Elektrodynamik",
     2.Auflage, Walter de Gruyter, Berlin·New York (1983)
1;3 Max Born, "Optik",
     Nachdruck der dritten Auflage, Springer Verlag (1985)
1;4 W.H. Beyer (Editor), "CRC Standard Mathematical Tables",
     25th edition, CRC"Press (1980)
1;5 A. Sommerfeld, "Über die Ausbreitung der Wellen in der
     drahtlosen Telegraphie", Ann.Phys. 28 (1909) 665-736 and
     Ann.Phys. 81 (1926) 1135-1153
1;6 T.P. Burghardt and N.L. Thompson, "Effect of planar di-
     electric interfaces on fluorescence emission and detec-
     tion", Biophys.J. 46 (1984) 729-737
1;7 J.P. Dowling et al., "Radiation pattern of a classical
     dipole in a cavity", Opt.Commun. 82 (1991) 415-419
1;8 M. Kawahigashi and S. Hirayama, "Microscopic fluorescence
     decay measurements on thin liquid films and droplets of
     concentrated dye solutions", J.Luminesc. 43 (1989) 207-212
1;9 A. Biswas et al., "Time-resolved spectroscopy of laser
     emission from dye-doped droplets",
     Opt.Lett. 14 (1989) 214-216
1;10 M.M. Asimov et al., "Possibility of investigating oxazine
     and xanthene dye vapours in an ultrasonic molecular jet",
     Opt.Spektrosk. 60 (1986) 1288-1289
1;11 P. Goy et al., "Small and sensitive systems interacting
     with millimeter and submillimeter waves: Rydberg atoms in
     a cavity", J.Appl.Phys 56 (1984) 627-633
1;12 H. Walther, "Single-atom oscillators",
     europhysics news 19 (1988) 105-108
1;13 M. Lai and J.-C. Diels, "Interference between spontaneous
     emission in different directions",
     Am.J.Phys 58 (1990) 928-930

2;1 W. Lukosz, "Light emission by multipole sources in thin layers. I. Radiation patterns of electric and magnetic dipoles", J.Opt.Soc.Am. 71 (1981) 744-754

2;2 W. Lukosz, "Theory of optical-environment-dependent spontaneous-emission rates for emitters in thin layers", Phys.Rev.B 22 (1980) 3030-3038

2;3 W. Lukosz and R.E. Kunz, "Fluorescence lifetime of magnetic and electric dipoles near a dielectric interface", Opt.Commun. 20 (1977) 195-199

2;4 W. Lukosz and R.E. Kunz, "Light emission by magnetic and electric dipoles close to a plane interface. I. Total radiated power", J.Opt.Soc.Am. 67 (1977) 1607-1615

2;5 W. Lukosz and R.E. Kunz, "II. Radiation patterns of perpendicular orientated dipoles", J.Opt.Soc.Am. 67 (1977) 1615-1619

2;6 W. Lukosz, "III. Radiation patterns of dipoles with arbitraty orientation", J.Opt.Soc.Am. 69 (1979) 1495-1503

3;1 Ch. Fattinger, "Laser Induced Luminescence of Molecules Near Interfaces", Diss. ETH No. 8222 (1987)

3;2 Th. Binkert, "Nanosekundenfluorometrie: Methodik und Anwendung der Messung zeitabhängiger und polarisierter Fluoreszenz", IAP-Bericht, Bern (1979)

3;3 S. Canonica, "Zeitaufgelöste Fluoreszenzspektroskopie und Brownsche Molekularbewegung", Diss. ETH Nr. 7634 (1984)

4;1 Theodor Förster, "Fluoreszenz Organischer Verbindungen", Vandenhoeck & Ruprecht, Göttingen (1951)

4;2 F.P. Schäfer (Editor), "Dye Lasers", Topics in Applied Physics Volume 1, Springer Verlag (1973)

4;3 F.J. Duarte and L.W. Hillman (Editors), "Dye Laser Principles", Academic Press (1990)

4;4 U. Brackmann, "Lambdachrome Laser Dyes", Lambda Physik GmbH (1987)

4;5 J. Arden, K.H. Drexhage et al., "Fluorescence and lasing properties of rhodamine dyes", J.Luminesc. 48 & 49 (1991) 352-358

4;6 L. Onsager, "Electric moments of molecules in liquids", J.Am.Chem.Soc. 58 (1936) 1486-1493

4;7 T. Govindanunny et al., "Solvent effects on the gain of rhodamine 6G", Appl.Phys. 23 (1980) 253-258

4;8   M. Meyer et al., "Ground state and singlet excited state
      of laser dye DCM: Dipole moments and solvent induced spec-
      tral shifts", Opt.Commun. $\underline{64}$ (1987) 264-268

4;9   S. Garoff et al., "Surface interactions of adsorbed mole-
      cules as probed by their optical properties",
      Opt.Commun. $\underline{41}$ (1982) 257-262

4;10 M. Lieberherr, Ch. Fattinger and W. Lukosz, "Optical-envi-
      ronment-dependent effects on the fluorescence of submono-
      molecular dye layers on interfaces",
      Surface Science 189/190 (1987) 954-959

4;11 M. Lieberherr, "Untersuchungen von laserinduzierter Lumi-
      neszenz adsorbierter, submonomolekularer Farbstoff-
      schichten", diploma thesis ETH (1986)

4;12 W. Lukosz and R.E. Kunz, "Changes in fluorescence life-
      times induced by variable optical environments",
      Phys.Rev.B $\underline{21}$ (1980) 4814-4828

4;13 N.L. Thompson and H.M. McConnel, "Order in supported phos-
      pholipid monolayers detected by the dichroism of fluores-
      cence excited with polarized evanescent illumination",
      Biophys.J. $\underline{46}$ (1984) 739-747

4;14 R.R. Chance et al., "Fluorescence and energy transfer near
      interfaces: The complete and quantitative description of
      the Eu^{+3}/mirror systems", J.Chem.Phys. $\underline{63}$ (1975) 1589-1595

4;15 F. De Martini et al., "Anomalous spontaneous emission in a
      microscopic optical cavity",
      Phys.Rev.Lett. $\underline{59}$ (1987) 2955-2958

4;16 M. Suzuki et al., "Observation of spontaneous emission
      lifetime change of dye-containing Langmuir-Blodgett films
      in optical microcavities",
      Appl.Phys.Lett. $\underline{58}$ (1991) 998-1000

4;17 B.D. Ryzhikov et al., "Effect of adsorption on the result
      of measuring the spectral characteristics of liquid dye
      solutions. 1: Absorption spectra",
      Opt.Spektrosk. $\underline{60}$ (1986) 267-271

4;18 B.D. Ryzhikov et al., "2: Excitation spectra and relative
      luminescence yield", Opt.Spektrosk. $\underline{61}$ (1986) 497-504

4;19 B.D. Ryzhikov et al., "3: Emission anisotropy and
      luminescence spectra", Opt.Spektrosk. $\underline{61}$ (1986) 1222-1227

- 74 -

4;20 B.D. Ryzhikov and N. R. Senatorova, "Spectroscopic study
     of rhodamine" 6G concentration distribution in aqueous so-
     lutions near an adsorbing surface",
     Opt.Spektrosk. 60 (1986) 1078-1081

5;1 J.L. Brash, T.A. Horbett, (Ed.), "Proteins at Interfaces",
     ACS Symposium Series 343 (1987) 290-305

5;2 J.D. Andrade et al., "Remote fiber-optic biosensors based
     on evanescent-excited fluoro-immunoassay: Concept and
     progress", IEEE Trans.Electr.Devices 32 (1985) 1175-1179

5;3 N.L. Thompson and D. Axelrod, "Immunoglobulin surface-
     binding kinetics studied by total internal reflection with
     fluorescence correlation spectroscopy",
     Biophys.J. 43 (1983) 103-114

5;4 Ph.M. Nellen and W. Lukosz, "Integrated Optical Input
     Grating Couplers as Chemo- and Immunosensors",
     Sensors and Actuators B1 (1990) 592-596

5;5 W. Lukosz, Ph.M. Nellen, Ch. Stamm, and P. Weiss, "Output
     Grating Couplers on Planar Waveguides as Integrated Opti-
     cal Chemical Sensors",
     Sensors and Actuators B1 (1990) 585-588

5;6 W. Lukosz and R.E. Kunz, "New method for determining re-
     fractive index and thickness of fluorescent thin films",
     Opt.Commun. 31 (1979) 251-256

6;1 M. Kerker, "The scattering of light and other electro-
     magnetic radiation", Academic Press, New York (1969)

6;2 M. Kerker (Ed.), "Selected Papers on Scattering",
     SPIE Milestone Series 951 (1988)

SYMBOLS AND ABBREVIATIONS

(2.x), [4;y]	reference to (formula) resp. list of [literature]
$\alpha_{1,2}$	emission angle in (x,z)-plane (in medium 1,2)
$\alpha_{c,i}$	critical angle of tot. internal reflection (medium i)
$\alpha_{e,i}$	angle of incidence of exciting radiation (medium i)
$A_{tot,r,nr}$	transition rate (total, radiative, non-radiative)
c	speed of light in vacuum, 299'792'458 m/s
cw	continuous wave, as opposed to pulsed
d_0	tickness of layer (n_0) containing the emitters
$\delta(*)$	Dirac's delta-distribution
E	electric field vector
$\hat{\varepsilon}_0$	permittivity of the vacuum $\approx 8.854 \cdot 10^{-12}$ As/Vm in SI
η	quantum efficiency or -yield
g_x, g_y, g_z	weight of dipole components in a radiation pattern
g'_x, g'_y, g'_z	weight of dipole comp. in an ensemble of emitters
I_F	fluorescence intensity (irradiance)
k, k_i	$k = 2\pi/\lambda_{vac}$, $k_i = n_i k$ (magnitude of wavevector)
λ, λ_F	emission wavelength (vacuum, F = fluorescence)
λ_e	excitation wavelength (vacuum)
$l_\perp^{(0)}$, $l_\parallel^{(0)}$	zero order term in Taylor series for $L_\perp(z_0)$, $L_\parallel(z_0)$
$L_\parallel(z_0)$	total radiated power by dipole parallel to interface
$L_\perp(z_0)$	power of a dipole perpendicular to the interface
n_i	refractive index of medium number i
$P(\alpha)$	radiation pattern = angular distribution of power
p$_{abs}$, **p**$_{em}$	absorption- and emission dipole moments
ψ	angle between **p**$_{abs}$ and **p**$_{em}$
s,p	polarization, s(TE): **E** $\parallel$ y-axis, p(TM): **E** $\perp$ y-axis
(ss),(sp),…	polarizations of (exciting emitted) em. waves
τ, τ_F	fluorescence lifetime = $1/A_{tot}$
τ_R	Brownian rotational diffusion time
ϑ	angle between a single dipole and z-axis
θ	weight (fit parameter) for a radiation pattern
ω	$= kc = 2\pi c/\lambda_{vac}$, angular frequency
x-axis	coordinate-axis parallel to and on the interface 0/2
y-axis	coordinate-axis perpendicular to the (x,z)-plane of incidence/emission in which α,α_e are measured
z-axis	coordinate-axis perpendicular to interface(s)
z_0	distance of dipole in medium 0 or 1 to medium 2

ACKNOWLEDGEMENTS

CURRICULUM VITAE

19. April 1962   born as son of Elisabeth Lieberherr-Müller and Jakob Lieberherr in Wetzikon, Switzerland

1969-1975   primary school in Wittenbach

1975-1977   Sekundarschule in St. Gallen

1977-1981   Mathematisch naturwissenschaftliches Gymnasium in St. Gallen

1981-1986   student of physics at the Swiss Federal Institute of Technology in Zurich

1986-   assistant in the optics group of Prof. Dr. W."Lukosz in the Institute of Quantum Electronics at the Swiss Federal Institute of Technology in Zurich